Sulfide-silicate textures in magmatic Ni-Cu-PGE sulfide ore deposits. 1. Disseminated and net-textured ores.

(Revision 1)

Stephen J. Barnes[1], James E. Mungall[2], Margaux Le Vaillant[1], Belinda Godel[1], C. Michael Lesher[3], David Holwell[4], Peter C. Lightfoot[5], Nadya Krivolutskaya[6] , Bo Wei[7]

[1]CSIRO Mineral Resources, Perth, Australia; [2]Dept of Earth Sciences, University of Toronto; [3]Dept of Earth Sciences, Laurentian University, Sudbury, Canada; [4]Dept of Earth Sciences, University of Leicester, UK; [5]Vale Ltd., Sudbury, Canada; [6]Vernadsky Institute, Moscow; [7]Chinese Academy of Sciences, Key Laboratory for Geochemistry, Guangzhou, China

steve.barnes@csiro.au, mungall@geology.utoronto.ca, Margaux.Levaillant@csiro.au, belinda.godel@csiro.au, mlesher@laurentian.ca, dah29@leicester.ac.uk, peter.lightfoot@vale.com, nakriv@mail.ru, bowei1986@hotmail.com

Abstract

A large proportion of ores in magmatic sulfide deposits consist of mixtures of cumulus silicate minerals, sulfide liquid and silicate melt, with characteristic textural relationships that provide essential clues to their origin. Within silicate-sulfide cumulates, there is a range of sulfide abundance in magmatic-textured silicate-sulfide ores between ores with up to about five modal percent sulfides, called “disseminated ores”, and “net-textured” (or “matrix”) ores containing about 30 to 70 modal percent sulfide forming continuous networks enclosing cumulus silicates. Disseminated ores in cumulates have a variety of textural types relating to the presence or absence of trapped interstitial silicate melt and (rarely) vapour bubbles. Spherical or oblate spherical globules with smooth menisci, as in the Black Swan disseminated ores, are associated with silicate-filled cavities interpreted as amygdales or segregation vesicles. More irregular globules lacking internal differentiation and having partially facetted margins are interpreted as entrainment of previously segregated, partially solidified sulfide. There is a textural continuum between various types of disseminated and net-textured ores, intermediate types commonly taking the form of “patchy net-textured ores” containing sulfide-rich and sulfide-poor domains at cm to dm scale. These textures are ascribed primarily to the process of sulfide percolation, itself triggered by the process of competitive wetting whereby the silicate melt preferentially wets silicate crystal surfaces. The process is self-reinforcing as sulfide migration causes sulfide networks to grow by coalescence, with a larger rise height and hence a greater gravitational driving force for percolation and silicate melt displacement. Many of the textural variants catalogued here, including poikilitic or leopard-textured ores, can be explained in these terms. Additional complexity is added by factors such as the presence of oikocrysts and segregation of sulfide liquid during strain-rate dependent thixotropic behaviour of partially consolidated cumulates. Integrated textural and geochemical studies are critical to full understanding of ore-forming systems.

Keywords: nickel deposits, magmatic sulfides, komatiites, layered intrusions

1 Introduction

Magmatic sulfide ore deposits account for some of the world's most valuable metal accumulations, currently accounting for ~56% of the world's nickel production and over 96% of supply of platinum, palladium and the other platinum group elements (Mudd and Jowitt, 2014; Zientek et al., 2014; Peck and Huminicki, 2016). They form by the accumulation of immiscible sulfide liquid that has scavenged chalcophile elements from a coexisting silicate magma, in a variety of settings:

1. Stratiform accumulations of disseminated sulfide in cumulates within layered mafic-ultramafic intrusions, including PGE-enriched "Reefs" (Mungall and Naldrett, 2008; Naldrett, 2011);
2. Accumulations of widely varying proportions of sulfide in small mafic or mafic-ultramafic intrusions, usually identifiable as magma conduits (Barnes et al., 2016a; Lightfoot and Evans-Lamswood, 2015);
3. Accumulations of widely varying proportions of sulfide in komatiite (Lesher, 1989; Lesher and Keays, 2002; Barnes, 2006) or ferropicrite (Hanski, 1992; Keays, 1995; Hanski et al., 2001) lava flows or associated shallow subvolcanic intrusions, commonly identifiable as magma conduits or feeder tubes;
4. Sulfide disseminations, commonly PGE-rich, in the marginal facies of large layered intrusions; the Platreef of the Bushveld Complex is the type example (Holwell and McDonald, 2006)
5. Sulfide accumulation from an impact-generated crustal melt sheet: the unique example of Sudbury (Keays and Lightfoot, 2004; Naldrett, 2004).

Within all these settings, sulfides occur as composite aggregates or “blebs” of the typical mineral assemblage formed by solidification of the original sulfide liquid, which in most cases has Fe as the dominant metal component, and subsequent subsolidus unmixing of that assemblage (Craig and Kullerud, 1969). The predominant minerals under most circumstances are pyrrhotite, pentlandite and chalcopyrite, forming aggregates that in many cases preserve the original physical form of the sulfide component as it existed in the liquid state. The nature and diversity of the physical form of the sulfide liquid, as droplets, pools, veins and networks, provide essential clues to understanding the physical processes of ore formation. In this contribution, we focus on “sulfide-silicate textures”, that is, the range in morphologies of intergrowths between sulfide and associated gangue silicate and oxide minerals. Textures and intergrowths in massive ores, semi-massive breccia ores and other variants of sulfide-dominated ores will be described in a forthcoming companion paper.

Our main purpose in the study of textures is to make deductions about ore-forming processes (using the term “ore” in a loose sense to denote sulfide-bearing rocks, rather than in the strict sense of being economically exploitable). Ore textures are commonly the end product of multiple stages, and magmatic sulfides are no exception. For this reason, we restrict this study to the spectrum of textures ranging from those in disseminated ores, with a few percent sulfide in a predominantly silicate matrix, through to matrix or net-textured ores containing up to around 70% sulfide forming a continuous network enclosing cumulus silicate grains. In many deposits, disseminated sulfides form large discontinuous haloes around higher grade, more economically attractive bodies of sulfide-rich ores; hence a second major purpose of this study is to assess whether spatial variations in ore textures, coupled with geochemical observations, can be used as exploration proxies and vectors towards high-grade ore.

We interpret disseminated and net-textures to be the end result of a relatively restricted sequence of processes:

1. Generation of a dilute sulfide-silicate liquid emulsion, i.e. a small proportion of sulfide liquid droplets within a transporting silicate magma;
2. Physical separation of a mixture of sulfide liquid droplets and cumulus silicate minerals, containing varying proportions of trapped silicate melt, from this emulsion;
3. Migration of sulfide liquid droplets and networks through a porous crystal mush, driven by the balance between capillary and gravitational forces.

The first two processes are clearly indispensable components of any magmatic sulfide ore forming system, although there is plenty of scope to debate how they occur in individual deposits. The extent of the third process may be minimal in some cases and pervasive in others, but understanding it is essential in order to be able to make any useful deductions about the first two. For this reason, consideration of the empirical evidence and underlying physics of sulfide liquid migration in intercumulus pore space forms a central theme of this study. Further implications extend to understanding the behaviour of sulfide droplets during mantle melting, segregation of S-bearing metal melts in meteorites and hence the formation of planetary cores (Gaetani and Grove, 1999; Mare et al., 2014).

The results presented here are the culmination of an extended body of work using a variety of characterization techniques to investigate sulfide-silicate ore textures, with the core technology being x-ray computed tomography for investigating microtextures in 3D. Combining this methodology with other newly-available techniques, such as high-resolution microbeam XRF mapping, opens a range of observations impossible to obtain using conventional petrographic techniques, particularly on the size, morphology and connectivity of phases and grain aggregates. We have made extensive use of supplementary online materials and the CSIRO online data repository to display animations and interactive visualizations of the 3D images. We strongly encourage the reader to make use of these resources in order to get the full value from the observations we present here.

1.1 Terminology

There is a spectrum of sulfide abundances in many magmatic sulfide ore deposits. In many cases, particularly in komatiite-hosted ores and also at Voisey's Bay (Fig. 1) there is a broadly trimodal distribution between massive ores typically containing 80-100% sulfide, ores with up to about five modal percent sulfides, called "disseminated ores", and ores containing about 30 to 70 modal percent sulfide forming continuous networks enclosing cumulus silicates (usually but not always olivine). The 30-70% sulfide type has gone by two completely synonymous terms: "matrix ore", commonly used in Australia, and "net-textured ore", used in Canada and elsewhere. Here we stick to the more descriptive term "net-textured". Ores with intermediate abundance between disseminated and net-textured do exist, and in some deposits are the predominant ore type, as in the giant Jinchuan deposit in China (Tonnelier, 2009). As we will see, these ores commonly have the characteristic of being mixtures of cm-scale domains of net-textured and disseminated ores.

Discrete sulfide mineral aggregates in magmatic sulfide ores (or sulfide-bearing igneous rocks in general) have commonly been referred to as "blebs". This was originally a medical term referring to spheroidal fluid-filled skin blisters, but it has become widespread in the petrology literature referring to bodies of originally immiscible liquids at mm to cm scale. The term "ocelli", meaning eye-like spots, has also been used to refer to immiscible liquids, usually silica-rich melt in a more mafic Fe-rich matrix (Frost and Groves, 1989), but has generally not been used for sulfide liquids. Given the diversity of size and morphology, we need to establish a consistent terminology to describe "sulfide aggregates", which we define as any contiguous body of minerals derived entirely from original immiscible sulfide or sulfide-oxide melt regardless of size or morphology. We retain the word "bleb" in recognition of its common usage, but attempt to define it specifically as a composite aggregate, at a scale from tens of microns to a few cm, regardless of its textural relationship to associated gangue silicate phases. Where blebs have sub-spherical morphologies, as in cases that have tended to be referred to in the literature as "blebby ores", we refer to them as "globules" and the ore type as "globular ore". Cuspate to round blebs that are developed within the interstitial space of silicate mineral cumulates are referred to as "interstitial blebs"; as we will see, there is a continuous spectrum between interstitial blebs and globules.

1.2 Silicate-sulfide wetting and dihedral angles

A fundamental control on the development of sulfide-silicate textures is the extent to which sulfide liquid wets silicate and oxide phases. Where three phases come together along a contact line, the angles between the phases perpendicular to the contact line can be described in several ways, illustrated in Fig.2. The angle between the faces of two solids (S) in contact with a liquid (L) is an interfacial angle (Fig. 2a). At equilibrium the interplay between the interfacial energies of the three contacts (e.g., S-S, S-L, S-L) leads to the establishment of an equilibrium dihedral angle θ (Fig. 2b) which generally is not equivalent to the interfacial angle outside the immediate vicinity of the contact line. At the contact line where two fluid phases meet a planar solid surface, an equilibrium wetting angle can be defined as in Figure 2c. In the example the wetting angle is 160°, as measured by Mungall and Su for sulfide melt and silicate melt against an alumina crucible (2005). Similar wetting angles have been observed in many other experiments e.g. (Brenan, 2003; Mungall and Brenan, 2014). Figure 2d shows cross sections of channels occupied by silicate melt along contact lines where three crystals meet. If the equilibrium dihedral angle is < 60° as in the two upper sketches, the walls of the channel are convex into the channel. If the dihedral angle θ is > 60° then the walls of the pore are concave into the channel, as in the lower example. In Figure 2e the same channels are shown with an immiscible sulfide liquid occupying the centre of each channel, making a contact angle of 160° with the channel walls. If $\theta < 60°$, the melt is defined as "wetting" and occupies prismatic grain edge channels, giving rise to an interconnected melt phase in three dimensions (Fig. 3), even at melt fractions below 1% by volume (Von Bargen and Waff, 1986; Jung and Waff, 1998; Wark et al., 2003). Conversely, in cases where $\theta >$ 60°, the melt is defined as "non-wetting" and grain edges become dry as a result of the liquid phase "beading-up" at grain-edge intersections. For $\theta > 60°$, melt connectivity is achieved only above a finite fraction that is a strong function of θ. In the descriptions that follow, we use the terms wetting and non-wetting in this specific sense. However, in sulfide-bearing cumulates the situation is complicated by the presence of not one but two potentially wetting liquids: silicate and sulfide. We will show that the wetting behaviour of sulfide liquid against solid silicates is strongly influenced by the presence and absence of coexisting silicate melt. If both liquid phases are present then the sulfide melt does not wet the crystals because of the very large wetting angle as shown in Figures 2e and 3c. If only sulfide melt is present then it is not prevented from making contact with the solids. Depending on the solid-solid-liquid dihedral angle the sulfide melt will either bead up in isolated pores (Fig. 3a) or spread into a well-connected network of channels as shown in Figure 3b. Whereas basaltic liquids have low dihedral angles against olivine and form networks resembling Figure 3b, measured dihedral angles for sulfide against olivine and chromite are sensitive functions of temperature and melt composition (Ballhaus and Ellis, 1996; Gaetani and Grove, 1999; Rose and Brenan, 2001). At typical moderately reducing conditions, sulfide liquids with appreciable Ni and Cu contents have dihedral angles > 60 and will not form interconnected networks. One therefore anticipates that in texturally equilibrated olivine cumulates entirely lacking silicate melt, the sulfide melt should form isolated blebs at four-grain contact points, but that small amounts of silicate melt will force the generation of an extended network of open channels along which the sulfide melt is able to propagate as shown in Figure 2c. These principles guide the physics behind sulfide-silicate textures.

2 Methods and samples

In this contribution, we focus on the diversity of intergrowths between original sulfide liquid and associated gangue silicate minerals, using the term "sulfide-silicate textures" to cover these intergrowths. The underlying assumption is the textures described are essentially magmatic and have not been substantially modified by deformation and alteration. To this end, we take examples as far as possible from undeformed deposits that have undergone little or no post-magmatic alteration or metamorphic modification. This criterion is very hard to satisfy in deposits hosted within ultramafic rocks, particularly komatiites which are almost universally hydrated or carbonated to some degree. However, it has been well established that under most circumstances the process of serpentinization faithfully pseudomorphs original igneous textures, even where primary silicate and sulfide mineralogy is completely transformed. Consequently, most of the komatiite-associated examples are from serpentinized rocks. This is necessary because komatiite-hosted ores are some of the simplest and best understood ore systems, forming under conditions of rapid cooling where primary depositional textures have the best chance of being frozen in. Hence they give some of the least ambiguous and most useful textural information. Localities discussed and illustrated here are summarized in Table 1.

Table 1.

A variety of imaging techniques has been used to illustrate sulfide-silicate textures, the most revealing being 3D X-ray computed tomography (XCT). Data are represented from low resolution (~mm scale) imaging using medical XCT scanning technology, on decimetre scale samples with coarse sulfide aggregates (Robertson et al., 2016), and also from high resolution HRXCT techniques (Godel, 2013) that can achieve resolutions of 0.7-10 μm on mm to cm scale samples (or volumes of interest within larger samples) at very much greater cost in instrument time.

The Medical X-Ray Computed Tomography system used for this study is a SOMATON Definition AS Medical CT Scanner. This instrument is composed of a rotating X-Ray source producing a fan-shaped X-ray beam, along with a rotating set of X-Ray detectors (Multislice UFC™ detectors), and a 100 kW generator. The X-Ray source is fitted with an STRATON MX P High Performance CT-X-Ray tube, with intensity and voltage ranging from 20 to 800 mA and from 70 to 140 kV, allowing the X-Ray to be transmitted through dense and complex material such as disseminated to blebby magmatic Fe-Ni-Cu sulphides. Reconstruction to produce the tomographic dataset was done on the Syngo® Acquisition Workspace, and involves correction for anisotropic voxel sizes.

High resolution micro-scale computed tomography was collected on two different instruments: a Skyscan (now Bruker) 1172 desktop scanner at CSIRO's Waterford Laboratory, and an XRadia (now Zeiss) Versa-XRM 500 3D x-ray microscope at CSIRO-Australian Resource Research Centre (both in Perth, Australia). Details for the Skyscan instrumental conditions are given by Godel (2013) and Godel et al. (2013), and for the XRadia instrument by Godel et al. (2014), Godel (2013) and Prichard et al. (2015). The resulting dataset after reconstruction using each of these instruments represents a regular volumetric grid, where each voxel has a unique grey-scale value. This grid is then processed and analysed with AvizoFire® (FEI). Digital image filters are applied to enhance and remove instrumental noise from the image (generally a non-local mean filter was applied), and a 3D gradient watershed segmentation process is carried out, attributing a range of grey-scale values to a given phase, with phase boundaries being located at the point of maximum gradient in grey-scale (Godel, 2013).

Conventional 2-D petrographic images are combined with X-ray fluorescence element maps using two different techniques: desktop microbeam XRF using the Bruker Tornado instrument at spatial resolutions around 40 μm (Barnes et al., 2016b), and 2-4 μm resolution images collected using the Maia multi-detector array on the XFM beamline of the Australian Synchrotron (Ryan et al., 2010; Paterson et al., 2011; Ryan et al., 2014; Fisher et al., 2015), the latter being referred to hereafter as MAIA-XFM images. Visualization of textures using combinations of 2D and 3D images by these various techniques has given us new insights into the diversity and origin of sulfide-silicate textures.

Textures are described from a number of deposits exemplifying all of the four main settings described above. Brief descriptions and sources of data and previously published images are given in Supplementary Material.

3 Disseminated sulfide textures

This section is concerned with sulfide-silicate textures in ores containing less than 10 modal percent sulfide, most typically in the range 0.5-2.5%. We begin with the simplest examples: disseminated sufides in komatiitic olivine cumulates (Figs. 4 - 6).

3.1 Disseminated sulfides in komatiitic dunites and peridotites

Barnes et al. (2008b) used high resolution X-ray tomography to obtain 3D images of sulfide textures in komatiitic disseminated ores, comparing the two typical host rock cumulate types, olivine adcumulates and olivine orthocumulates from several mineralized localities within the Norseman-Wiluna Greenstone Belt of the Yilgarn Craton in Western Australia. Images are shown from the adcumulate-dominated Mt. Keith MKD5 (Barnes et al., 2011a) and Dumont (Sciortino et al., 2015) deposits (Figs. 4-6) and the orthocumulate-dominant Black Swan deposit (Dowling et al., 2004; Barnes et al., 2009) (Fig. 7). The Mt Keith samples comprise nearly pure olivine-sulfide adcumulates, with less than 5% trapped intercumulus silicate melt component and a sulfide mode of less than 5%; whereas the Black Swan olivine-sulfide orthocumulates contain an original interstitial silicate liquid abundance of around 30% and 1-5% modal percent sulfide. The samples have all undergone secondary serpentinization which produces complete pseudomorphic replacement of the original olivine grains, but extensive observation of large numbers of samples with varying degrees of serpentinization convinces us that the degree of modification of the original igneous morphology of the sulfide blebs is minor. This conclusion is backed up by a synchrotron XFM image of disseminated sulfides in almost completely fresh olivine adcumulate from Dumont (Fig. 6 c,d) (and see also previously published images of sulfides in fresh dunite from the Betheno locality – Barnes et al., 2011b). Sulfide aggregates in the Black Swan olivine orthocumulates tend to form rounded globules within the interstitial space, in comparison with the more lobate morphologies of sulfides in the adcumulate rocks from Mt Keith. Olivine grain size in the dunite hosted deposits at Mt Keith and Yakabindie is systematically finer within sulfide-bearing domains relative to sulfide-free domains, at a scale of decimetres or about ten times the characteristic olivine grain size (Godel et al., 2013), but this relationship is not evident at Black Swan.

The CT-scan images of Barnes et al. (2008b) and Godel et al. (2013) indicate that a proportion of sulfides in the Mount Keith adcumulate-textured samples appear to wet the former olivine grains with highly variable dihedral angles (Fig. 3) ranging down to less than 30 degrees (as estimated in the 3D image), but some samples also contain a population of typically coarser more globular sulfides with high dihedral angles. (See supplementary materials for animated rotating 3D images, which give a much clearer impression of the true geometry of the sulfide blebs). Sulfides in the more "wetting" samples form well-connected "channels" along the triple-grain boundaries even at low sulfide abundance of less than 3%, with sulfide channels extending on a scale of about 2-4 times the characteristic olivine grain size. In the Dumont sample, the wetting angle is evidently much higher, such that sulfide liquid forms completely isolated triple-point blebs with high dihedral angles (Figure 6). With decreasing abundance in the Mt Keith samples, sulfides tend to occupy triple-point "channels" to a limited degree, but the degree of interconnectivity between blebs is low, and there is a high proportion of small isolated blebs. In marked contrast, sulfides from the orthocumulate-textured samples from Black Swan (Fig. 7) exclusively form isolated sub-spherical blebs with poor connectivity despite having a sulfide content similar to that of the Mt. Keith samples. Larger blebs in the Black Swan samples show irregular "coalesced" morphologies occupying interstitial space, in some cases occupying olivine grain faces but for the most part forming rounded non-wetting boundaries with no measurable dihedral angle.

We conclude that sulfides either form isolated patches in the complete absence of silicate melt, or interconnected frameworks along olivine triple grain boundaries that were lined by small quantities of silicate melt (Fig. 3a,c).

3.2 Disseminated sulfides in layered intrusion cumulates

Disseminated sulfides in peridotitic and pyroxenitic cumulates have been studied in a number of deposits, with examples being given here from four: Kevitsa in arctic Finland (Yang et al., 2013; Santaguida et al., 2015; Le Vaillant et al., 2016), the Mirabela Intrusion (Santa Rita deposit) in north-eastern Brazil (Barnes et al., 2011c), the Merensky Reef of the Bushveld Complex in South Africa (Godel et al., 2010), and the JM Reef of the Stillwater Complex in the USA (Godel et al., 2006).

In the Kevitsa and Mirabela intrusions, sulfides form typical interstitial disseminated blebs within wehrlite and poikilitic clinopyroxenite (Kevitsa), and poikilitic harzburgites and orthopyroxenites (Mirabela). Blebs are characteristically less than 1 mm in size and poorly interconnected, and are characteristically isolated at olivine/pyroxene triple and quadruple point grain boundaries (Figs. 8, 9). They show some interesting textural variants as the result of some additional factors: presence of pyroxene oikocrysts (Figure 8), presence of chromite, and in the case of Mirabela, differentiation of the sulfide blebs producing Cu-rich residual liquids coexisting with fractionated trapped liquid (Figure 9).

The Kevitsa sulfides are dominated by small interstitial blebs, with more than 95% of the number of blebs having sizes expressed as equivalent sphere diameters of less than 500 microns (see discussion of bleb sizes below). Dihedral angles are generally high and interconnectivity low. However, in the sample illustrated in Figure 8, containing 6.3 volume percent sulfide, the three largest blebs, representing 52% of the total volume of sulfide in the sample, occur as much larger networks forming interconnected triple-boundary channels extending at scales tens to hundreds of times the characteristic cumulus silicate grain size (Fig. 8a – this is best seen in the animated image in the supplementary material). A similar observation was made by Godel et al. (2013) on some of the sulfide-rich (>3 modal %) samples from Mt Keith; there appears to be a threshold value of around 3-5% sulfide at which sulfide networks begin to form and coexist with much finer isolated blebs. This texture appears to represent a transition between typical interstitial disseminated and patchy net-texture, an important point to which we will return.

The Kevitsa disseminated sulfides also display a characteristic feature evident in a wide variety of other deposits displaying a range of sulfide abundances. Where poikilitic phases are present, in this case clinopyroxenes enclosing chadacrysts of orthopyroxene or olivine, the oikocrysts are characteristically free of sulfide inclusions. A striking example of this texture is seen in 3D in Fig. 8e,f: the "holes" in the sulfide "cloud" are subhedral equant clinopyroxene oikocrysts.

Disseminated sulfides in the mesocumulate orthopyroxenite and harzburgites of the Mirabela intrusion show broadly similar textures to those at Kevitsa (Fig. 9), but also have a tendency to be associated with patches of late-crystallising postcumulus silicate and oxide phases representing the "dregs" of the trapped liquid solidification process. An additional complexity at Mirabela is that chalcopyrite, formed from the liquid residual to solidification of mss from the sulfide melt fraction, commonly forms complex, almost symplectic intergrowths in these late postcumulus patches (Fig. 9b). This texture is attributed to migration of both silicate and sulfide residual liquids during the late stages of compaction and solidification of the crystal pile, such that both accumulate in the same remnant pore space. These late stage Cu-rich liquids are evidently strongly wetting against silicates. A similar feature was noted in the Mordor intrusion in central Australia (Barnes et al., 2008a) where residual Cu-rich sulfides form complex intergrowths with late-forming mica and oxide grains.

The chromite content of the disseminated sulfide zone at Mirabela ranges up to about 5%, and in the more chromite-rich samples sulfide blebs show a strong tendency to associate with and interconnect between chromite grains (Fig. 9d,e). This is attributable to a tendency for sulfide liquids to wet oxide minerals in preference to silicate minerals (Rose and Brenan, 2001; Brenan and Rose, 2002). A similar preference for sulfide blebs (and platinum group element minerals) to be attached to chromite grains is apparent in the Merensky Reef (Godel et al., 2010), although measured dihedral angles in the Merensky chromitite seams appear to indicate non-wetting behaviour (Godel et al., 2006). Similar discrepancies between grain scale textures and dihedral angles, and wide-short range variability in wetting angles, are a common theme in these investigations.

In the olivine gabbronorite from the J-M Reef (Fig. 10a and b) and the gabbronorite from the Merensky Reef (Fig. 10c), the sulfide forms 3D-interconnected networks that extend over variable length based on the sample considered. These networks tend to be elongated parallel to the paleo-vertical and occur at both pyroxene/pyroxene and pyroxene/plagioclase boundaries This particular sulfide topology is inferred to be due to downward percolation of sulfide liquid during the early stage of compaction, resulting in the formation of vertical dilantancy triggered by local extension in the plane of the layering (Godel, 2006). Similar features are seen in sulfides from the JM Reef of the Stillwater Complex (Godel, 2015).

3.3 Globular sulfides

Globular ores are defined by the presence of convex, typically sub-spherical or ellipsoidal sulfide aggregates with diameters ranging from hundreds of microns to several cm. These occur in two major varieties, with and without associated polymineralic silicate caps ("capped" and "uncapped"), and in several settings:

1. in the chilled margins and interiors of mafic dikes as both capped and uncapped varieties
2. in komatiitic olivine orthocumulates, as capped and uncapped varieties
3. in xenolith-bearing cumulate rocks from subvolcanic sills and chonoliths, most notably in the Noril'sk - Talnakh camp but also in a number of other intrusion-hosted deposits worldwide. The Noril'sk-Talnakh examples include both capped and uncapped varieties, but examples in mineralized olivine cumulate layers in the lower portions of the chonoliths are mostly capped.
4. in Offset Dikes of the Sudbury Igneous Complex, where they are closely associated with xenolith-bearing sulfide breccias; these are exclusively uncapped.

3.3.1 Globular sulfides in dikes.

Capped globules trapped within chilled dike margins have been described in detail from two localities: one of a suite of mafic "macrodikes" associated with the Tertiary basaltic volcanic province in in the Kangerlussuaq area of East Greenland (Holwell et al., 2012), and from a mafic dike occurrence in Uruguay (Prichard et al., 2004). Fig. 11 illustrates the textures from the gabbroic Togeda Macrodike, where spherical globules are present up to a maximum diameter of around 10 mm (Fig. 11A-F). Larger globules are present, up to several centimetres, but they do not preserve the spherical shape, and become transitional with interstitial disseminated textures. In most cases, the spherical globules display a coarse-grained silicate cap (Fig. 11A-D) made up of plagioclase and clinopyroxene, above and partially intergrown with the top of the sulfide globule, which has a spherical bowl shape at its base. Identical textures were also observed by Prichard et al. (2004) in sulfide globules in a mafic dyke from Uruguay. Prichard et al. (2004) interpreted the textures to have formed from sinking of the sulfide during crystallization, leaving a void into which the coarse silicates grew. However, there are a number of explanations to explain these caps, including the association with vapour bubbles, which are discussed below. Notwithstanding this, such textures are reliable geopetal indicators in such intrusions.

Interestingly, the S isotope signatures of the globules in the Togeda Macrodike indicate a sulfur source from sediments present stratigraphically hundreds of metres higher than the present position of the dike-hosted globules (Holwell et al., 2012). This provides compelling evidence for downward transport of these sulfide globules; similar isotopic evidence for downward transport of sulfides on a scale of tens of metres has been found in ultramafic-mafic plugs on the Isle of Rum, Scotland (Hughes et al., 2016).

3.3.2 Globular sulfides in komatiitic cumulates

These are relatively widespread, although usually not a large proportion of the total volume of sulfide in individual deposits, exceptions being some of the Kambalda deposits and particularly the Marriott's deposit in Western Australia where almost the entire deposit is comprized of flattened ellipsoidal sulfide globules. As shown above, there is a complete transition, sometimes within the same few cubic centimetres of rock, between interstitial disseminated and globular blebs, with globules becoming more predominant in more orthocumulate rocks.

The Black Swan disseminated deposit is dominated by transitional sulfide morphologies (Fig. 7) but is marked by one of the best-developed known examples of capped globules (Fig. 12). Here, sulfide globules are associated with rounded segregations of chlorite-rich material containing weakly pseudomorphed microspinifex texture (Fig. 12e), occupying convex spaces between cumulus olivine grains). These are interpreted by Barnes et al. (2009) as segregation vesicles, analogous to those seen in basalts (Anderson et al., 1984; Caroff et al., 2000) and described in unmineralized komatiite by Siegel et al. (2015) and Beresford et al.

(2000).The caps are originally gas filled vesicles that subsequently become filled with evolving interstitial silicate melt due to vapour pressure gradients generated during the late stages of solidification, a process referred to as gas filter-pressing (Anderson et al., 1984). Sulfide globules occupy the bottom contacts of these vesicles, and have characteristic concave-up menisci against the silicate infill material. In rare cases (Fig. 12b,c,d) the sulfide globules have rinds of skeletal chromite that is unlikely to have crystallized from the segregated melt within the vesicle on mass balance grounds; these provide evidence that the vesicles formed after the sulfide droplet, which itself must have reacted with a large volume of silicate melt before becoming embedded in the olivine orthocumulate crystal pile.

The experimental observations of Mungall et al. (2015) provide the essential clue to the processes in action here. Where sulfide melt, silicate melt and vapour bubbles coexist, vapour bubbles have a strong tendency to nucleate against and then to remain attached to sulfide droplets owing to surface tension effects. Depending on the proportion of the phases, this may enable sulfide droplets to float within a much less dense mafic magma like a basket beneath a hot-air balloon. This process may explain the retention of coarse silicate-capped sulfide globules in mafic dykes in the examples cited above. Sulfide flotation may have played a role in the formation of the Black Swan globular ores, but these only form a small proportion of the orebody, and much of the sulfide at Black Swan occurs as sub-rounded blebby aggregates (Fig. 7) with no evidence of an attached vapour phase. The Black Swan komatiites are highly contaminated and probably contained high proportions of assimilated water, such that vapour saturation would have been achieved during solidification of the trapped interstitial melt (Barnes et al., 2004). We therefore prefer the interpretation that the droplet-bubble association at Black Swan arose from in-situ nucleation of a hydrous vapour phase from the fractionated intercumulus silicate melt fraction, with the vapour bubbles nucleating preferentially on the already-accumulated sulfide droplets due to surface energy effects. Interestingly, capped globules associated with probable amygdales, similar to those at Black Swan, have also been reported from komatiitic flow tops (Keele and Nickel, 1974; Stone et al., 1996), implying that the sulfides may have floated in free melt by the “balloon basket” mechanism in these cases.

3.3.3 Globular sulfides at Insizwa and Noril’sk-Talnakh

Globular sulfides in intrusions associated with flood basalt volcanism are known from two localities: the Insizwa Complex (Waterfall Gorge locality) in the Karoo Province in South Africa (Lightfoot et al., 1984), and in the mineralized chonolith intrusions of the Noril’sk-

Talnakh camp (Dodin, 1971; Genkin et al., 1982; Distler et al., 1988) (Fig. 13). The Noril'sk-Talnakh bodies form part of the intrusive component of the super-giant Siberian Traps flood basalt province, formed at the Permian-Triassic boundary during a mantle plume arrival event (Fedorenko, 1994; Naldrett, 1999; Naldrett and Lightfoot, 1999; Campbell, 2007; Arndt, 2011). Globular sulfides are abundant within the olivine cumulates that form the lower layers of the ore-bearing intrusions, typically immediately above the large basal pools of sulfide liquid now preserved as massive sulfide. These include the heterogeneous, highly contaminated olivine cumulates called "taxitic picrodolerites", whose characteristic texture is a continuous framework of olivine crystals that in some case develop skeletal textures, with interstitial space filled primarily by clinopyroxene and plagioclase. Globules are also abundant in the more homogeneous, conventionally orthocumulate textured olivine gabbros (locally called "picrodolerites") that form continuous layers above the lower taxites within the lower third of the mineralized intrusions (Torgashin, 1994; Czamanske et al., 1995; Sluzhenikin et al., 2014). The globules in these rocks have a number of very distinctive features (Fig. 13), notably a pronounced flattening in the plane of the layering, preferentially developed (within the same sample) by the larger globules (Fig. 13a). In some samples globules show complex external morphologies reminiscent of squeezed balloons (Figure 13e), implying that they have retained their surface integrity while being deformed. They show an almost universal differentiation into MSS (now pyrrhotite plus exsolved pentlandite) in the lower half and chalcopyrite in the upper half, this being attributed to fractional crystallization of the sulfide liquid as described in a number of previous publications (e.g. Barnes et al., 2006). The individual droplets form microcosms of the large-scale process of differentiation into Cu-rich and Cu-poor components evident within the massive sulfide orebodies of the Kharealakh intrusion (Sukhanova, 1968; Torgashin, 1994; Naldrett et al., 1997; Distler et al., 1999). On close inspection, a large proportion of Noril'sk globules from the picrodolerites are "capped" (Fig. 13) in a similar way to the Black Swan, as is the globule from the Insizwa locality shown in Fig. 13e. The silicate caps are developed above the sulfide globules, the caps being occupied by variable proportions of plagioclase, clinopyroxene, orthopyroxene, Ti-rich magnetite, ilmenite, hornblende, phlogopite, titanite, apatite and rarely anhydrite. Details are discussed by Le Vaillant et al. (in review).

3.3.4 Globular sulfides at Sudbury

Globular sulfide ores are well-known in the Sudbury ore deposits and were discussed by Naldrett (1969), under the term "buckshot ore", in one of the first papers to address the mechanisms of sulfide ore texture formation. They are found in two main settings: within the quartz diorite-hosted sulfide ores and ore breccias within the Offset Dikes (Lightfoot et al., 1997b), and much less commonly within the Mafic Norite unit that forms the lowermost layer of silicate cumulates within the Sudbury Intrusive Complex and also within the Sublayer (Souch and Podolsky, 1969; Mungall, 2002). The Offset Dikes are extensive composite dikes that extend to depths of up to several thousand metres below the base of the Sudbury Intrusive Complex (SIC), typically comprising an outer chilled margin of fine-grained sulfide-poor quartz diorite, an inner zone of inclusion-rich quartz diorite and a central mineralized zone that ranges from sulfide-matrix breccias to complex mixtures of quartz diorite matrix, inclusions of quartz diorite, SIC cumulates and wall rocks, and sulfide blebs ranging from sub-spherical globules to irregular elongate cm-sized blebs (Lightfoot et al., 1997a; Lightfoot et al., 1997b; Lightfoot and Farrow, 2002). Medical CT images and Tornado XRF maps of typical offset dike globular ores from the Copper Cliff mine are shown in Fig. 14.

A number of features of the Copper Cliff globular sulfides are distinct from those described above. Internal differentiation into Cu-rich and Fe+Ni-rich components is common, but they lack the consistent geopetal relationship of Cu-rich sulfide at the top that is so characteristic of the globules at Noril'sk. The globules are only rarely smooth and subspherical, and there are no silicate caps. Size distributions measured in 3D show a similar characteristic to most other disseminated sulfides in that particle sizes define a log-linear negative slope on the equivalent of crystal-size distribution (CSD) plots, as discussed below. Margins of the globules are in many cases angular and faceted, and there is fine scale intergrowth with matrix silicates. Grain boundary ("loop-texture") exsolution of pentlandite defines the margins of original MSS grains, now pyrrhotite, and in some cases idiomorphic hexagonal facets define the margins of the globules (Fig. 14c). These relationships are consistent with the proposal by Naldrett (1969) that the textures are the result of an almost complete temperature overlap in the melting ranges of the sulfide melt and the host quartz diorite liquid; the morphology of the sulfide globules was frozen in at an early stage due to a framework of growing MSS crystals that formed while the transporting silicate melt was still largely liquid and flowing. It is possible that these textures arise from the disruption and mechanical remobilization of a cumulus MSS-enriched component of a previously segregated and partially crystalline sulfide melt (Lesher et al., 2008). This explanation would resolve an old argument about the apparent heterogeneity of composition of individual sulfide blebs, an observation which led Fleet (1977) to question the magmatic origin of very similar ores in the Frood offset deposit.

Very similar textures are found in the small Piaohechuan prospect in northern China, a Ni sulfide occurrence hosted within a small differentiated mafic intrusion with hydrous mafic parent magma (Wei et al., 2015). The deposit incorporates globular, network and breccia textures, the latter types to be discussed in a companion paper. The globular textures show irregular and locally facetted morphologies of similar size and morphology to those at Sudbury (Fig. 15), as well as very similar sulfide mineral relationships. They are distinctly depleted in Cu relative to the deposit as a whole. Wei et al. (2015) show 2D images indicating the presence of rounded silicate inclusions within the globules, but 3D scanning of the same sample (Fig. 15c) reveals that these are 2D artefacts of complex indented 3D morphologies similar to those at Copper Cliff. The margins of the globules locally truncate grain boundaries between plagioclase and hornblende in the silicate matrix (altered olivine orthocumulate), leading to the initial suggestions of post-solidification replacement; however, Wei et al. (2015) interpret them as the result of growth impingement of late-crystallising silicates from hydrous magma against already partially solidified sulfide globules. We regard these textures, like those at Sudbury, as the result of entrainment and redeposition of a partially solidified and differentiated sulfide liquid pool from elsewhere in the mineralized system.

4 Net-Textured Ores

Net-textured ores, also called matrix ores, are defined by the presence of a continuous matrix of sulfide containing a connected framework of cumulus silicate crystals, usually olivine. They are most commonly found in komatiitic or komatiitic basaltic settings, where they typically form a component of a regular vertical sequence, from bottom to top: massive sulfide from tens of centimetres to several metres in thickness with a sharp upper contact; net-textured ore, up to tens of metres thick in some of the larger deposits; a gradational upper contact over tens of centimetres to a metre, into olivine cumulates containing less than 5 % disseminated sulfides. This sequence, first described from komatiite settings at Kambalda, Western Australia (Ewers and Hudson, 1972; Marston, 1984) and Alexo, Ontario (Naldrett, 1973; Houle and Lesher, 2011; Houle et al., 2012), became the basis for the “billiard-ball model” of Naldrett (1973), in which the succession of textures was interpreted in terms of Archimedes Law buoyancy equilibrium, as discussed below.

Some of the best developed net-textured ores are found in the komatiitic basalt-hosted deposits of the Raglan Belt in the Ungava Peninsula of north-eastern Canada (Barnes et al., 1982; Lesher, 2007) (Fig. 16). In the sample shown here from the Katinniq deposit, olivine is the only enclosed silicate phase, forming a relatively open framework of interconnected grains ranging in abundance from about 30-50 volume percent. As a general rule the abundance of olivine in net-textured ores is considerably less than the theoretical proportion of around 60% from close-packed individual particles, implying that the olivines accumulated not as isolated crystals but as chains and clusters formed either by heterogeneous self-nucleation (Campbell, 1978) or by the process of random agglomeration of crystals referred to as synneusis (Schwindinger, 1999). Net-textured ores thereby constitute one the best lines of evidence for crystal clustering in cumulates (Jerram et al., 2003). These textures often cause terminological confusion in that the olivine framework is typical of that seen in sulfide-free olivine orthocumulates (Hill et al., 1995), but the rocks are commonly free of a trapped intercumulus silicate liquid component and are actually adcumulates (strictly, heteradcumulates), the cumulus phases being olivine and sulfide liquid.

Simple olivine-sulfide (give or take minor chromite or magnetite) net-textures are an end-member of a family of variants, two of the most widespread and genetically significant being poikilitic net-textures (often informally called “leopard textures”) (Fig.16b,c,d) and patchy net-textures (Fig. 17).

4.1 Poikilitic net-textures (“Leopard ore”)

Poikilitic net-texture is particularly well developed at Katinniq in the Raglan belt. The large “leopard spots” in this case (Fig. 16b,c,d) are 1-2 cm subhedral oikocrysts of orthopyroxene (now altered to antigorite in the illustrated example) with Cr-rich cores (Fig. 16d), corresponding to the presence of chromite as well as olivine chadacrysts. Similar examples with clinopyroxene instead of orthopyroxene are also known in the same deposit. These oikocrysts are almost completely devoid of sulfide inclusions. We have already encountered this relationship in the case of disseminated ores in pyroxene rich cumulates at Kevitsa (Fig. 8). Similar examples exist in other deposits including Ntaka Hill, Tanzania (Barnes et al., 2016b). The absence of sulfide inclusions from poikilitic phases is evidently a widespread feature that imparts useful clues as to the origins of net-textures, percolation and migration of sulfides in crystal mushes, and the origin of poikilitic textures themselves.

4.2 Patchy net-textures

Patchy net-textures are a widespread variant where the sulfide content of the rock is less than the typical 50-60%, in some cases grading down to less than 10%, but the texture of the rock is heterogeneous at a scale of ten to a hundred times the characteristic silicate grain size. The rock is divided into irregular three-dimensional domains of sulfide-poor orthocumulate, where crystallization products of trapped parent silicate melt form the matrix to the cumulus silicates (usually olivine), and sharply-bounded domains of true net texture, free of visible interstitial silicate melt components. An example of patchy net-textured ore from the komatiite-hosted deposit at Alexo, Ontario (the original type locality for the “billiard ball model”) is shown in Fig. 17. Within the net-textured domains, dihedral angles between olivine and sulfide are typically low implying wetting of olivine silicate melt channels which in turn have served to permit infiltration by sulfide. In the silicate orthocumulate domains, what little sulfide there is forms non-wetting globular blebs in the intercumulus pore space, now occupied by relict acicular clinopyroxene and chlorite as an alteration product of trapped liquid and possible plagioclase. The Alexo sample shown here is also of interest in that it contains a component of spherical sulfide globules. The significance of this particular combination of features is discussed below in the framework of the physics of sulfide melt migration in crystal mushes. It is important to note that the paucity of perfectly fresh and unaltered examples of these textures makes it nearly impossible to determine with confidence whether or not small volumes of silicate melt persisted at the cuspate terminations of the sulfide-filled channels as illustrated in Figures 1e and 2c

Exactly the same relationship has been reported in the giant Jinchuan deposit in China (Lehmann et al., 2007; Tonnelier, 2009; Tonnelier et al., 2009), which is important in this context in two respects: firstly, almost the entire orebody, probably the largest single contiguous accumulation of magmatic sulfides in the world, is composed of patchy net textured ores, with domains of true net texture and only very minor massive ores (Tonnelier, 2009). Secondly, it is by far the largest accumulation of net-textured ores in an intrusive non-komatiitic setting.

4.3 “Leopard” net-textures at Voisey’s Bay

“Leopard-textured” ores are widespread in the Eastern Deeps, Ovoid, and Reid Brook orebodies that comprise the Voisey’s Bay system. They are mainly associated with mineralization hosted in the dike system that connects the major orebodies. They form the lower-grade haloes around the massive sulfide orebodies such as the Ovoid and the Eastern

Deeps that occur at or close to the entry point of the dyke into the chamber (Evans-Lamswood et al., 2000). Unlike the "leopard ore" example from the Katinniq deposit, at Voisey's Bay the term applies to net-textured sulphides including sulfide-free pyroxene and olivine oikocrysts surrounding primary plagioclase. In the example illustrated in Fig. 18, plagioclase is clearly a liquidus phase forming a 3D framework (confirmed by x-ray tomography), whereas olivine and lesser orthopyroxene form oikocrysts enclosing multiple plagioclase laths. Again, the oikocrysts are almost entirely free of sulfide inclusions, imparting the “leopard spot” appearance to the rock in hand sample. The textural relationship is the same as that observed in the Katinniq example, but the phases are different. We therefore recommend caution in the use of the term "leopard texture", it being applicable to a variety of textures involving the presence of sulfide-free oikocrysts within net-textured domains. Poikilitic net texture is a preferable term.

4.4 Combined globular and patchy net-textured ores

A distinctive feature of the Alexo patchy net-textured ore in Fig. 17 is the presence of globular sulfides, forming very regular flattened ellipsoids with almost perfectly circular morphologies in plan view, flattened parallel to the mineral lamination defined by platy olivines in the rock. Unfortunately the original orientation of the sample is not known, but by analogy with other occurrences we take the flatter side of the globules to be the base, with an upwardly convex meniscus at the top. These globules occur primarily within the relatively sulfide-poor domains in between the net-textured patches. In some samples these globules are seen to be associated with silicate caps (Fig. 17g,h) that show strong similarities to those at Black Swan; here the caps are occupied by very fine grained serpentine, probably derived by Mg-metasomatism of an original amygdale filling, rather than being original segregated melt.

The deposits of the South Raglan trend in the Cape Smith Belt (Mungall, 2007a) are primarily hosted within the lower margins of blade-shaped dykes, and consist of a mixture of massive, net-textured and composite globular and patchy net textures (Fig. 20). These textures are different from those described above from Alexo in that they are developed within altered “pyroxenitic” marginal rocks of the dykes: felted intergrowths of acicular pyroxene grains (now amphibole) with interstitial silicate melt (now amphibole plus chlorite) and sulfide blebs. Sulfides form patchy net textures interstitial to the pyroxenes, which are thought to grow in situ as a form of microspinifex texture. These deposits also contain poikilitic olivine-bearing patchy net-textures, and patchy net-textures where clinopyroxene is the cumulus phase. Sulfides also form spheroidal or ellipsoidal globules, in some cases within the net-textured domains but also in between them (Fig. 19).

4.5 Interspinifex ore

Interspinifex ore is a very rare but distinctive textural type, unique to komatiite-settings. It forms a category of its own but can be regarded as a special case of net-textured ore in that sulfide forms an interconnected framework interstitial to olivine (Fig. 20). In this case, the olivine takes the form of skeletal spinifex plates characteristic of the upper, liquid-rich portions of komatiite flows (Arndt et al., 2008). Interspinifex ore has been described from Kambalda localities by Groves et al. (1986), Beresford et al. (2005) and Barnes et al. (2016a), in the Langmuir deposit in Ontario by Green and Naldrett (Green and Naldrett, 1981) and mentioned at the Alexo deposit, Ontario by Houle et al. (2012) (Fig. 21 B,C). In the Lunnon Shoot locality described by Groves et al. (1986) a massive sulfide pool overlies the basal komatiite flow, the top of which has been eroded such that the A1 and A2 quenched flow top and random spinifex zone have been removed, leaving the coarse parallel-plate A2 spinifex zone in direct contact with the base of the sulfide pool (Fig. 20A). The original silicate melt component of this A2 zone is missing, and the space is now occupied by a typical magmatic Fe-Ni sulfide assemblage that has either replaced or displaced that silicate melt component. The spinifex plates are curved, bent and slightly crumpled, indicative of high temperature deformation. At the top of this zone, at the interface with the massive sulfide, small plumes of quenched silicate melt about 10-20 mm in size are partially enclosed within the lower few cm of the sulfide pool. Each plume has a narrow rim of fine, wiry skeletal spinel, a hallmark of primary contacts between massive sulfide ores and komatiite melt and a feature also seen in the Langmuir interspinifex ores. Groves et al. (1986) concluded that heat from the sulfide had caused interstitial komatiitic melt between the olivine plates to be physically displaced upward by dense, downward percolating sulfide liquid. Several tens of centimetre at least of originally quenched komatiite flow top must have been removed altogether. As well as providing an outstanding piece of evidence for thermal erosion beneath komatiite flows, this ore type also provides clear evidence for the process of downward migration of sulfide liquid through interstitial pore space on a scale of decimetres; this is an important observation for the interpretation of net-textured ores as a whole.

4.6 Lobate-symplectic sulfide-silicate intergrowths at Duke Island.

An unusual variant on net-textured ores is described from the Duke Island intrusion in the Alaskan Panhandle by Stifter et al. (2014). These textures are developed within olivine-clinopyroxene-sulfide adcumulates where, instead of entirely occupying the interstitial space between the cumulus silicates, the sulfides also develop complex symplectic intergrowths with clinopyroxene and form subspherical inclusions (in two dimensions) in olivine. There are no 3D images available for these samples, but it is likely that these sulfide inclusions and intergrowths actually represent interconnected networks that are intimately intergrown with the silicate phases. Stifter et al. (2014) propose that these intriguing textures reflect downward percolation of sulfide melt and displacement of original silicate melt, along the lines of the mechanism proposed above for spinifex ore. We further suggest that the complex textures here may reflect an origin of the cumulus silicates as crescumulate dendritic (harrisitic) phases, which underwent partial textural equilibration before displacement of the interstitial silicate melt by percolating sulfide. It is noteworthy that the sulfide included in the symplectic intergrowths appears to be exclusively pyrrhotite, perhaps indicating that represents a true solid-solid symplectite produced by simultaneous growth of mss and pyroxene under water-rich conditions where both sulfide and silicate melts were between their liquidus and solidus over the same range of temperatures. Further 3D investigation of these textures is warranted, as they may provide critical evidence for or against the mechanisms discussed here.

5 Discussion

5.1 The Billiard-Ball Model reconsidered – origins of net-textured ores

The billiard-ball model was originally proposed by Naldrett (1973) to account for the characteristic vertical progression of massive to net-textured to disseminated ores in any komatiite-hosted deposits. In the analogy, the sulfide liquid is represented by mercury, olivine by billiard balls and komatiite magma by water (Fig. 21). The mercury (sulfide liquid) sinks to the bottom, while a column of billiard balls (olivine) sinks in the water and floats in the mercury to the point where the upward and downward buoyancy forces balance. The model was criticized by Groves et al. (1979) on the grounds that the thickness of the olivine cumulate pile in most Kambalda komatiite flows was too great to allow the retention of any olivine-free sulfide liquid to make the basal massive ore. This issue was addressed in a quantitative thermal model by Usselman et al. (1979), who showed that the massive sulfide could be explained by upward solidification of the sulfide liquid pool simultaneously with sinking of olivine crystals. The olivine column sinks to meet the ascending sulfide solidification front (Fig. 21B).

Subsequently a number of other challenges have arisen to the model, the main one being the recognition that this deposit type forms by sequential accumulation in dynamic flow channels rather than by static accumulation from stagnant magma. In detail, ore profiles are commonly more complex than the stereotype (Lesher, 2007; Houle et al., 2012). In a number of cases the composition of the sulfide fraction is not homogeneous, but shows a systematic variation from Cu- and Pt-Pd poor, Ir-Ru-Os-Rh enriched massive ore, indicative of an origin as MSS cumulate, to net textured ores with the opposite characteristics (Keays et al., 1981; Barnes and Naldrett, 1986; Barnes et al., 1988; Heggie et al., 2012). These complexities could still be accommodated within the basic theory, but the presence of leopard-textured poikilitic matrix ores as well as patchy net-textured ores, especially patchy net-texture with sulfide globules as described above from Alexo and the South Raglan deposits, become very hard to explain. Poikilitic ores arise as a result of the early and probably liquidus heteradcumulate origin of the oikocrysts (Barnes et al., 2016b); clearly, olivine or pyroxene oikocrysts could not have grown from the sulfide liquid, so their presence attests to early growth from now-displaced silicate melt.

As an alternative, or in some cases complementary, mechanism to the billiard-ball model, we propose that much net-textured ore, and particularly the globular-net texture combination, is the result of downward percolation of sulfide through originally silicate melt-filled porosity in unconsolidated olivine-sulfide orthocumulate mush, with concomitant upward displacement of the silicate melt. We have seen clear evidence for the operation of this process in the example of interspinifex ores (Fig. 20).

We propose that patchy net textures arise from self-organized gravity-driven migration of both sulfide and silicate melt through the intercumulus pore space of original sulfide-olivine (or sulfide-pyroxene) orthocumulates, mediated by the presence of thin films of silicate melt lining inter-crystalline channels and pores as illustrated in Figure 3c. The critical extra factor is the linking up of sulfide blebs into chains or aggregates with sufficient rise height to overcome the capillary barrier to migration of sulfide blebs through the silicate pore throats (Mungall and Su, 2005; Chung and Mungall, 2009) Fig. 3c).

Chung and Mungall’s theoretical analysis considered the sulfide bleb dimensions relative to the characteristic silicate grain size. Where sulfide blebs are significantly smaller than the pore throats between the cumulus grains, sulfide microdroplets are capable of migrating distances of hundreds to thousands of meters vertically through crystal mushes as long as silicate melt remains between the crystals. However, larger droplets, comparable in size to the cumulus minerals, become stranded as a result of capillary forces preventing droplet deformation as they attempt to pass into pore throats narrower than themselves (Fig. 3). Only in very coarse-grained mushes with grain sizes greater than about 2 cm can droplets the size of intergranular pores migrate downwards.

Extensive drainage and coupled melt migration occurs when coalescence of many microdroplets generates connected net-textured domains (networks) of the dense liquid that are many times larger than the grain size of the mush. An example of this is observed in the Kevitsa sample imaged in Fig. 8. When the vertical height of the connected network is great enough, the pressure gradient inside the dense phase exceeds the capillary force impeding downward motion through narrow pore throats and the immiscible phase is able to move down along vertically-oriented networks, displacing silicate melt upward as it migrates. The process is closely similar to that which forms interspinifex ores. As the sulfide networks migrate they grow by coalescing with previously stranded droplets; this progressive coalescence increases the rise height of the interconnected sulfide droplets, hence increasing their tendency to drain downward and further displacing silicate melt. Patchy net-textures are the result of this feedback-driven self-organization within the sulfide-bearing mush, whereas leopard textures are the result of the sulfide flowing around early formed, essentially cumulus oikocrysts (Fig. 22).

The common persistence of globular textures in net-textured sulfide ores is a key textural observation in support of the notion that net-textures form by infiltration of sulfide melt into formerly disseminated or sulfide-free orthocumulates (Figures 15-17). A globule is a textural record of a large drop of sulfide melt that maintained its form to minimize surface energy in a deformable mushy silicate magma (Figure 22a). After consolidation of the mush into a rigid framework, subsequent infiltration of the now-rigid mush by sulfide melt (Figure 22b,c) caused the globular shape of the original bleb to be retained even after it no longer marked the boundary of an isolated drop. Globular blebs of this nature cannot have formed from a crystal mush that was already filled with intercumulus sulfide melt, because in that situation there would be no sulfide-silicate melt interface whose surface tension could generate the globular shape.

It has been noted above (e.g. Figs. 4-5 and associated discussion) that sulfide-silicate wetting relationships are often inconsistent at very fine scales. The apparent local wetting of silicate minerals by sulfide may in some cases be a result of the efficient displacement of the former interstitial silicate melt. Dihedral angles in cumulate rocks adjust themselves towards equilibrium by diffusive migration of the "wetted" component through the wetting liquid (Holness et al., 2013). Where the cumulus silicates are insoluble in the liquid, as in the case of olivine and sulfide, this adjustment is not possible, and the original silicate-silicate dihedral angel is inherited by the sulfide-olivine interface. Where small amounts of silicate liquid remain as a film between sulfide and olivine along the solid-solid-melt contact lines, this may give rise to the complex bleb morphologies and highly inconsistent wetting relationships observed in some disseminated interstitial ores.

We suggest that under ideal circumstances, runaway sulfide percolation within original olivine-sulfide-silicate liquid mushes forms true net-textured ores, and even potentially allows sulfides to drain all the way to the bottom of the cumulate pile to form massive ores. It is unlikely that this is the mechanism for forming all of the typical Kambalda-style "billiard ball" intersections, where the original Naldrett mechanism may also operate in ideal circumstances, but the presence of patchy and globular net-textured ores suggests strongly that feedback-driven, self-organized sulfide drainage plays an important role in the generation of high-sulfide magmatic ores.

5.2 Implications for sulfide migration and ore genesis

5.2.1 Origins of massive ore veins

The typical mode of occurrence for massive sulfide ores in all the settings mentioned in the introduction is as basal accumulations in flows or intrusions. However, in many cases the situation is more complex; massive sulfides commonly occur as cross-cutting veins in floor rocks and in host intrusions. Such veins range in scale from a few mm (Fig. 23) to tens of metres at Noril'sk and Sudbury (Lightfoot and Zotov, 2005; Lightfoot and Zotov, 2014).

Figure 23 a and b show examples of small-scale vein-type segregations of massive sulfide within dominantly disseminated ore, which we attribute to a combination of two factors: downward migration of an interconnected sulfide liquid network, coupled with transient fracturing of the crystal mush during sudden stress events such as earthquakes. We propose that partially solidified cumulates have thixotropic rheology like water-saturated sand; they flow under low strain rates, but fracture during rapid shocks. Where sulfide melt is migrating through a mush, such events could cause transient fractures to be occupied by dense migrating sulfide melt. This process may operate at a range of scales, giving rise to sulfide veins ranging from mm to metres wide. An incipient stage may be recorded in the sheet-like sulfide aggregates identified by Godel et al. (2006) in the Merensky Reef (Fig. 10). This process is a small-scale analogue to the migration of sulfide liquid into fractures in floor rocks, often accompanied by melting of those rocks and incorporation of silicate rock fragments into massive sulfide, as documented in a komatiite setting by Dowling et al. (2004) and illustrated in a variety of settings by Barnes et al. (2016a). The various manifestations of this process are discussed in a companion paper (Barnes et al., in prep).

Figure 23c shows a complex intermingling of textures observed along auto-intrusive contacts at the base of the Tootoo deposit in the Cape Smith Belt of northern Quebec. In this view there are lobate margins between domains of net-textured ore and other domains of fine-grained "pyroxenitic" chilled margin containing isolated sulfide globules. Also present are patches of massive sulfide with ragged margins against net-textured ore. This complex texture is interpreted to have resulted from rupture of the lower boundary of a net-textured crystal mush and intrusion of mingled sulfide-free to globular-textured magma with net-textured and massive sulfide together into a keel-shaped extension of the intrusion below its original floor (Liu et al., 2016).

5.2.2 Tenor variability within deposits

The compositions of magmatic sulfide ores are often characterized by variability at a range of scales: between different textural zones of the same mineral system (Naldrett et al., 1996; Naldrett et al., 2000; Lightfoot et al., 2012) and short-range variability on decimetre scale within orebodies (Tonnelier, 2009). This variability is caused primarily by a combination of magmatic controls during deposition (parent magma composition, silicate sulfide mass balance) and subsequent differentiation of the sulfide liquid itself during solidification. This variability is a complex topic beyond the scope of this paper, but some of the textural evidence presented here throws light on the origin of short-range variability.

An example of short range variability is seen in Figure 19, where domains of Cu-rich and Ni-rich sulfides are observed at cm scale in patchy net-textured ore. This variability is interpreted as the result of simultaneous migration and fractional crystallization of MSS from the migrating sulfide liquid. Crystallization of MSS (monosulfide solid solution, the liquidus phase for almost all natural sulfide magmas) results in Cu-depleted zones of partially solidified sulfide, while the relatively Cu-enriched residual sulfide liquid continues to migrate, solidifying deeper in the system. This process leads to differentiation at a range of scales: mm-scale, in the case of the Cu-rich interstitial intergrowths described at Mirabela (Figure 9) and up to several metres in the case of Jinchuan (Tonnelier, 2009). Striking evidence of this phenomenon is offered by the common observation that pyrrhotite forms giant oikocrysts in net-textured ores at the Mequillon deposit in the Cape Smith Belt of northern Quebec (Fig. 19e); these oikocrysts are thought to have formed originally as oikocrysts of monosulfide solid solution (now inverted to pyrrhotite plus pentlandite) during solidification of the intercumulus sulfide melt, and occur together with nearby domains that are greatly enriched in chalcopyrite that crystallized from the sulfide melt residual to early mss crystallization. Similar poikilitic pyrrhotite is also commonly observed in net-textured sulfides at the Eagle's Nest deposit (Mungall et al., 2010) in northwestern Ontario.

It is widely believed that the formation of Cu-rich veins and patches is enhanced by a higher tendency of Cu-rich sulfide liquids to wet silicates. Ebel and Naldrett (1996) reported experimental evidence suggesting that wetting of glass tubes by sulfide liquid in the presence of a vapour phase was more extensive in more Cu-rich liquids, although the surface tension measurements of Mungall and Su (2005) did not find this effect. Textural evidence from globular ores at Noril'sk tends to argue against it; differentiated sulfide globules such as those shown in Figure 12 show no tendency for the Cu-rich residual component to leak preferentially into the intercumulus pore space. It is important to bear in mind that the wetting angle between sulfide melt, silica glass, and vapour should not be expected to bear any resemblance to the wetting angle in the completely different physical environment of silicate melt, sulfide melt, and solids that obtains in ore deposits. However, there may be an indirect surface-wetting effect. Residual copper-rich liquids tend to form at lower temperatures where the associated silicate melt is more likely to have crystallized; hence there may be a tendency for Cu-rich liquids to migrate preferentially under certain circumstances owing to the absence of the competitive wetting effect discussed above.

At conditions below the solidus of an enclosing silicate assemblage, sulfide may remain partially molten. Under these circumstances, MSS may remain stranded in formerly isolated blebs while residual sulfide liquid rich in Cu and PGE may be free to migrate along microfractures (Mungall, 2002; Mungall and Su, 2005; Mungall, 2007b). At Sudbury there are domains of disseminated sulfide mineralization hosted by norite extending tens to hundreds of meters above the net-textured to massive contact ores. These disseminated haloes have compositions clearly representative of MSS rather than of the sulfide melt that was originally trapped in the intercumulus space. Whereas Mungall (2002) argued that the missing fractionated sulfide liquid might have risen to form a halo above the disseminated mineralization, this idea was modified by Mungall (2007b) to suggest that the missing fractionated sulfide melt descended along microfractures after solidification of the norite.

According to this interpretation, this mobile sulfide joined the residual sulfide melt streaming off the contact ores below, eventually moving into the footwall of the Sudbury Igneous Complex to form the Ni-, Cu-, and PGE-rich sharp-walled vein systems.

5.3 Bleb sizes and implications for transport and deposition mechanisms

Clues to the transport and deposition mechanisms of sulfide liquids in magma can be obtained from the study of sulfide bleb sizes, which can only be measured meaningfully from 3D images. Published data on disseminated sulfides from komatiites and mafic intrusions (Godel et al., 2013; Robertson et al., 2016) are combined with new data from Sudbury and Kevitsa (this study) in a series of particle size distribution plots (PSDs) (Fig. 24). These plots take the same form as crystal size distribution (CSD) plots widely used in petrology and materials science (Marsh, 1998), being frequency distributions of the number of particles within a size range (size being defined as the diameter of a sphere of the same volume as the particle) per cubic cm of sample volume, normalized to the width of the size bin on the x axis. Populations of growing crystals from a cooling magma generate linear tends of negative slope on such plots, which can then be modified by processes such as textural maturation, mechanical sorting and accumulation of phenocrysts (Marsh, 1998).

Almost all measured bleb size distributions show broadly linear and variably convex-up patterns on PSD plots, and most show similar slopes at the fine-grained end of the distribution. Godel et al. (2013) suggested that the concave-up distributions in sulfide blebs in komatiitic dunites were the result of a mixture of two linear components: a mechanically sedimented population of transported droplets, and a finer (and steeper) population of cotectic sulfide droplets that had nucleated and grown in situ. Robertson et al. (2016) pointed out that linear negative slopes on PSD plots could also be generated by dynamic breakup of transported liquid droplets. They showed that this process is likely to be dominant over coalescence during flow of magmatic emulsions, consistent with previous experimental and theoretical work (de Bremond d'Ars et al., 2001). They interpreted sulfide bleb and droplet PSDs as the result of multiple superimposed processes which are active on different portions of the droplet size distribution: growth of sulfide droplets from sulfide-saturated silicate magma, and mechanical accumulations of transported assimilated droplets that have undergone break-up by a variety of mechanisms during transport.

The observations presented here suggest that coalescence is also an important factor in generating the strongly convex-up PSD observed at Kevitsa. In the Kevitsa case, this coalescence is post-accumulation, and takes place during self-organized percolation of sulfide liquid networks through the crystal pile. The geometry of some of the larger more irregular blebs at Copper Cliff and Kharelakh is also strongly suggestive of post-deposition coalescence of larger droplets. However, the predominance of broadly linear negative slopes on PSDs for all globular ores strongly suggests a control by dynamic droplet breakup during flow, with a relatively minor degree of mechanical sorting during deposition. This implies that sulfide droplet accumulation to form orebodies occurs by a type of "avalanche" process, whereby a sulfide liquid rich slurry accumulates in a cascade of strongly interacting particles, rather than by simple Stokes-Law settling of non-interacting individual particles (Robertson et al., 2014). The presence of large uncapped sulfide globules of the Copper Cliff type described above, in excess of 1 cm, is a strong indicator of proximity either to a massive sulfide accumulation, or to a site of assimilation of sulfide-rich country rock. Where such globules are Cu and/or Ni enriched, requiring enough time for effective equilibration with the host magma, they are an indicator of proximity to sulfide-rich ore.

6 Conclusions

The diversity of the major textural types of disseminated and net-textured sulfides arises from the interplay of a relatively small number of factors: the modal abundance of sulfide; the modal abundance of co-existing silicate melt; the relative liquidus and solidus temperatures of the co-existing melts; the presence or absence of a co-existing vapour phase; the proportion of silicate melt to solid cumulus (or phenocryst) silicates and oxides; and the cooling history. These relationships are summarized in the classification scheme in Table 2.

Disseminated sulfides fall into two major categories:

1. Interstitial blebs, which may be more or less concave and globule-like depending on the abundance of silicate melt in the local micro-environment.
2. Globules. These in turn can be subdivided into (a) typically rounded and sub-spherical globules associated with amygdales and/or segregation vesicles; and (b) equant but non-spherical, locally facetted globules without any associated amygdales or vesicles. The latter (b) type, as at Sudbury, are associated with silicate magmas with relatively low solidus temperatures. The morphology of these blebs may be the result of disruption and re-deposition of partially solidified pre-existing sulfide concentrations. The former (a) type may form either as a result of flotation of sulfide droplets on vapour bubbles in high-level emplacement settings, or by nucleation of bubbles on

sulfide droplets due to post-cumulus vapour saturation of intercumulus silicate liquid. Vapour saturation of the solidifying sulfide melt itself may also be a factor.

A continuum exists between relatively sulfide-rich disseminated ores and net-textured ores, but the intermediate ore types are typically patchy net-textured ores consisting of domains of sulfide-rich net-texture with low wetting angles, separated by sulfide-poor domains where silicate melt occupies the pore space. This texture is driven by self-organized sulfide percolation, itself triggered by the process of competitive wetting whereby the silicate melt preferentially wets silicate crystal surfaces. The process is self-reinforcing as sulfide migration causes sulfide networks to become larger, with a larger rise height and hence a greater gravitational driving force for percolation and silicate melt displacement.

The sulfide percolation process is coupled with upward displacement of silicate melt, and in ideal circumstances gives rise to fully net-textured ores. Interspinifex ores are a special case, providing convincing evidence of this migration-displacement process. The poikilitic "leopard-textured" ores at Voisey's Bay (Fig. 19) are likely to be another manifestation of this process, where the cumulus framework is made up of plagioclase and olivine rather than olivine alone. The presence of globular sulfides within patchy net-textured ores is attributed to a two stage process: formation of low-sulfide globular disseminated ore, followed by infiltration by downward percolating sulfide from above. Poikilitic ores probably reflect a similar two-stage process: deposition of a poikilitic orthocumulate, followed by displacement of silicate melt by percolating sulfide. The leopard-textured troctolite-hosted ores at Voisey's Bay are from a process point of view simply another variety of net-textured ore, but with plagioclase as the predominant cumulus phase. They could be seen as the plagioclase-bearing equivalent of interspinifex ore.

Where sulfide abundances are too low, less than about 3 modal percent, sulfide blebs remain unconnected, and gravitational forces are too small to drive percolation. Sulfides then become trapped in pore space to form disseminated ores. This accounts for the broadly bimodal distribution of sulfide abundances between disseminated and net-textured ores as seen at Voisey's Bay.

Strain-rate dependent thixotropic behaviour of sulfide bearing-crystal mushes gives rise to localized opening of fractures during sudden shock events such as earthquakes. This results in the formation of sulfide veins and veinlets at a variety of scales within net-textured and disseminated ore profiles, as percolating sulfide liquid flows into transient high-permeability pathways.

The Naldrett (1973) “billiard ball model” for net-textured ores may have operated under some circumstances, but is likely to be coupled with the various other processes outlined here. The initial step may be transport and co-deposition of a slurry of silicate and sulfide melt with olivine or pyroxene crystals, followed by gravitationally-driven percolation and textural re-organization.

7 Implications

The panoply of sulfide textures described here provides important genetic clues to the origin of some of the world’s most valuable ore deposits. Furthermore, from an exploration point of view, the textures and size distributions of disseminated sulfide populations may be incorporated with standard geochemical data sets to infer vectors towards sulfide-rich Ni-Cu-PGE ores and potential for high-grade ore in the system. The presence of large uncapped sulfide globules, in excess of 1 cm, is a strong indicator that the transporting magma was capable of generating a massive sulfide accumulation. This is particularly true for the large, irregular Ni- and Cu-enriched globules of the type observed at Sudbury. Restriction of sulfide populations to low modal abundance and steep log-normal particle size distributions is indicative of a dominant origin by in-situ nucleation of newly-formed sulfide droplets growing from the host magma (Godel et al., 2013; Robertson et al., 2016), which represents a more distal environment to sulfide-rich ore deposition, and may not be associated with sulfide-rich ores at all. A transition from the latter case to ores with coarse blebs of any form can be taken as a potential vector towards high-grade sulfide-rich mineralization. Systematic and consistent mapping out of textural types within individual orebodies has potential to be just as important and instructive as standard geochemical and petrographic investigations,. Complementary textural and geochemical investigations are necessary for the full understanding of magmatic sulfide ore deposits.

8 Acknowledgements

We are grateful to many industry collaborators for providing access to the deposits covered in this review. In particular we thank Vale Brownfields Exploration for access to samples from Voisey’s Bay and Sudbury; and Norilsk Nickel and the organisers of the 13th International Platinum Conference in Russia for samples from the Noril’sk-Talnakh orebodies etc. The synchrotron X-ray fluorescence maps were collected on the X-ray fluorescence microscopy beam line at the Australian Synchrotron, Clayton, Victoria, Australia, and we acknowledge the assistance of Daryl Howard, David Paterson, Martin De Jonge and Kathryn Spiers. We acknowledge financial support for this facility from the Science and Industry Endowment Fund (SIEF). Michael Verrall provided essential support for the Tornado microbeam XRF mapping and the high-resolution X-ray microtomography. We thank the National Geosequestration Lab and Lionel Esteban for access to the medical CT scanner, and iVEC and Andrew Squelch for access to and assistance with computer hardware and processing software. Danielle Giovennazzo and Chusi Li provided helpful reviews.

9 References

Anderson, A.T., Swihart, G.H., Artoli, G., and Geiger, C.A. (1984) Segregation vesicles, gas filter-pressing, and igneous differentiation. Journal of Geology, 92, 55-72.

Arndt, N.T. (2011) Insights into the Geologic Setting and Origin of Ni-Cu-PGE Sulfide Deposits of the Norilsk-Talnakh Region, Siberia. Reviews in Economic Geology, 17, 199-215.

Arndt, N.T., Lesher, C.M., and Barnes, S.J. (2008) Komatiite. 467 p. Cambridge University Press, Cambridge.

Ballhaus, C., and Ellis, D.J. (1996) Mobility of core melts during Earth's accretion. Earth and Planetary Science Letters, 143(1-4), 137-145.

Barnes, Sarah-J., and Naldrett, A.J. (1986) Variations in platinum group element concentrations in the Alexo mine komatiite, Abitibi greenstone belt, northern Ontario. Geological Magazine, 123, 515-524.

Barnes, Sarah-J., Cox, R.A., and Zientek, M.L. (2006) Platinum-Group Element, Gold, Silver and Base Metal Distribution in Compositionally Zoned Sulfide Droplets From the Medvezky Creek Mine, Noril'sk, Russia. Contributions to Mineralogy and Petrology, 152(2), 187-200.

Barnes, S.J. (2006) Komatiite-hosted nickel sulfide deposits: geology, geochemistry, and genesis. Society of Economic Geologists Special Publication, 13, 51-118.

Barnes, S.J., Anderson, J.A.C., Smith, T.R., and Bagas, L. (2008a) The Mordor Alkaline Igneous Complex, Central Australia: PGE-enriched disseminated sulfide layers in cumulates from a lamprophyric magma. Mineralium Deposita, 43, 641-662.

Barnes, S.J., Beresford, S.W., and Le Vaillant, M. (2016b) Interspinifex Ni sulfide ore from the Coronet Shoot, Kambalda: characterization using microbeam XRF mapping and 3D X-ray computed tomography. Economic Geology, in review.

Barnes, S.J., Coats, C.J.A., and Naldrett, A.J. (1982) Petrogenesis of a Proterozoic nickel sulphide - komatiite association: the Katiniq Sill, Ungava, Quebec. Economic Geology, 77, 413-429.

Barnes, S.J., Cruden, A.R., Arndt, N.T., and Saumur, B.M. (2016a) The mineral system approach applied to magmatic Ni-Cu-PGE sulphide deposits. Ore Geology Reviews, online.

Barnes, S.J., Fiorentini, M.L., Austin, P., Gessner, K., Hough, R., and Squelch, A. (2008b) Three-dimensional morphology of magmatic sulfides sheds light on ore formation and sulfide melt migration. Geology, 36, 655-658.

Barnes, S.J., Fiorentini, M.L., Duuring, P., Grguric, B.A., and Perring, C.S. (2011a) The Perseverance and Mount Keith Ni deposits of the Agnew-Wiluna Belt, Yilgarn Craton, Western Australia. Reviews in Economic Geology, 17, 51-88.

Barnes, S.J., Godel, B.M., Locmelis, M., Fiorentini, M.L., and Ryan, C.G. (2011b) Extremely Ni-rich Fe-Ni sulfide assemblages in komatiitic dunite at Betheno, Western Australia: results from synchrotron X-ray fluorescence mapping. Australian Journal of Earth Sciences, 58, 691-709.

Barnes, S.J., Gole, M.J., and Hill, R.E.T. (1988) The Agnew Nickel Deposit, Western Australia: part II. Sulfide geochemistry, with emphasis on the platinum-group elements. Economic Geology, 83, 537-550.

Barnes, S.J., Hill, R.E.T., and Evans, N.J. (2004) Komatiites and Nickel Sulfide Ores of the Black Swan area, Yilgarn Craton, Western Australia. 3. Komatiite geochemistry, and implications for ore forming processes. Mineralium Deposita, 39, 729-751.

Barnes, S.J., Mole, D.R., Le Vaillant, M., Campbell, M., Verrall, M., Roberts, M., and Evans, N.J. (2016b) Poikilitic textures, heteradcumulates and zoned orthopyroxenes in the Ntaka Ultramafic Complex, Tanzania: implications for crystallization mechanisms of oikocrysts. Journal of Petrology, in revision.

Barnes, S.J., Osborne, G.A., Cook, D., Barnes, L., Maier, W.D., and Godel, B.M. (2011c) The Santa Rita Nickel Sulfide Deposit in the Fazenda Mirabela Intrusion, Bahia, Brazil: geology, sulfide geochemistry and genesis. Economic Geology, 106, 1083-1110.

Barnes, S.J., Wells, M.A., and Verrall, M.R. (2009) Effects of magmatic processes, serpentinization and talc carbonate alteration on sulfide mineralogy and ore textures in the Black Swan disseminated nickel sulfide deposit, Yilgarn Craton. Economic Geology, 104 (4), 539-562.

Beresford, S., Stone, W.E., Cas, R., Lahaye, Y., and Jane, M. (2005) Volcanological Controls on the Localization of the Komatiite-Hosted Ni-Cu-(Pge) Coronet Deposit, Kambalda, Western Australia. Economic Geology, 100(7), 1457-1467.

Beresford, S.W., Cas, R.A.F., Lambert, D.D., and Stone, W.E. (2000) Vesicles in thick komatiite lava flows, Kambalda, Western Australia. Journal of the Geological Society, 157, 11- 14.

Brenan, J.M. (2003) Effects of fO2, fS2, temperature, and melt composition on Fe-Ni exchange between olivine and sulfide liquid: Implications for natural olivine–sulfide assemblages. Geochimica et Cosmochimica Acta, 67, 2663-2681.

Brenan, J.M., and Rose, L.A. (2002) Experimental constraints on the wetting of chromite by sulfide liquid. Canadian Mineralogist, 40, 1113-1126.

Campbell, I.H. (1978) Some problems with the cumulus theory. Lithos, 11, 311-323.

Campbell, I.H. (2007) Testing the plume theory. Chemical Geology, 241, 153-176.

Caroff, M., Maury, R.C., Cotten, J., and Clement, J.P. (2000) Segregation structures in vapor-differentiated basaltic flows. Bulletin of Volcanology, 62, 171- 187.

Chung, H.-Y., and Mungall, J.E. (2009) Physical constraints on the migration of immiscible fluids through partially molten silicates, with special reference to magmatic sulfide ores. Earth and Planetary Science Letters, 286(1-2), 14-22.

Craig, J.R., and Kullerud, G. (1969) Phase relations in the Cu-Fe-Ni-S system and their application to magmatic ore deposits. Economic Geology Monograph, 4, 344-358.

Czamanske, G.K., Kunilov, V.E., Zientek, M.L., Cabri, L.J., Likhachev, A.P., Calk, L.C., and Oscarson, R.L. (1992) A proton-microprobe study of magmatic sulfide ores from the Noril'sk-Talnakh district, Siberia. Canadian Mineralogist, 30, 249-287.

Czamanske, G.K., Zen'ko, K.E., Fedorenko, V., Calk, L.C., Budahn, J.R., Bullock, J.H.J., Fries, T.L., King, B.S., and Siems, D.F. (1995) Petrographic and geochemical characterization of ore-bearing intrusions of the Noril'sk Type, Siberia; with discussion of their origin. Resource Geology Special Issue, 18, 1-48.

de Bremond d'Ars, J., Arndt, N.T., and Hallot, E. (2001) Analog experimental insights into the formation of magmatic sulfide deposits. Earth and Planetary Science Letters, 186, 371-381.

Distler, V.V., Grokhovskaya, T.L., Evstigneeva, T.L., Sluzheninkin S.F., Filimonova A.A., Dyuzhikov O.A., and I.P, L. (1988) Petrology of Magmatic Sulfide Ore Mineralization. Nauka, Moscow.

Distler, V.V., Sluzhenikin, S.F., Cabri, L.J., Krivolutskaya, N.A., Turovtsev, D.M., Golovanova, T.A., Mokhov, A.V., Knauf, V.V., and Oleshkevich, O.I. (1999) Platinum ores of the Noril'sk layered intrusions: Magmatic and fluid concentration of noble metals. Geology of Ore Deposits, 41, 214- 237.

Dodin, D.A., Batuev, B.N., Mitenkov, G.A., and Izoitko, V.M. . (1971) Atlas of Rocks and Ores of the Noril’sk Copper–Nickel Deposits. Nedra, Leningrad.

Dowling, S.E., Barnes, S.J., Hill, R.E.T., and Hicks, J. (2004) Komatiites and Nickel Sulfide Ores of the Black Swan area, Yilgarn Craton, Western Australia. 2. Geology and Genesis of the Orebodies. Mineralium Deposita, 39, 707-728.

Ebel, D.S., and Naldrett, A.J. (1996) Fractional crystallization of sulfide ore liquids at high temperature. Economic Geology, 91(3), 607-621.

Evans-Lamswood, D.M., Butt, D.P., Jackson, R.S., Lee, D.V., Muggridge, M.G., Wheeler, R.I., and Wilton, D.H.C. (2000) Physical controls associated with the distribution of sulfides in the Voisey's Bay Ni-Cu-Co deposit, Labrador. Economic geology and the Bulletin Of the Society Of Economic Geologists, 95(4), 749.

Ewers, W.E., and Hudson, D.R. (1972) An interpretive study of a nickel-iron sulfide ore intersection, Lunnon Shoot, Kambalda. Economic Geology, 67, 1075-1092.

Fedorenko, V.A. (1994) Evolution of magmatism as reflected in the volcanic sequence of the Noril'sk region. In P.C. Lightfoot, and A.J. Naldrett, Eds. Proceedings of the Sudbury-Noril'sk Symposium, Ontario Geological Survey Special Publication 5, 5, p. 171-184. Ontario Geological Survey, Toronto.

Fisher, L.A., Fougerouse, D., Halfpenny, A., Ryan, C.G., Micklethwaite, S., Hough, R.M., Cleverley, J.S., Gee, M., Paterson, D., and Howard, D. (2015) Fully quantified, multi-scale element mapping of mineral system samples using the Maia detector array: recognizing chemical variation on micron to cm scales. Mineralium Deposita, 50, 665-674.

Fleet, M.E. (1977) Origin of disseminated copper-nickel sulfide ore at Frood, Sudbury, Ontario. Economic Geology and the Bulletin of the Society of Economic Geologists, 72(8), 1449-1456.

Frost, K.M., and Groves, D.I. (1989) Ocellar units at Kambalda: evidence for sediment assimilation by komatiite lavas. In M.D. Prendergast, and M.J. Jones, Eds. Magmatic sulphides - the Zimbabwe Volume, p. 207-214. Institute of Mining and Metallurgy, London.

Gaetani, G.A., and Grove, T.L. (1999) Wetting of mantle olivine by sulfide melt: implications for Re/Os ratios in mantle peridotite and late-stage core formation. Earth and Planetary Science Letters, 169, 147- 163.

Genkin, A.D., Distler, V.V., Gladyshev, G.D., Filimonova, A.A., Evstigneeva, T.L., Kovalenker, V.A., Laputina, I.P., Smirnov, A.V., and Grokhovskaya, T.L. (1982) Copper-nickel sulphide ores from the Noril'sk deposits. 446 p.

Godel, B. (2013) High-Resolution X-Ray Computed Tomography and Its Application to Ore Deposits: From Data Acquisition to Quantitative Three-Dimensional Measurements with Case Studies from Ni-Cu-PGE Deposits Economic Geology, 108, 2005-2019

-. (2015) Chapter 9: Platinum-Group Element Deposits in Layered Intrusions: Recent Advances in the Understanding of the Ore Forming Processes. Layered Intrusions, p. 379-432. Springer Geology, Netherlands.

Godel, B., Barnes, Sarah-J., and Maier, W.D. (2006) 3-D distribution of sulphide minerals in the Merensky Reef (Bushveld Complex, South Africa) and the J-M Reef (Stillwater Complex, USA) and their relationship to microstructures using X-ray computed tomography. Journal of Petrology, 47, 1853-1872.

Godel, B., Barnes, S.J., and Barnes, Sarah-J. (2013) Deposition mechanisms of magmatic sulphide liquids: evidence from high-resolution X-ray computed tomography and trace element chemistry of komatiite-hosted disseminated sulphides. Journal of Petrology, 54, 1455-1481.

Godel, B., Rudashevsky, N.S., Nielsen, T.F.D., Barnes, S.J., and Rudashevsky, V.N. (2014) New constraints on the origin of the Skaergaard Intrusion Cu-Pd-Au mineralization: Insights from high-resolution X-ray computed tomography. Lithos, 190-191, 27-36.

Godel, B.M., Barnes, S.J., Barnes, Sarah-J., and Maier, W.D. (2010) Platinum ore in 3D: Insights from high-resolution X-ray computed tomography. Geology, 38, 1127-1130.

Green, A.H., and Naldrett, A.J. (1981) The Langmuir volcanic peridotite-associated nickel sulphide deposits: Canadian equivalents of the Western Australian occurrences. Economic Geology, 76, 1503-1523.

Groves, D.I., Barrett, F.M., and McQueen, K.G. (1979) The relative roles of magmatic segregation, volcanic exhalation and regional metamorphism in the generation of volcanic-associated nickel ores of Western Australia. Canadian Mineralogist, 17, 319-336.

Groves, D.I., Korkiakoski, E.A., McNaughton, N.J., Lesher, C.M., and Cowden, A. (1986) Thermal erosion by komatiites at Kambalda, Western Australia and the genesis of nickel ores. Nature, 319, 136-139.

Hanski, E., Huhma, H., Rastas, P., and Kamenetsky, V.S. (2001) The Palaeoproterozoic komatiite-picrite association of Finnish lapland. Journal of Petrology, 42, 855- 876.

Hanski, E.J. (1992) Petrology of the Pechenga ferropicrites and cogenetic Ni-bearing gabbro-wehrlite intrusions, Kola Peninsula, Russia. Geological Survey of Finland. Bulletin, 367.

Heggie, G.J., Fiorentini, M.L., Barnes, S.J., and Barley, M.E. (2012) Maggie Hays nickel deposit: Part 2. Nickel mineralization and the spatial distribution of PGE ore forming signatures in the Maggie Hays Ni system, Lake Johnston greenstone belt, Yilgarn Craton, Western Australia. Economic Geology, 107, 817-833.

Hill, R.E.T., Barnes, S.J., Gole, M.J., and Dowling, S.E. (1995) The volcanology of komatiites as deduced from field relationships in the Norseman-Wiluna greenstone belt, Western Australia. Lithos, 34, 159-188.

Holness, M.B., Namur, O., and Cawthorn, R.G. (2013) Disequilibrium Dihedral Angles in Layered Intrusions: a Microstructural Record of Fractionation. Journal of Petrology, 54(10), 2067-2093.

Holwell, D.A., Abraham-James, T., Keays, R.R., and Boyce, A.J. (2012) The nature and genesis of marginal Cu-PGE-Au sulphide mineralization in Paleogene Macrodykes of the Kangerlussuaq region, East Greenland. Mineralium Deposita, 47(1-2), 3-21.

Holwell, D.A., and McDonald, I. (2006) Petrology, geochemistry and the mechanisms determining the distribution of platinum group element and base metal sulfide mineralization in the Platreef at Overysel, northern Bushveld Complex, South Africa. Mineralium Deposita, 41(6), 575-598.

Houle, M.G., and Lesher, C.M. (2011) Komatiite-Associated Ni-Cu-(PGE) Deposits, Abitibi Greenstone Belt, Superior Province, Canada. Reviews in Economic Geology, 17, 89-121.

Houle, M.G., Lesher, C.M., and Davis, P.C. (2012) Thermomechanical erosion at the Alexo Mine, Abitibi greenstone belt, Ontario: implications for the genesis of komatiite-associated Ni-Cu-(PGE) mineralization. Mineralium Deposita, 47(1-2), 105-128.

Hughes, H.S.R., McDonald, I., Holwell, D.A., Boyce, A.J., and Kerr, A.C. (2016) Sulphide sinking in magma conduits: evidence from mafic-ultramafic plugs on Rum and the wider North Atlantic Igneous Province. Journal of Petrology, in press.

Jerram, D.A., Cheadle, M.J., and Philpotts, A.R. (2003) Quantifying the building blocks of igneous rocks; are clustered crystal frameworks the foundation? Journal of Petrology, 44, 2033-2051.

Jung, H., and Waff, H.S. (1998) Olivine Crystallographic Control and Anisotropic Melt Distribution In Ultramafic Partial Melts. Geophysical Research Letters, 25, 2901-2904.

Keays, R.R. (1995) The role of komatiitic and picritic magmatism and S-saturation in the formation of ore deposits. Lithos, 34, 1-18.

Keays, R.R., and Lightfoot, P.C. (2004) Formation of Ni-Cu-platinum group element sulfide mineralization in the Sudbury impact melt sheet. Mineralogy and Petrology, 82, 217-258.

Keays, R.R., Ross, J.R., and Woolrich, P. (1981) Precious metals in volcanic peridotite-associated nickel sulfide deposits in Western Australia, II. Distribution within ores and host rocks at Kambalda. Economic Geology, 76, 1645-1674.

Keele, R.A., and Nickel, E.H. (1974) The geology of a primary millerite-bearing sulfide assemblage and supergene alteration at the Otter Shoot, Kambalda, Western Australia. Economic Geology, 69, 1102-1117.

Le Vaillant, M., Barnes, S.J., Fiorentini, M.L., Santaguida, F., and Törmäla, T. (2016) Effects of hydrous alteration on the distribution of base metals and platinum group elements within the Kevitsa magmatic nickel sulphide deposit. Ore Geology Reviews, 72, 128-148.

Lehmann, J., Arndt, N., Windley, B., Zhou, M.F., Wang, C.Y., and Harris, C. (2007) Field Relationships and Geochemical Constraints on the Emplacement of the Jinchuan Intrusion and Its Ni-Cu-Pge Sulfide Deposit, Gansu, China. Economic Geology, 102(1), 75-94.

Lesher, C.M. (1989) Komatiite-associated nickel sulfide deposits. In J.A. Whitney, and A.J. Naldrett, Eds. Ore Deposition Associated with Magmas, 4, p. 44-101. Economic Geology Publishing Company, El Paso.

Lesher, C.M. (2007) Ni-Cu-(PGE) deposits in the Raglan area, Cape Smith Belt, New Québec. In W.D. Goodfellow, Ed. Mineral Deposits of Canada: A Synthesis of Major Deposit-Types, District Metallogeny, the Evolution of Geological Provinces, and Exploration Methods Special Publication 5, p. 351-386. Geological Associaton of Canada, Mineral Deposits Division, St. John's (NL).

Lesher, C.M., Golightly, J., Huminicki, M.A.E., and Gregory, S. (2008) Magmatic-hydrothermal fractionation of Fe-Ni-Cu-PGE mineralization in the Sudbury Igneous Complex (abstract). Geochimica et Cosmochemica Acta, 72, A536.

Lesher, C.M., and Keays, R.R. (2002) Komatiite-associated Ni-Cu-PGE deposits: geology, mineralogy, geochemistry and genesis. In L.J. Cabri, Ed. The Geology, Geochemistry Mineralogy and Mineral Beneficiation of Platinum Group Elements., p. 579-617. Canadian Institute of Mining Metallurgy and Petroleum Special Volume 54.

Lightfoot, P.C., and Evans-Lamswood, D.M. (2015) Structural controls on the primary distribution of mafic–ultramafic intrusions containing Ni–Cu–Co–(PGE) sulfide mineralization in the roots of large igneous provinces. Ore Geology Reviews, 64, 354-386.

Lightfoot, P.C., and Farrow, C.E.G. (2002) Geology, geochemistry, and mineralogy of the Worthington offset dike: A genetic model for offset dike mineralization in the Sudbury Igneous Complex. Economic Geology and the Bulletin of the Society of Economic Geologists, 97, 1419- 1446.

Lightfoot, P.C., Keays, R.R., Evans-Lamswood, D., and Wheeler, R. (2012) S saturation history of Nain plutonic suite mafic intrusions; origin of the Voisey's Bay Ni-Cu-Co sulfide deposit, Labrador, Canada. Mineralium Deposita, 47(1-2), 23-50.

Lightfoot, P.C., Keays, R.R., Morrison, G.G., Bite, A., and Farrell, K.P. (1997a) Geochemical relationships in the Sudbury Igneous Complex - origin of the Main Mass and Offset Dykes. Economic Geology, 92(3), 289-307.

Lightfoot, P.C., Keays, R.R., Morrison, G.G., Bite, A., and Farrell, K.P. (1997b) Geologic and geochemical relationships between the contact sublayer, inclusions, and the main mass of the Sudbury Igneous Complex; a case study of the Whistle Mine Embayment. Economic Geology and the Bulletin of the Society of Economic Geologists, 92(6), 647-673.

Lightfoot, P.C., Naldrett, A.J., and Hawkesworth, C.J. (1984) The geology and geochemistry of the Waterfall Gorge section of the Insizwa Complex with particular reference to the origin of the nickel sulphide deposits. Economic Geology, 79, 1857-1879.

Lightfoot, P.C., and Zotov, I.A. (2005) Geology and Geochemistry of the Sudbury Igneous Complex, Ontario, Canada: Origin of Nickel Sulfide Mineralization Associated With an Impact-Generated Melt Sheet. Geology of Ore Deposits, 47(5), 349-381.

Lightfoot, P.C., and Zotov, I.A. (2014) Geological relationships between the intrusions, country rocks and Ni-Cu-PGE sulfides of the Kharealakh Intrusion, Noril'sk region: Implications for the role of sulfide differentiation and metasomatism in their genesis. Northwestern Geology, 47, 1-35.

Liu, Y.X., Mungall, J.E., and Ames, D. (2016) Hydrothermal Redistribution and Local Enrichment of Platinum Group Elements in the Tootoo and Mequillon Magmatic Sulfide Deposits, South Raglan Trend, Cape Smith Belt, New Quebec Orogen Economic Geology, 111, 467-485.

Mare, E.R., Tomkins, A.G., and Godel, B. (2014) Restriction of parent body heating by metal-troilite melting: Thermal models for the ordinary chondrites. Meteoritics & Planetary Science, 49, 636-651.

Marsh, B.D. (1998) On the Interpretation Of Crystal Size Distributions In Magmatic Systems. Journal Of Petrology, 39, 553- 599.

Marston, R.J. (1984) Nickel mineralization in Western Australia. Geological Survey of Western Australia Mineral Resources Bulletin, 14, 271.

Mudd, G.M., and Jowitt, S.M. (2014) A Detailed Assessment of Global Nickel Resource Trends and Endowments. Economic Geology, 109, 1813-1841.

Mungall, J.E. (2002) Late-stage sulfide liquid mobility in the main mass of the Sudbury Igneous Complex: Examples from the Victor Deep, McCreedy East, and Trillabelle deposits. Economic Geology and the Bulletin of the Society of Economic Geologists, 97, 1563- 1576.

-. (2007a) Crustal Contamination of Picritic Magmas During Transport Through Dikes: the Expo Intrusive Suite, Cape Smith Fold Belt, New Quebec. Journal of Petrology, 48(5), 1021-1039.

Mungall, J.E. (2007b) Crystallization of magmatic sulfides; an empirical model and application to Sudbury ores. Geochimica et Cosmochimica Acta, 71(11), 2809.

Mungall, J.E., and Brenan, J.M. (2014) Partitioning of platinum-group elements and Au between sulfide liquid and basalt and the origins of mantle-crust fractionation of the chalcophile elements. Geochimica et Cosmichimica Acta, 125, 265-289.

Mungall, J.E., Brenan, J.M., Godel, B., Barnes, S.J., and Gailard, F. (2015) Transport of S, Cu and Au in magmas by flotation of sulphide melt on vapour bubbles. Nature Geoscience, 8, 216-219.

Mungall, J.E., Harvey, J.D., Balch, S.J., Azar, B., Atkinson, J., and Hamilton, M.A. (2010) Eagle's Nest: a magmatic Ni-sulfide deposit in the James Bay Lowlands, Ontario, Canada. Society of Economic Geologists Special Publication 15, 539-557.

Mungall, J.E., and Naldrett, A.J. (2008) Ore deposits of the platinum-group elements. Elements, 4(4), 253-258.

Mungall, J.E., and Su, S. (2005) Interfacial tension between magmatic sulfide and silicate liquids: constraints on the kinetics of sulfide liquation and sulfide migration through silicate rocks. Earth and Planetary Science Letters, 234, 135-149.

Naldrett, A. (2011) Fundamentals of Magmatic Sulfide Deposits. Reviews in Economic Geology, 17, 1-50.

Naldrett, A.J. (1969) A portion of the system Fe-S-O and its application to sulfide ore magmas. Journal of Petrology, 10, 171-202.

-. (1973) Nickel sulphide deposits: their classification and genesis, with special emphasis on deposits of volcanic association. Canadian Institute of Mining and Metallurgy Bulletin, 66, 45-63.

-. (1999) World-class Ni-Cu-PGE deposits: key factors in their genesis. Mineralium Deposita, 34, 227- 240.

Naldrett, A.J. (2004) Magmatic Sulfide Deposits: Geology, Geochemistry and Exploration. 727 p. Springer, Heidelberg.

Naldrett, A.J., Asif, M., Krstic, S., and Li, C.S. (2000) The composition of mineralization at the Voisey's Bay Ni-Cu sulfide deposit, with special reference to platinum-group elements. Economic Geology and the Bulletin of the Society of Economic Geologists, 95, 845- 865.

Naldrett, A.J., Ebel, D.S., Asif, M., Morrison, G., and Moore, C.M. (1997) Fractional crystallization of sulfide melts as ilustrated at Noril'sk and Sudbury. European Journal of Mineralogy, 9(2), 365-377.

Naldrett, A.J., Fedorenko, V.A., Asif, M., Lin, S., Kunilov, V.E., Stekhin, A.I., Lightfoot, P.C., and Gorbachev, N.S. (1996) Controls on the composition of Ni-Cu sulfide deposits as illustrated by those at Noril'sk, Siberia. Economic Geology and the Bulletin of the Society of Economic Geologists, 91(4), 751-773.

Naldrett, A.J., and Lightfoot, P.C. (1999) Ni-Cu-PGE deposits of the Noril'sk region, Siberia: their formation in conduits for flood basalt volcanism. In R.R. R.R. Keays, C.M. C.M. Lesher, P.C. P.C. Lightfoot, and C.E.G. Farrow, Eds, p. 195-249. Geological Association of Canada Short Course 13, Sudbury.

Paterson, D., de Jonge, M.D., Howard, D.L., Lewis, W., McKinlay, J., Starritt, A., Kusel, M., Ryan, C.G., Kirkham, R., Moorhead, G., and Siddons, D.P. (2011) The X-ray Fluorescence Microscopy Beamline at the Australian Synchrotron. Proceedings of the Australian Institute of Physics, 1365, 219-222.

Peck, D.C., and Huminicki, M.A.E. (2016) Value of mineral deposits associated with mafic and ultramafic magmatism: Implications for exploration strategies. Ore Geology Reviews, 72, 269-298.

Prichard, H.M., Barnes, S.J., Godel, B., Reddy, S.M., Vukamanovic, Z., Halfpenny, A., Neary, C., and Fisher, P.C. (2015) The structure of and origin of nodular chromite from the Troodos ophiolite, Cyprus, revealed using high-resolution X-ray computed tomography and Electron Backscatter Diffraction. Lithos, 218-219, 87-98.

Prichard, H.M., Hutchinson, D., and Fisher, P.C. (2004) Petrology and Crystallization History of Multiphase Sulfide Droplets in a Mafic Dike From Uruguay: Implications for the Origin of Cu-Ni-Pge Sulfide Deposits. Economic Geology and the Bulletin of the Society of Economic Geologists, 99(2), 365-376.

Robertson, J.C., Barnes, S.J., and Le Vaillant, M. (2016) Dynamics of magmatic sulphide droplets during transport in silicate melts and implications for magmatic sulphide ore formation. Journal of Petrology, 56, 2445-2472.

Robertson, J.C., Barnes, S.J., and Metcalfe, G. (2014) Chaotic entrainment can drive sulfide remobilization at low magma flow rates. 13th International Platinum Symposium, p. 47-48. Russian Academy of Sciences, Ural Branch, Yekaterinburg, Russia.

Rose, L.A., and Brenan, J.M. (2001) Wetting properties of Fe-Ni-Co-Cu-O-S melts against olivine: implications for sulfide melt mobility. Economic Geology, 96, 145-157.

Ryan, C.G., Kirkham, R., Hough, R.M., Moorhead, G., Siddons, D.P., de Jonge, M.D., Paterson, D.J., De Geronimo, G., Howard, D.L., and Cleverley, J.S. (2010) Elemental X-ray imaging using the Maia detector array: The benefits and challenges of large solid-angle. Nuclear Instruments & Methods in Physics Research Section A - Accelerators Spectrometers Detectors and Associated Equipment, 619, 37-43.

Ryan, C.G., Siddons, D.P., Kirkham, R., Li, Z.Y., de Jonge, M.D., Paterson, D.J., Kuczewski, A., Howard, D.L., Dunn, P.A., Falkenberg, G., U , Boesenberg, U., De Geronimo, G., Fisher, L.A., Halfpenny, A., Lintern, M.J., Lombi, E., Dyl, K.A., Jensen, M., Moorhead, G.F., Cleverley, J.S., Hough, R.M., Godel, B., Barnes, S.J., James, S.A., Spiers, K.M., Alfeld, M., Wellenreuther, G., Vukmanovic, Z., and Borg, S. (2014) Maia X-ray fluorescence imaging: Capturing detail in complex natural samples. Journal of Physics: Conference Series, 499, p. 012002.

Santaguida, F., Luolavirta, K., Lappalainen, M., Ylinen, J., Voipio, S., and Jones, S. (2015) The Kevitsa Ni-Cu-PGE deposit in the Central Lapland Greenstone Belt in Finland. Mineral Deposits of Finland, p. 195-210. Elsevier.

Schwindinger, K.R. (1999) Particle dynamics and aggregation of crystals in a magma chamber with application to Kilauea Iki olivines. Journal Of Volcanology and Geothermal Research, 88, 209- 238.

Sciortino, M., Mungall, J.E., and Muinonen, J. (2015) Generation of High-Ni Sulfide and Alloy Phases During Serpentinization of Dunite in the Dumont Sill, Quebec Economic Geology, 110, 733-761.

Siegel, C., Arndt, N.T., Barnes, S.J., Henriot, A.-L., Haenecour, P., Debaille, V., and Mattielli, N. (2015) Fred’s Flow (Canada) and Murphy Well (Australia): thick komatiitic lava flows with contrasting compositions, emplacement mechanisms and water contents. Contribution to Mineralogy and Petrology, 168.

Sluzhenikin, S.F., Krivolutskaya, N.A., Rad'ko, V., Malitch, K.N., Distler, V.V., and Fedorenko, V.A. (2014) Ultramafic-mafic intrusions, volcanic rocks and PGE-Cu-Ni sulfide deposits of the Noril’sk Province, Polar Siberia, Field Trip Guidebook. Institute of Geology of Ore Deposits, Petrography, Mineralogy and Geochemistry., Yekaterinburg, Russia.

Souch, B.E., and Podolsky, T. (1969) The sulfide ores of Sudbury; their particular relationship to a distinctive inclusion-bearing facies of the nickel irruptive. Economic Geology Monograph, 4, 252-261.

Stifter, E.C., Ripley, E.M., and Li, C. (2014) Silicate melt removal and sulfide liquid retention in ultramafic rocks of the Duke Island Complex, Southeastern Alaska. Mineralogy and Petrolgy, 108, 727-740.

Stone, W.E., Crocket, J.H., and Fleet, M.E. (1996) Platinum-group mineral occurrence associated with flow top amygdule sulfides in komatiitic basalt, Abitibi Greenstone Belt, Ontario. Mineralogy and Petrology, 56(1-2), 1-24.

Sukhanova, E.N. (1968) Zoning of orebodies, intrusions, and tectonomagmatic clusters and its applied implications (in Russian). Geology and mineral resources of the Noril'sk mining district, p. 139-142. NTO Tsvetmet, Noril'sk.

Tonnelier, N. (2009) Geology and Genesis of the Jinchuan Ni-Cu-(PGE) Deposit, China, PhD, p. 251. Laurntian University, Sudbury.

Tonnelier, N., Lesher, C.M., and Arndt, N.T. (2009) Petrology and geochemistry of the Jinchuan intrusion and asssociated Ni-Cu-(PGE) mineralization, Xi'an Ni-Cu Symposium, Xi'an, China. Xi'an Ni-Cu Symposium, Xi'an (China).

Torgashin, A.S. (1994) Geology of the Massive and Copper Ores of the Western Part of the Oktyabr'sky Deposit. In P.C. Lightfoot, and A.J. Naldrett, Eds. Proceedings of the Sudbury-Noril'sk Symposium. Ontario Geological Survey Special Publication 5, 5, p. 231-260. Ontario Geological Survey, Toronto, ON.

Usselman, T.M., Hodge, D.S., Naldrett, A.J., and Campbell, I.H. (1979) Physical constraints on the characteristics of nickel-sulfide ore in ultramafic lavas. Canadian Mineralogist, 17, 361-372.

Von Bargen, N., and Waff, H.S. (1986) Permeabilities, interfacial areas, and curvatures of partially molten systems; results of numerical computations of equilibrium microstructures. Journal of Geophysical Research, 91B, 9261-9276.

Wark, D.A., Williams, C.A., Watson, E.B., and Price, J.D. (2003) Reassessment of pore shapes in microstructurally equilibrated rocks, with implications for permeability of the upper mantle. Journal of Geophysical Research, 108(B1), 12.

Wei, B., Wang, C.Y., Arndt, N.T., Prichard, H.M., and Fisher, P.C. (2015) Textural Relationship of Sulfide Ores, PGE, and Sr-Nd-Os Isotope Compositions of the Triassic Piaohechuan Ni-Cu Sulfide Deposit in NE China. Economic Geology, 110, 2041-2062.

Yang, S.-H., Maier, W.D., Hanski, E.J., Lappalainen, M., Santaguida, F., and Maatta, S. (2013) Origin of ultra-nickeliferous olivine in the Kevitsa Ni-Cu-PGE-mineralized intrusion, northern Finland. Contributions to Mineralogy and Petrology, 166(1), 81-95.

Zientek, M.L., Causey, J.D., Parks, H.L., and Miller, R.J. (2014) Platinum-group elements in southern Africa—Mineral inventory and an assessment of undiscovered mineral resources. U.S. Geological Survey Scientific Investigations Report, 2010–5090–Q, p. 126.

10 Figure Captions

Figure 1. Frequency distribution of S abundance in ores from the Ovoid and Eastern Deeps at Voisey's Bay, after Lightfoot et al. (Lightfoot et al., 2012), illustrating the typical pattern of distribution, with peaks corresponding to disseminated and massive ores and a long tail on the disseminated mode leading into a broad peak corresponding to net-textured ores.

Figure 2 Sketches of contact angles in partially molten rocks, drawn in the plane perpendicular to the tangent of the contact line or lines where three phases come together. S = solid, L = liquid, L1, L2 = two immiscible liquids. a. Interfacial angle of 28° between two planar crystal faces. b. An example of a contact where the interfacial angle is 28° but the equilibrium dihedral angle is 50°; the interfaces are deflected close to the contact line to achieve local textural equilibrium. c. Axial cross section of a sulfide liquid drop sessile on a planar olivine crystal face, both in contact with silicate melt. The wetting angle is 160° (Mungall and Su, 2005) and the drop is small enough not to be deformed under its own negative buoyancy; i.e., the system is small enough that surface tension predominates over body forces. d. Axial view down three linear channel separating three crystals (S) and occupied by liquid (L). e. Melt-filled channels as in d are now occupied by two liquids with a wetting angle of 160°; L2 in this case could correspond to sulfide liquid in a basalt-filled channel (L1) between olivine crystals (S).

Figure 3. Sketches of the distribution of melts and solids in idealized partially molten systems with very low melt fraction, corresponding closely to olivine adcumulate textures in dunites (after van Bargen and Waff, 1986; Mungall, 2015). a. Dihedral angle > 60°, as would occur in oxygen-rich sulfide melts hosted by olivine in the absence of silicate melt (Rose and Brenan, 2001). b. Dihedral angle < 60°, as would occur where basaltic liquid was hosted by olivine (Van Bargen and Waff, 1986). c. One wetting liquid has dihedral angle < 60° (e.g., basaltic liquid against olivine) but a second non-wetting liquid has a wetting angle of 160° (e.g., sulfide liquid). The presence of the network of channels of wetting basaltic liquid opens up a pathway for extended drops of sulfide liquid spanning several pores and channels; however sulfide melt cannot spontaneously migrate downwards as isolated drops unless they are small enough to fit through the smallest dimensions of the grain-edge channels (microdrop at top right). Larger isolated drops are stranded in pores at the junction of four

crystals, unable to move because capillary forces impede the deformation require to force them through grain-edge channels (stranded drop, deformed drop at right). Large, extended drops of sulfide melt within the basaltic melt channel network can only migrate downwards if the hydraulic head expressed over the vertical distance ζ exceeds the capillary force resisting downward motion at the bottom of the sulfide mass (Chung and Mungall, 2009).

Figure 4. Disseminated sulfides in komatiitic olivine adcumulates from Mt Keith (a to e), traced from polished sections. Note the wide variability of dihedral angle within the same sample and in some cases within the same bleb. Modified from Godel et al. (2013).

Figure 5 (a) Microbeam X-ray fluorescence (XFM) element map collected using the Maia detector array on the XFM beamline of the Australian Synchrotron. False colour image showing relative normalized abundances of Ni (red), Fe (green) and Cu (blue) in a polished section of interstitial disseminated ore from Mt Keith. (b): MAIA-XFM false colour image of disseminated sulfides in 95% fresh dunite from Dumont, same colour scheme as (f).

Figure 6. 3D textures in interstitial disseminated ores, perspective views of HRXCT images. (a) Disseminated sulfide blebs in olivine-sulfide adcumulate from Mt. Keith, showing triple-point "tubules" or micro-channels of sulfide along olivine triple grain boundaries – compare Fig.1a. (b) olivine-sulfide meso-adcumulate from Mt Keith, individual sulfide blebs colour-coded by size (after Godel et al., 2013). (Animations of 3D scans at https://www.youtube.com/watch?v=uJXfKNQx3nY). Blebs in this sample are primarily convex/globular. (c) perspective views of single 3D image of disseminated sulfides from Dumont (same sample as Fig. 5b) showing isolated, poorly interconnected non-wetting sulfides. Yellow = sulfide, red = awaruite (Ni-Fe alloy) – note presence of an awaruite grain in each sulfide bleb (See supplementary material for 3D animations of these images).

Figure 7. 2D and 3D images of globular sulfides from olivine-sulfide orthocumulates at Black Swan, Western Australia. A phase map traced from polished slab showing distribution of (alteration products of) olivine, interstitial silicate melt and sulfide blebs, after Barnes et al. (2009). B,c– 3D HRXCT image of sulfide globules in a similar olivine-sulfide orthocumulate rock, drill core approximately 4 cm across. Animation of 3D image at https://www.youtube.com/watch?v=U-wj_kx4ns0

Figure 8. Sulfide textures in pyroxenites from the Kevitsa intrusion, Finland. (a), (b), perspective views of 3D microCT image of disseminated sulfides in orthopyroxenite. Colours

indicate separate sulfide networks. (c), (d), same image, same view, showing only the largest interconnected network in the sample. See https://www.youtube.com/watch?v=OXC7ICRP1Iw for 3D animation. E, Tornado MicroXRF image of sample KV148-337, disseminated sulfide in poikilitic websterite. Relative normalized proportions of Ni (red), Cu (green) and Ca (blue). Oikocrysts of clinopyroxene (blue) enclosing orthopyroxene (black). Sulfides indicated by Ni and Cu – note exclusion of sulfides from interior of oikocrysts. F, perspective view of 3D image of same sample, sulfides in yellow. Sulfides primarily form poorly interconnected blebs; vacant volumes are occupied by oikocrysts.

Figure 9 Sulfide textures in the Mirabela Intrusion (a-e), after Barnes et al. (2011b) A, b: reflected light photomicrographs of interstitial blebs, pn=pentlandite, po = pyrrhotite, cp = chalcopyrite, py = pyrite. Note symplectic intergrowth of cp with pyroxene in (b). c, transmitted crossed polar light photomicrograph of sulfide (black) intergrown with intercumulus patch of plagioclase, amphibole, mica and apatite. (d,e), perspective view of 3D microCT image of non-connected interstitial disseminated sulfide in chromite-bearing harzburgite.

Figure 10. 3D rendering showing the 3D distribution and morphology of sulfides in samples from the JM-Reef of the Stillwater Complex (U.S.A) and the Merensky Reef of the Bushveld Complex (South-Africa). a) 3D distribution of sulfides in olivine-gabbronorite from the JM-Reef in red and yellow (modified from Godel, et al., 2006). The red colour represent the largest interconnected network in the specimen scanned. b) 3D morphology of sulfides-silicate boundaries in similar JM Reef sample obtained using HRXCT, modified after Godel (2015); c) 3D distribution of sulfides in gabbronorite from the Merensky Reef (modified from Godel, et al. (2006)) with three largest sulfide network coloured in red, blue and green.

Figure 11. Globules with silicate caps from Togeda macrodyke, after Holwell et al. (2012). A,b,c:; oblique view of horizontal slices and cylindrical edges of core sample located in d, microCT images. Note silicate cap occupied by plagioclase (pl), and clinopyroxene (cpx) intergrown with the top of the sulfide globule. D, 3D microCT image of drill core showing location of detailed slices a,b,c. E, outcrop photograph. F, medical CT image of multiple sulfide globules in outcrop sample (different sample from a,b,c,d). See https://data.csiro.au/dap/SupportingAttachment?collectionId=17878&fileId=1234

for a fully interactive 3D visualization and https://www.youtube.com/watch?v=lUm3sope5y0 for animation.

Figure 12. Capped sulfide globules associated with segregation vesicles in olivine orthocumulate, Black Swan komatiite-hosted deposit. A –C, drill core samples showing globules occupying lower portion of segregation vesicles (Seg-black), after Dowling et al. (2004). Sulf= sulfide, ol-Srp, SM = interstitial silicate melt. D, Tornado false colour microbeam XFM image, normalized relative abundances of Cr (red), Ni (green) and Fe (blue). Sulfide (blue, green – pyrite plus millerite) rimmed by skeletal chromite (Chr, pink) within skeletal textured olivine orthocumulate – olivine now pseudomorphed by serpentine (Ol-Srp) plus magnetite, interstitial space occupied by fine chlorite-serpentine intergrowth after original trapped silicate liquid. E, detail of D, synchrotron XFM image, Cr (red), log Ni (green), Fe (blue) – note fine-grained microspinifex texture (psp) within segregated silicate component (upper right).F, 3D perspective view of microCT image of same sample – note chromite rimming sulfide (yellow) interconnects with a larger octahedral chromite grain outside the vesicle – after Godel et al. 2014).

Figure 13. Polished slab photos of capped globules in samples of globular disseminated ore from the Noril'sk 1 and Kharelakh intrusions, Noril'sk-Talnakh, Siberia. A, B, olivine gabbro containing two sulfide populations: flattened globules with upper silicate caps, and interstitial blebs. Globules show characteristic differentiation into po-pn at the base, chalcopyrite-dominant at top, with a smooth meniscus between. Note variable degree of flattening of globules. C, Enlargement of capped bleb in (B), showing upper boundary of Cu-rich sulfide with silicate cap, and percolation of Fe-rich sulfide at bottom into interstitial space within the cumulus olivine framework of the rock. D, capped differentiated sulfide globule from Waterfall Gorge, Insizwa Intrusion, Karoo province. F, 3D medical CT image of globular disseminated sulfides from the Kharelakh intrusion. Colours have no compositional significance, but indicate individual non-interconnected globules. Note irregular multi-lobate morphologies of many globules. See https://data.csiro.au/dap/SupportingAttachment?collectionId=17878&fileId=1233 and https://data.csiro.au/dap/SupportingAttachment?collectionId=17878&fileId=1231 for interactive 3D visualizations.

Figure 14. Globular disseminated sulfides from Copper Cliff offset, Sudbury. A) photo mosaic of polished slab. B, c, Tornado XFM 3-element false colour maps of same slab. See

https://www.youtube.com/watch?v=-kVK3kNyqic for animation of moving slices through 3D image.

Figure 15. XRF and CT images of globular disseminated sulfides, Piaohechuan deposit, China. A) photo mosaic of polished slab. B, Tornado XFM 3-element false colour map of same slab. Pyrrhotite in blue, pentlandite pink, chalcopyrite green. c) representative slices through medical CT 3D image with sulfide globule intersections picked out in yellow. Note embayed morphologies of some of the larger globules. d) perspective view of 3D medical-CT image showing arbitrary colours for individual interconnected globules. Note that the large globules tend to be less spherical and more coalesced (see https://data.csiro.au/dap/SupportingAttachment?collectionId=17878&fileId=1230 for interactive 3D visualization and https://www.youtube.com/watch?v=pxnQeBjTwNA for animation.

Figure 16. Net-textured and poikilitic "leopard" net-textured ores from the Katinniq deposit, Raglan belt, Canada. A, typical oikocryst-free net-textured ore, B, poikilitic net-textured ore; inset enlargement showing chromite grains in orthopyroxene core. A-B reflected light photomicrographs. Note olivine, opx are completely replaced by serpentine. C, Tornado XFM map, normalized relative concentrations of Cr (red), Fe (green) and S (blue). Not Cr-enriched zones in cores of opx, Cr-poor outer opx zones, greatly reduced proportion of sulfide (blue/turquoise) inside oikocrysts. D, same, Ni (red), Cu (green) and S (blue).

Figure 17. Net-textured ore textures – combined patchy net-textured and globular sulfides, with and without silicate caps, Alexo, Ontario. A,b: photomosaics of polished slabs showing sulfide as interstitial network and ellipsoidal globules. Olivine pseudomorphs as equant and aligned platy grains (black). c, d: Tornado XFM images – ol=olivine, sul=sulfide, TL = trapped liquid alteration product, cpx=clinopyroxene. Note trapped-liquid rich orthocumulate micro-domains are relatively poor in sulfide and vice versa. E, transmitted light photomicrograph showing relic acicular cpx and chlorite interstitial to olivine pseudomorphs in orthocumulate domain. F, orthoslices through medical CT image showing oblate spheroid geometry of coarse sulfide globules (see supplementary material for animated version). g: photomosaic of polished slabs showing sulfide (sul) as interstitial network and ellipsoidal globules capped by amygdales (amg) filled with very fine-grained serpentine. Olivine pseudomorphs as equant and aligned platy grains (black). h: Tornado XFM image (S red, Ca green and Al blue) highlighting orthocumulate (ooc) micro-domains with low sulfide content

separated by sulfide-rich, trapped-liquid poor net-textured micro-domains. Interactive 3DE visualization at https://data.csiro.au/dap/SupportingAttachment?collectionId=17878&fileId=1235

Figure 18. Voisey's Bay "Leopard textured" ore. Net-textured ore with plagioclase as the main enclosed silicate, with oikocrysts of olivine and minor orthopyroxene that are free of sulfide inclusions.

Figure 19. Patchy net-textures combining matrix and globular sulfides, Mesamax (Raglan) developed within altered "pyroxenitic" marginal rocks of the dykes: felted intergrowths of acicular pyroxene grains (now amphibole) with interstitial silicate melt (now amphibole plus chlorite) and sulfide blebs. A,b, Sulfides form patchy net-textures interstitial to the pyroxenes, which are thought to grow in situ as a form of microspinifex texture. Sulfides also form spheroidal or ellipsoidal globules, in some cases within the matrix domains but also in between them. C, heavily disseminated sulfides with distinct globules– note Cu-rich composition reflecting decimetre scale variability in Ni/Cu ratio of sulfide component, d) same sample as C, perspective view of 3D medical CT scan with disseminated interstitial sulfides in yellow, largest globular sulfides in blue. Interactive 3D image at https://data.csiro.au/dap/SupportingAttachment?collectionId=17878&fileId=1232, animation at https://www.youtube.com/watch?v=BksdEnjBpec

E), net-textured ore from Mequillon deposit – dashes outline single crystal oikocrysts of pyrrhotite (formerly MSS).

Figure 20. Interspinifex ores. A) underground face photo from M.J. Donaldson, hanging wall ore at Lunnon Shoot. Massive ore overlying interspinifex ore – note mushroom-shaped plumes (arrowed) of displaced silicate melt at interface between interspinifex ore (ISO) and overlying massive sulfide (MS). Kom = host komatiite flows. B,c,d – Tornado images of interspinifex ore from Langmuir, Ontario. Optical photo-mosaic (b), Phase map showing olivine (green), sulfide (po + pn) in yellow, chromite in red. D) three-element false colour image with Ni red, Cu green and S blue. For moving slice animation through 3D medical CT scan see https://www.youtube.com/watch?v=szBQa0LCZOw

Figure 21. Cartoon illustrating the "billiard ball model" for the origin of net textured sulfide, after Naldrett (1973) and Usselman et al. (1979)

Figure 22. Cartoon illustrating evolution of patchy net-texture from coalescence and inter-pore drainage of originally disseminated sulfides.

Figure 23. Features related to sulfide liquid percolation. A,b: “soft-wall” sulfide-rich vein-like segregations (SV) developed within intervals of predominantly in disseminated ores. a) Kevitsa deposit, Finland; b) Ntaka Hill deposit, Tanzania – disseminated ores in coarse-grained orthopyroxenite. C, complex mixed sulfide textures in the Tootoo deposit, Cape Smith Belt, northern Quebec: lobate margins between domains of net-textured ore and other domains of fine-grained "pyroxenitic" chilled margin containing isolated globular blebs of sulfide. Also present are patches of massive sulfide with ragged margins against net-textured ore. C, complex mixed sulfide textures in the Tootoo deposit, Cape Smith Belt, northern Quebec: lobate margins between domains of net-textured ore and other domains of fine-grained "pyroxenitic" chilled margin containing isolated globular blebs of sulfide. Also present are patches of massive sulfide with ragged margins against net-textured ore.

Figure 24. Sulfide bleb sizes, modified from Robertson et al. (2015). (a) Particle size distribution plots (equivalent to CSD plots of Marsh (1988)) showing equivalent sphere diameter measurements for sulphide blebs from a number of disseminated ore deposits consisting of 2-5% disseminated sulphides in komatiitic olivine adcumulates. All measurements were made in 3D using x-ray microtomography on 2-5 cm3 samples following the procedure of Godel (2013). The Mount Keith population is composite of five samples. (b) data from three Noril’sk globular ore samples. (c) droplet size distributions for samples from Mesamax (Expo), Black Swan and Marriots. D) disseminated sulfide blebs from Kevitsa, same samples as shown in Fig. 8.

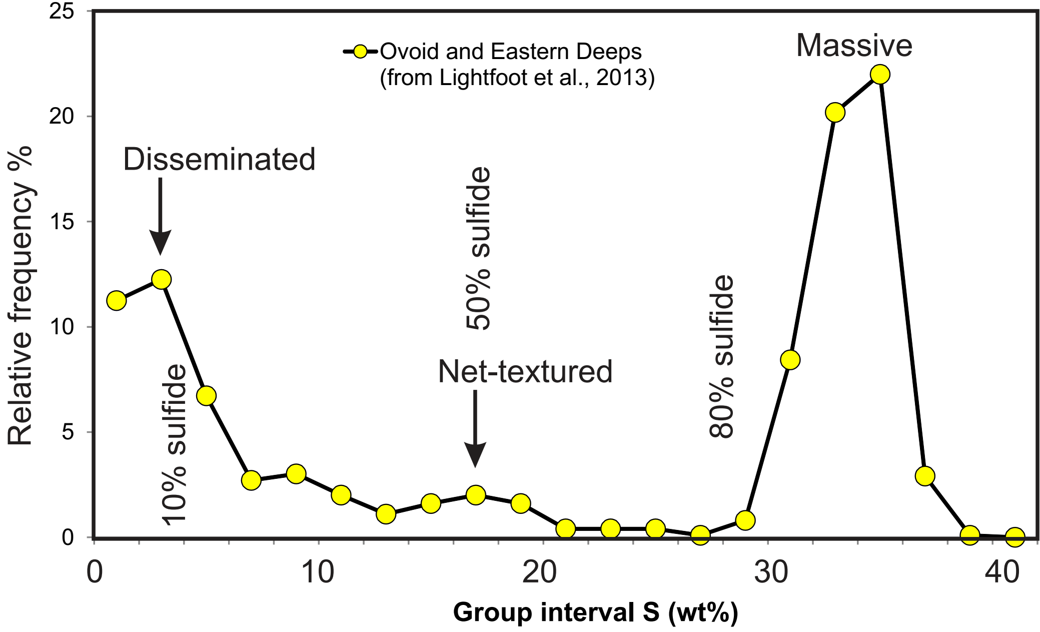

Ovoid and Eastern Deeps
(from Lightfoot et al., 2013)
Massive
Disseminated
50% sulfide
80% sulfide
10% sulfide
Net-textured
Relative frequency %
Group interval S (wt%)
0
5
10
15
20
25
0
10
20
30
40

Figure 1

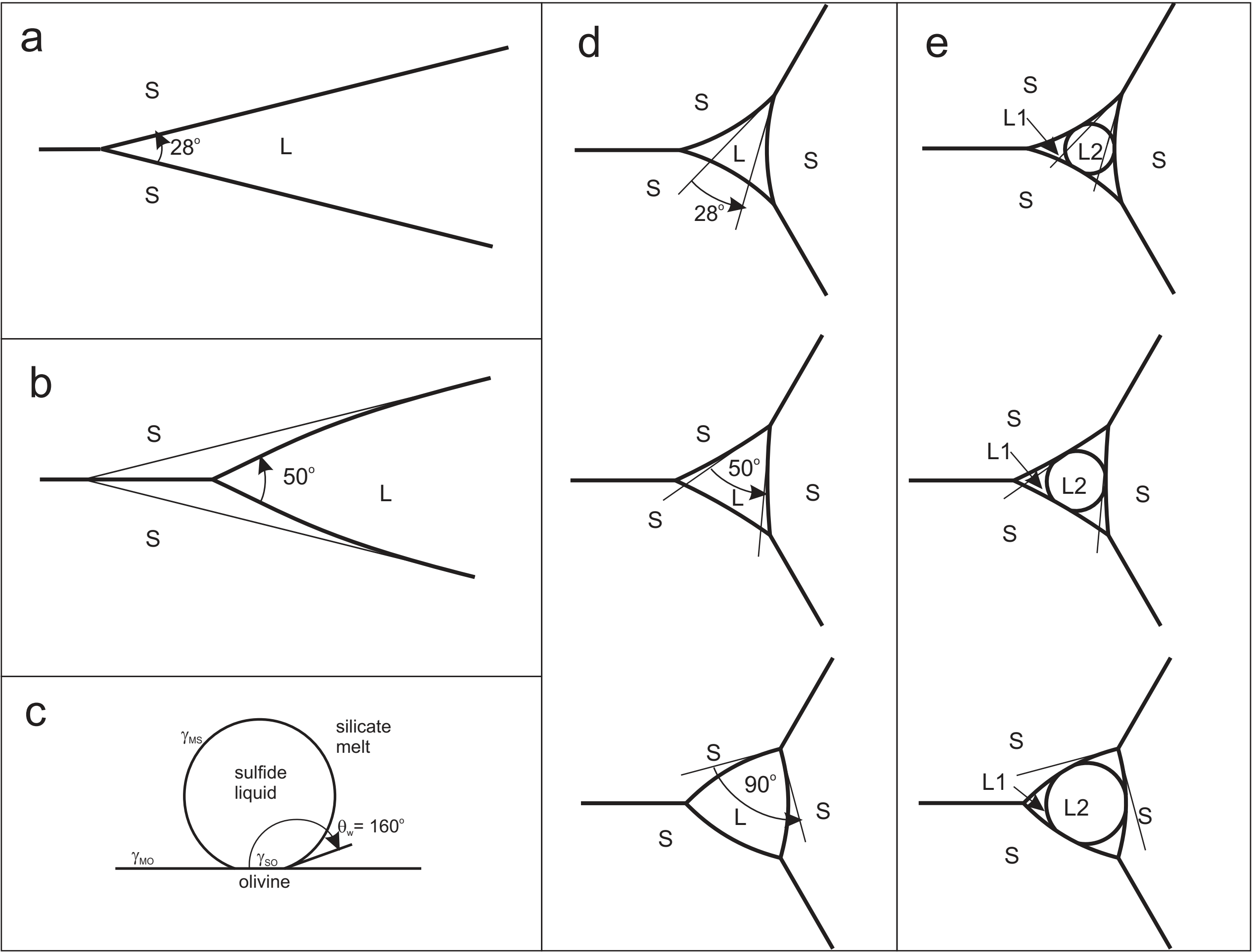
a
S
28°
L
S
b
S
50°
L
S
c
silicate
melt
γMS
sulfide
liquid
θw= 160°
γMO
γSO
olivine
d
S
L
S
S
28°
S
50°
L
S
S
S
90°
L
S
S
e
S
L1
L2
S
S
S
L1
L2
S
S
S
L1
L2
S
S

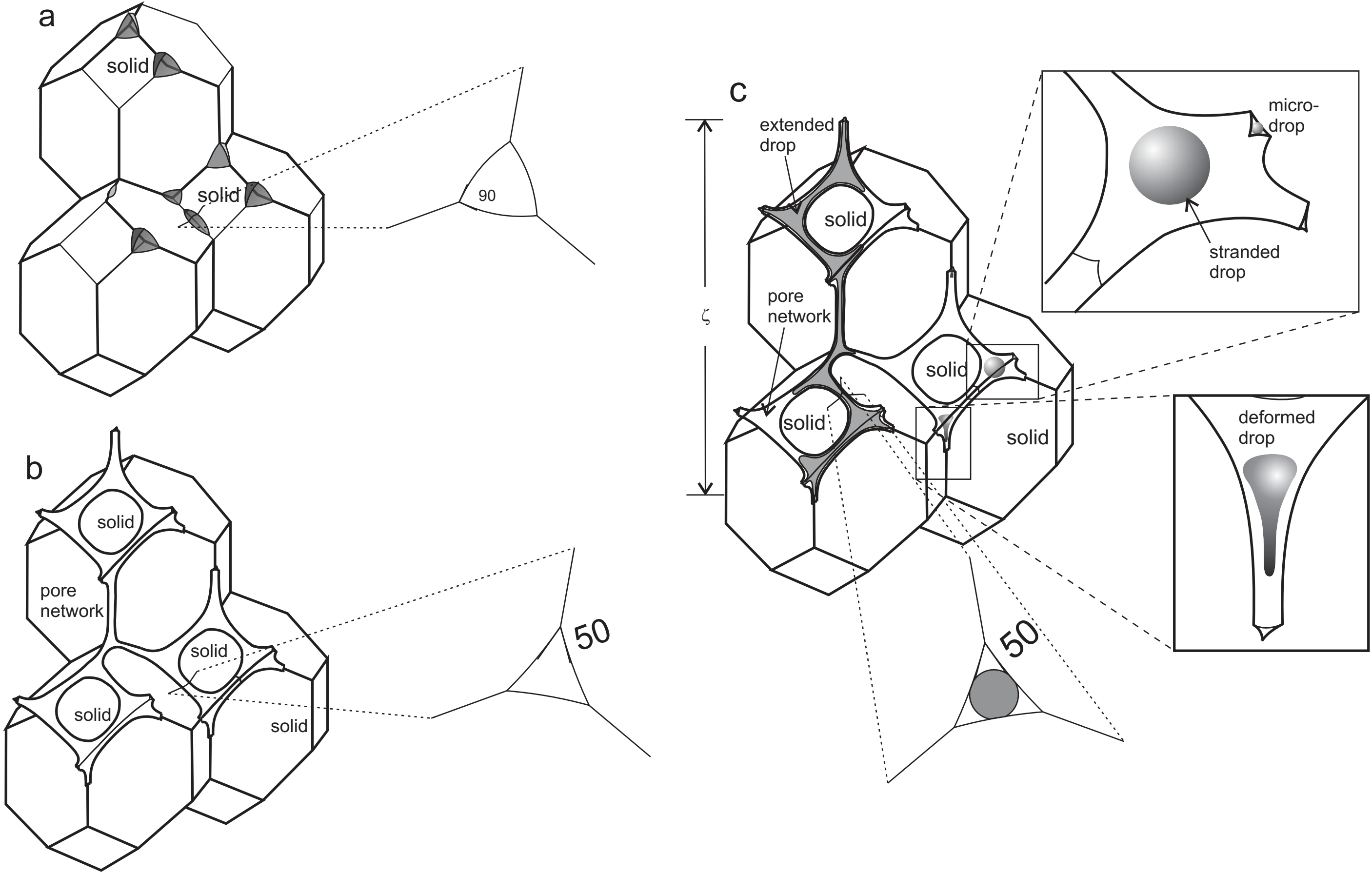

a
solid
solid
90
b
solid
pore
network
solid
solid
solid
50
c
extended
drop
solid
pore
network
ζ
solid
solid
solid
micro-
drop
stranded
drop
deformed
drop
50

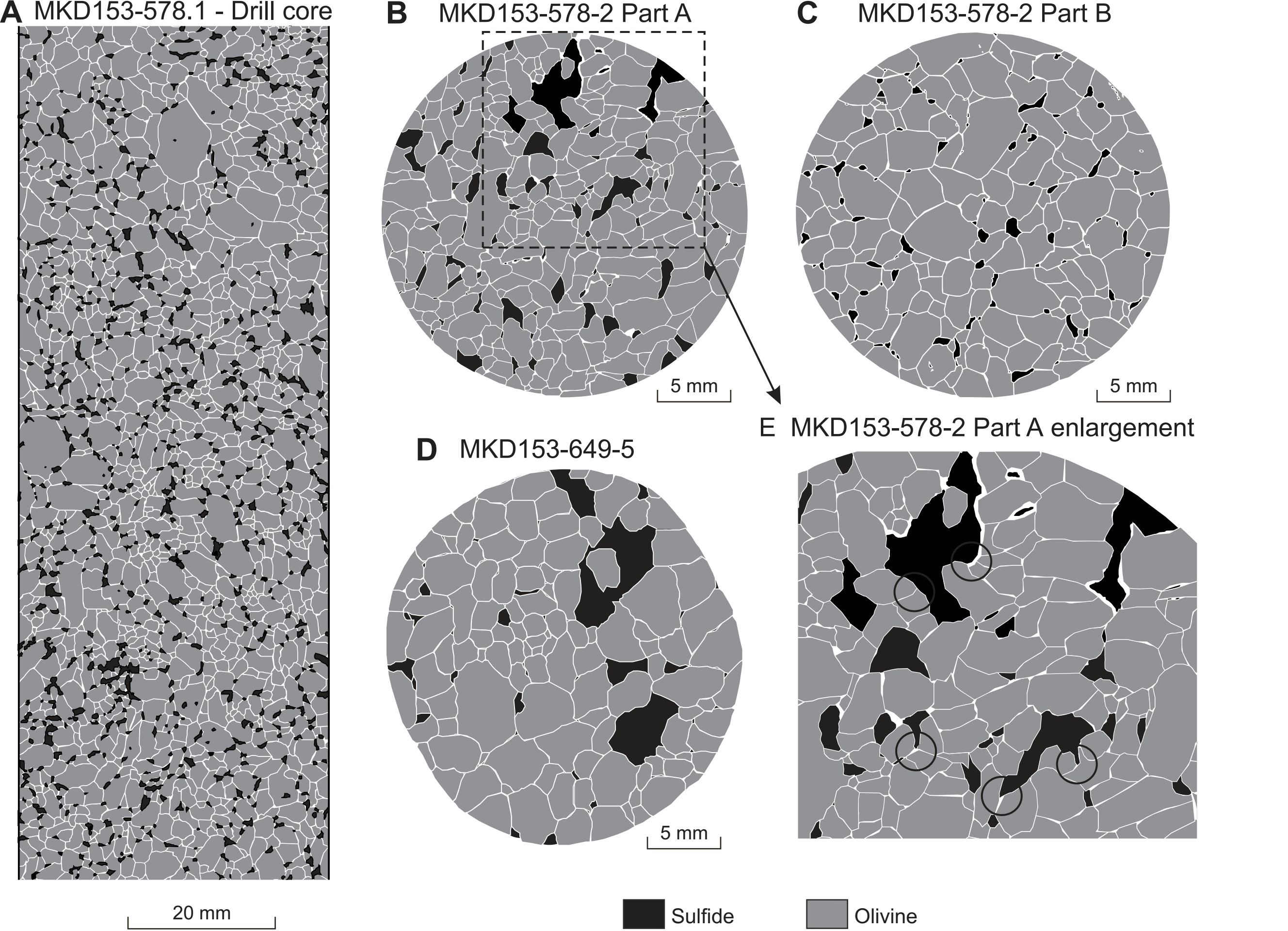
A MKD153-578.1 - Drill core
B MKD153-578-2 Part A
C MKD153-578-2 Part B
D MKD153-649-5
E MKD153-578-2 Part A enlargement
5 mm
5 mm
5 mm
20 mm
Sulfide
Olivine

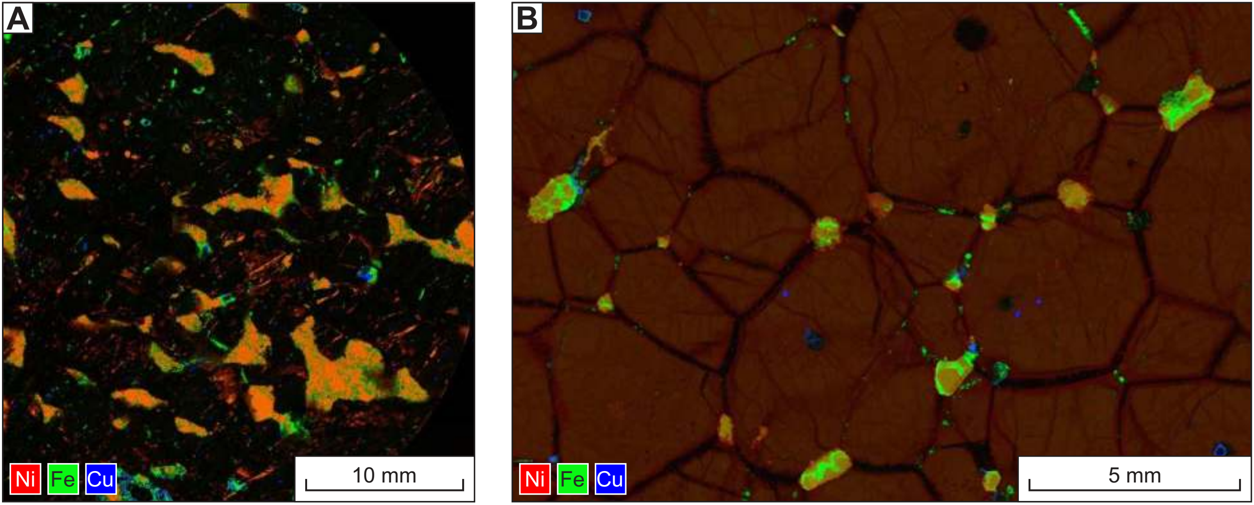
A
Ni
Fe
Cu
10 mm
B
Ni
Fe
Cu
5 mm

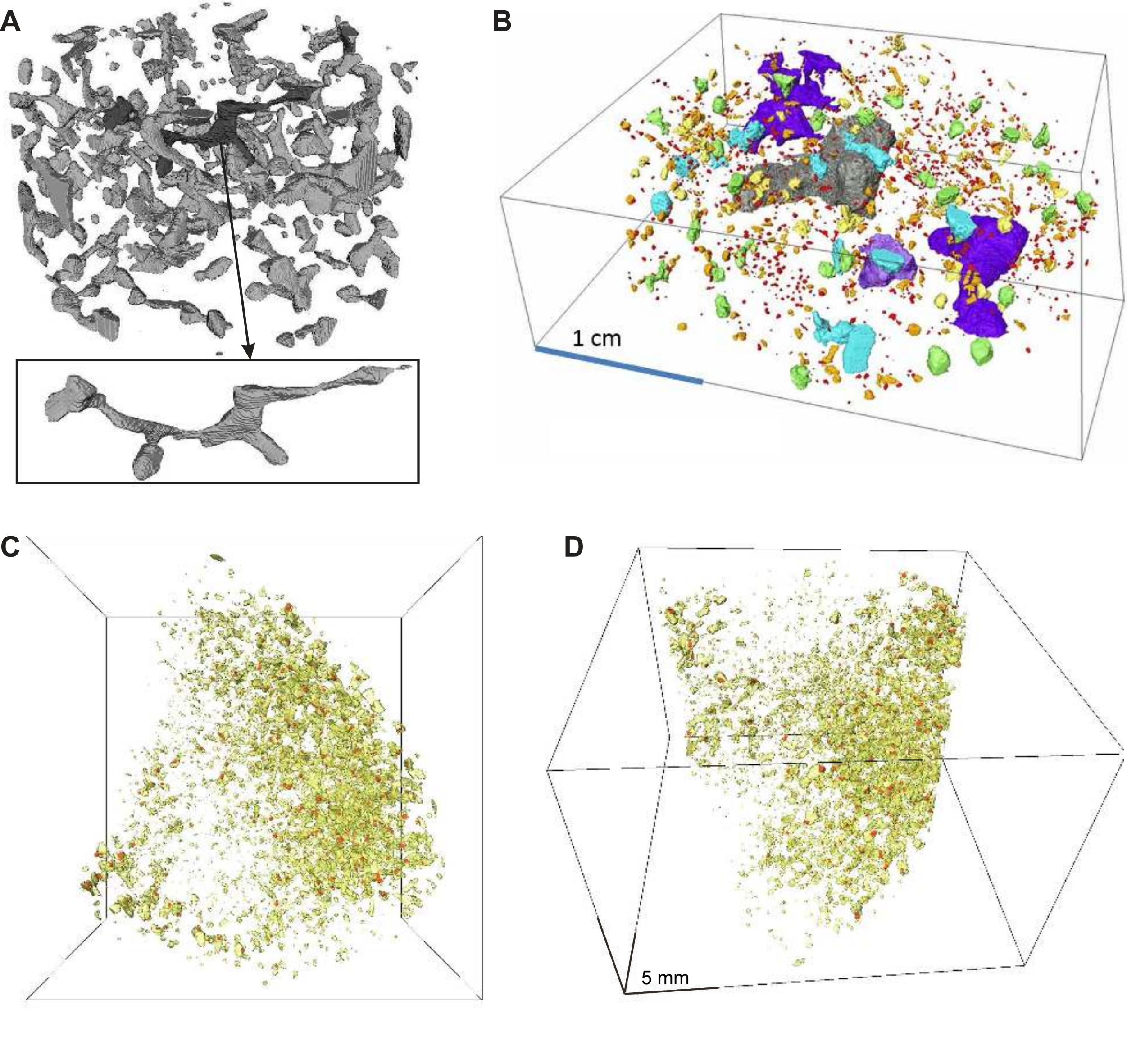

Figure 6

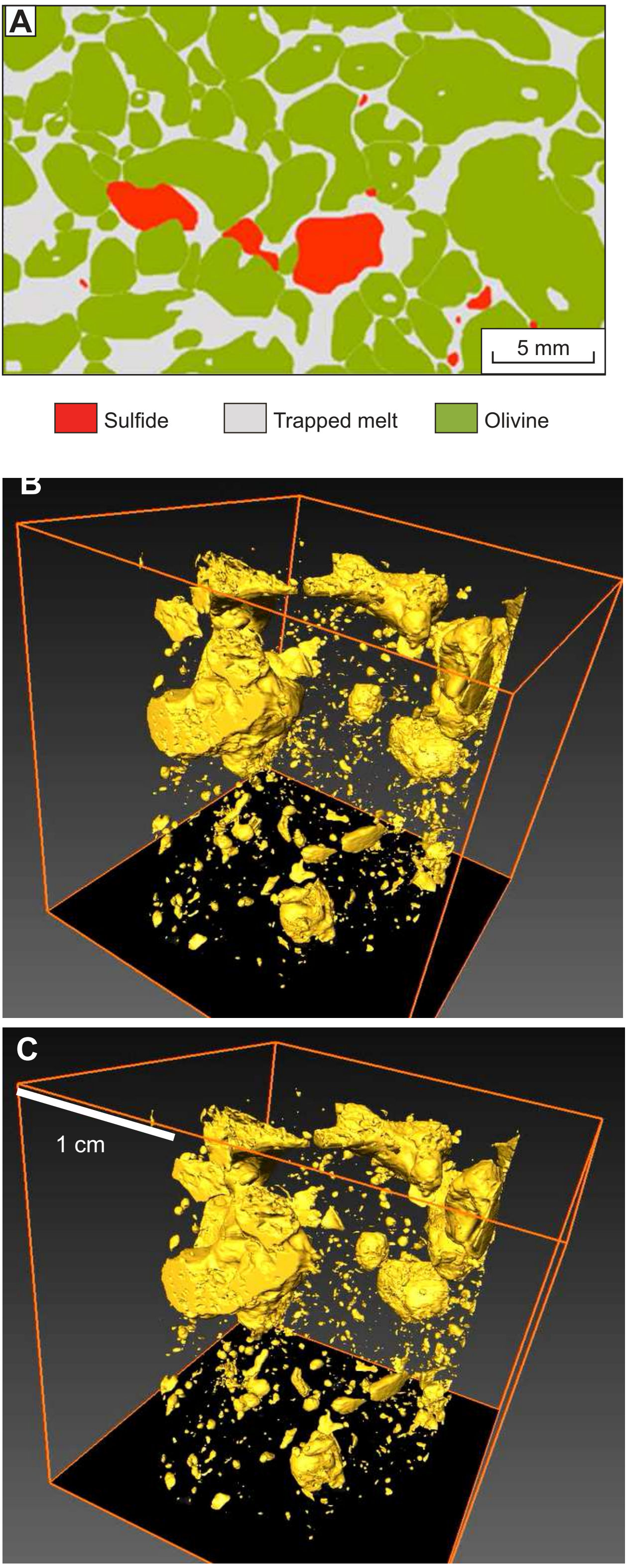

Fig 7

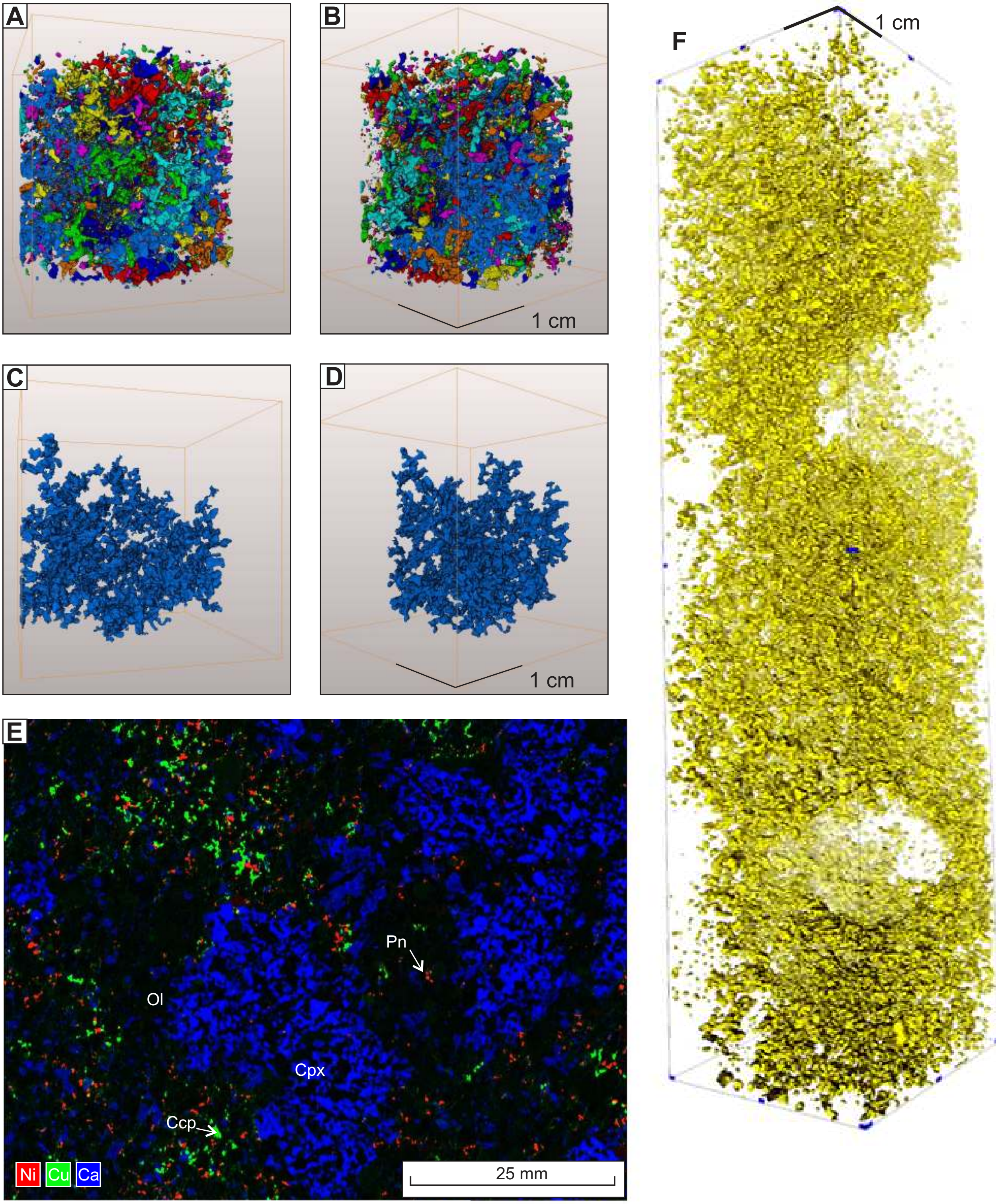

Figure 8

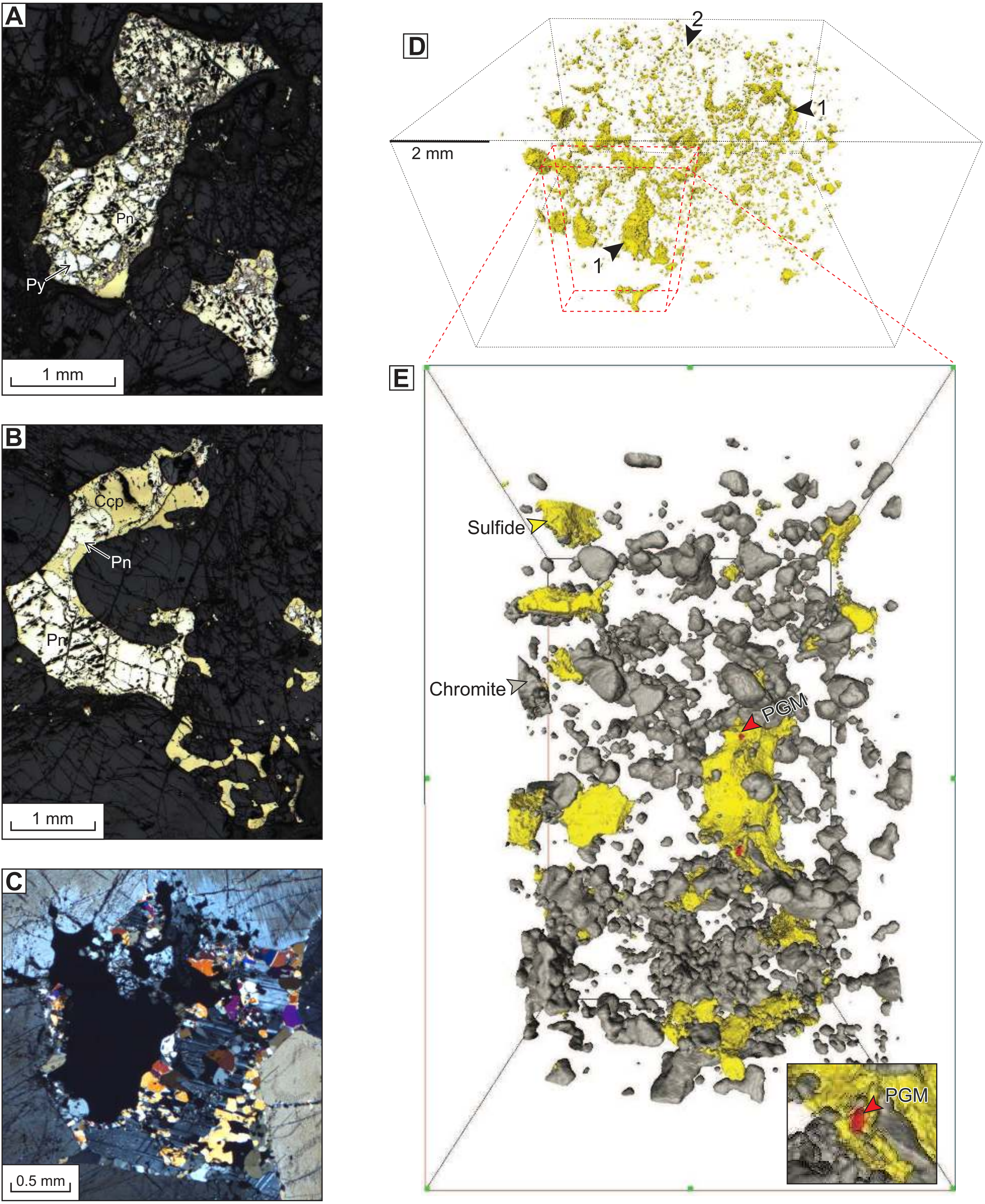
A
Pn
Py
1 mm
B
Ccp
Pn
Pn
1 mm
C
0.5 mm
D
2
1
2 mm
1
E
Sulfide
Chromite
PGM
PGM

Figure 9

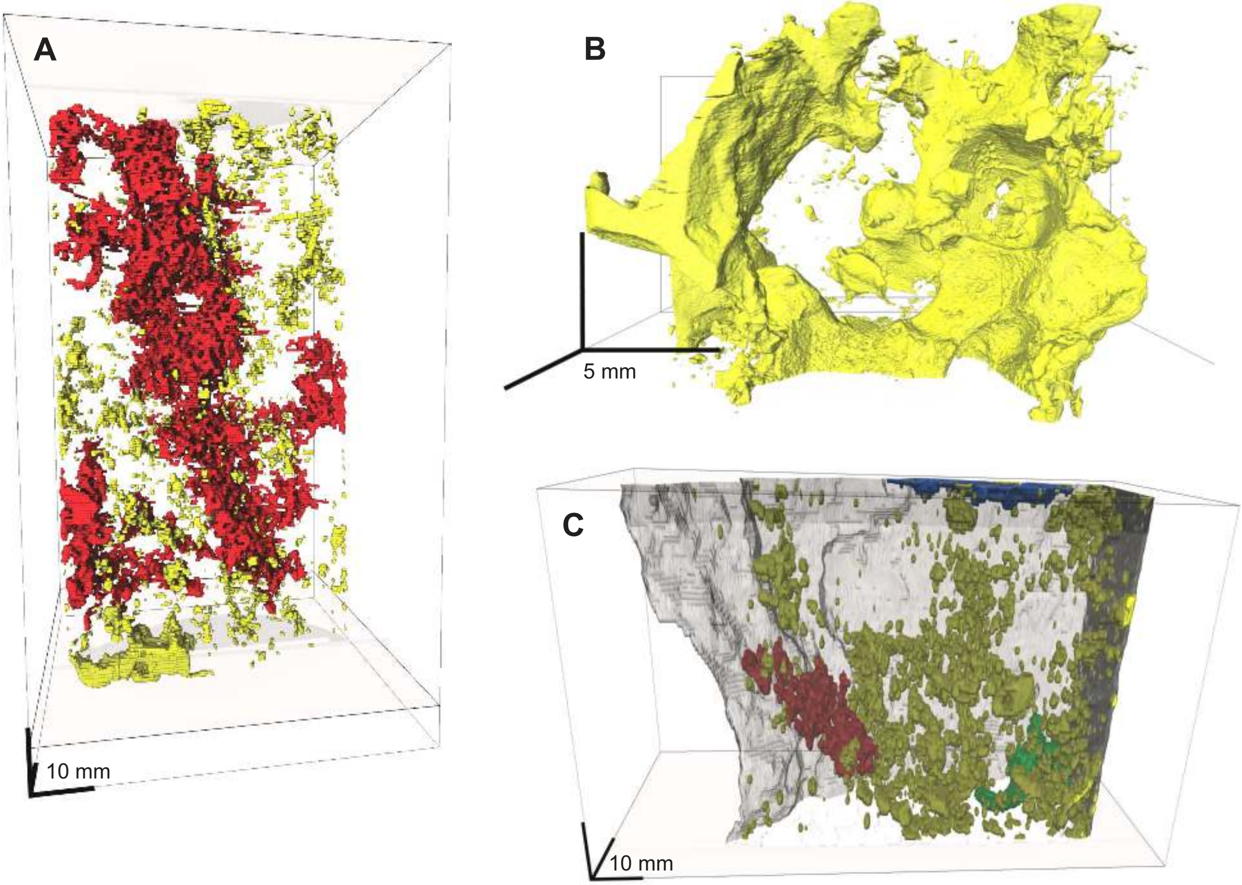

Figure 10

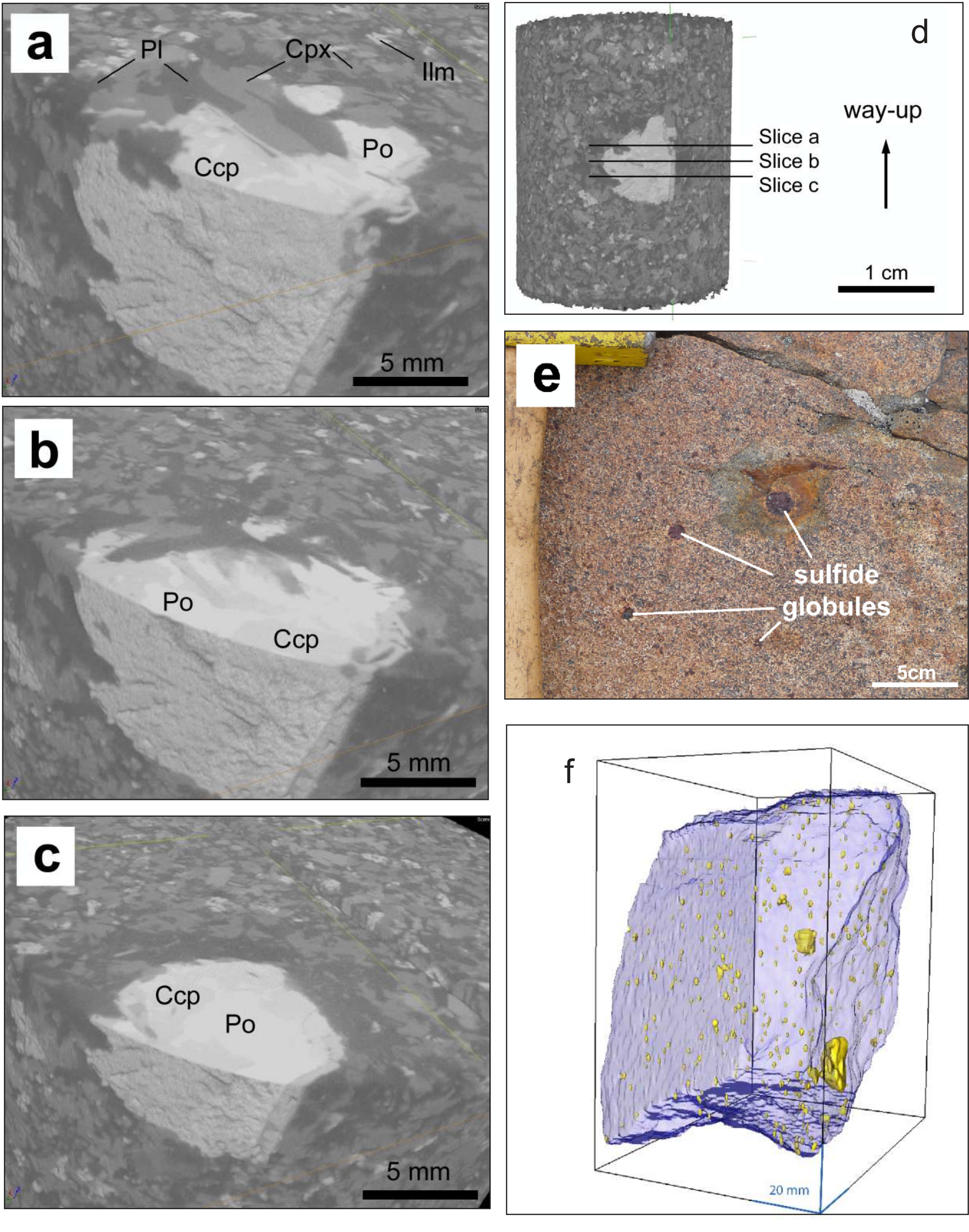
a
Pl
Cpx
Ilm
Ccp
Po
5 mm
b
Po
Ccp
5 mm
c
Ccp
Po
5 mm
d
way-up
Slice a
Slice b
Slice c
1 cm
e
sulfide
globules
5cm
f
20 mm

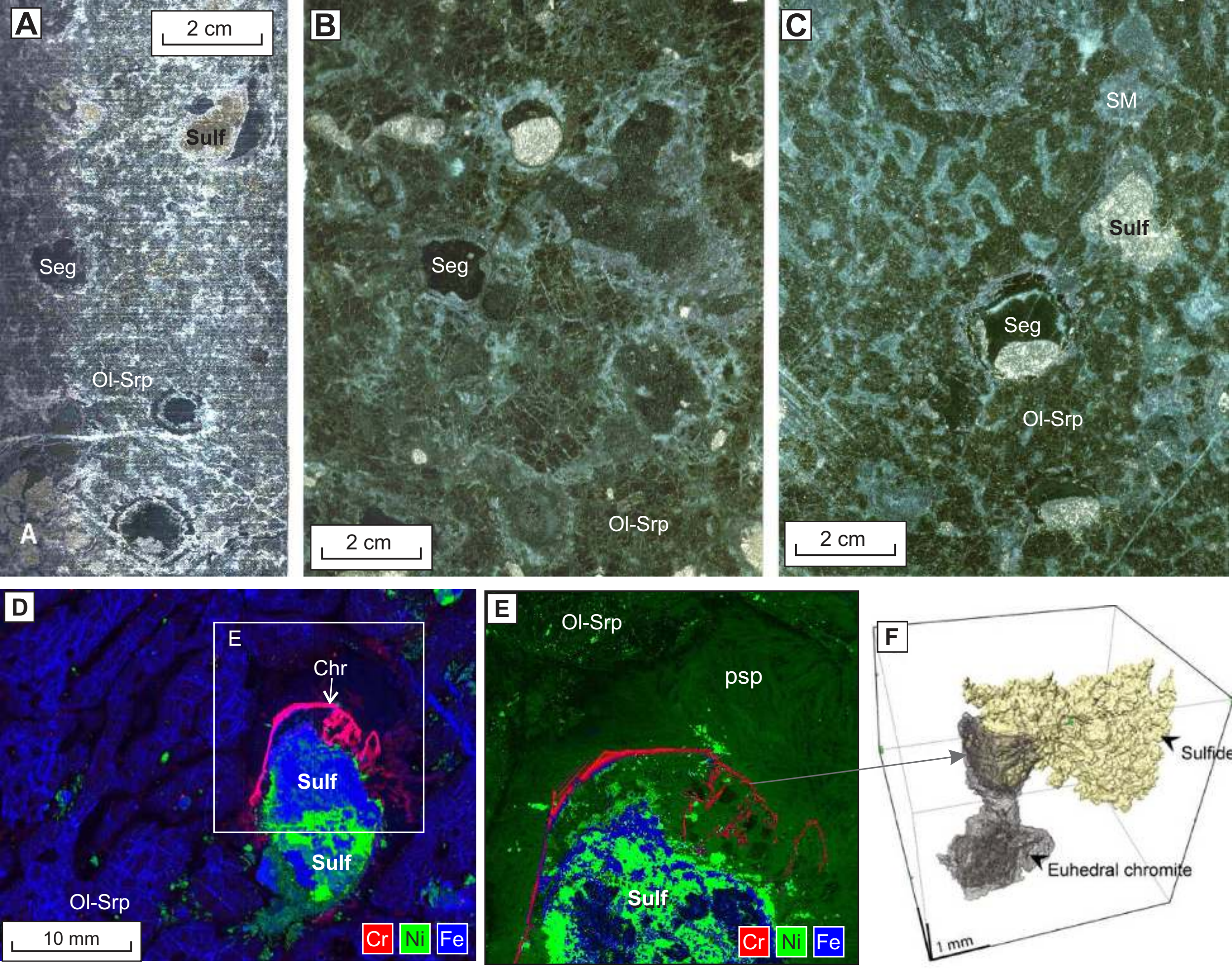
A
2 cm
Sulf
Seg
Ol-Srp
A
B
Seg
Ol-Srp
2 cm
C
SM
Sulf
Seg
Ol-Srp
2 cm
D
E
Chr
Sulf
Sulf
Ol-Srp
10 mm
Cr
Ni
Fe
E
Ol-Srp
psp
Sulf
Cr
Ni
Fe
F
Sulfide
Euhedral chromite
1 mm

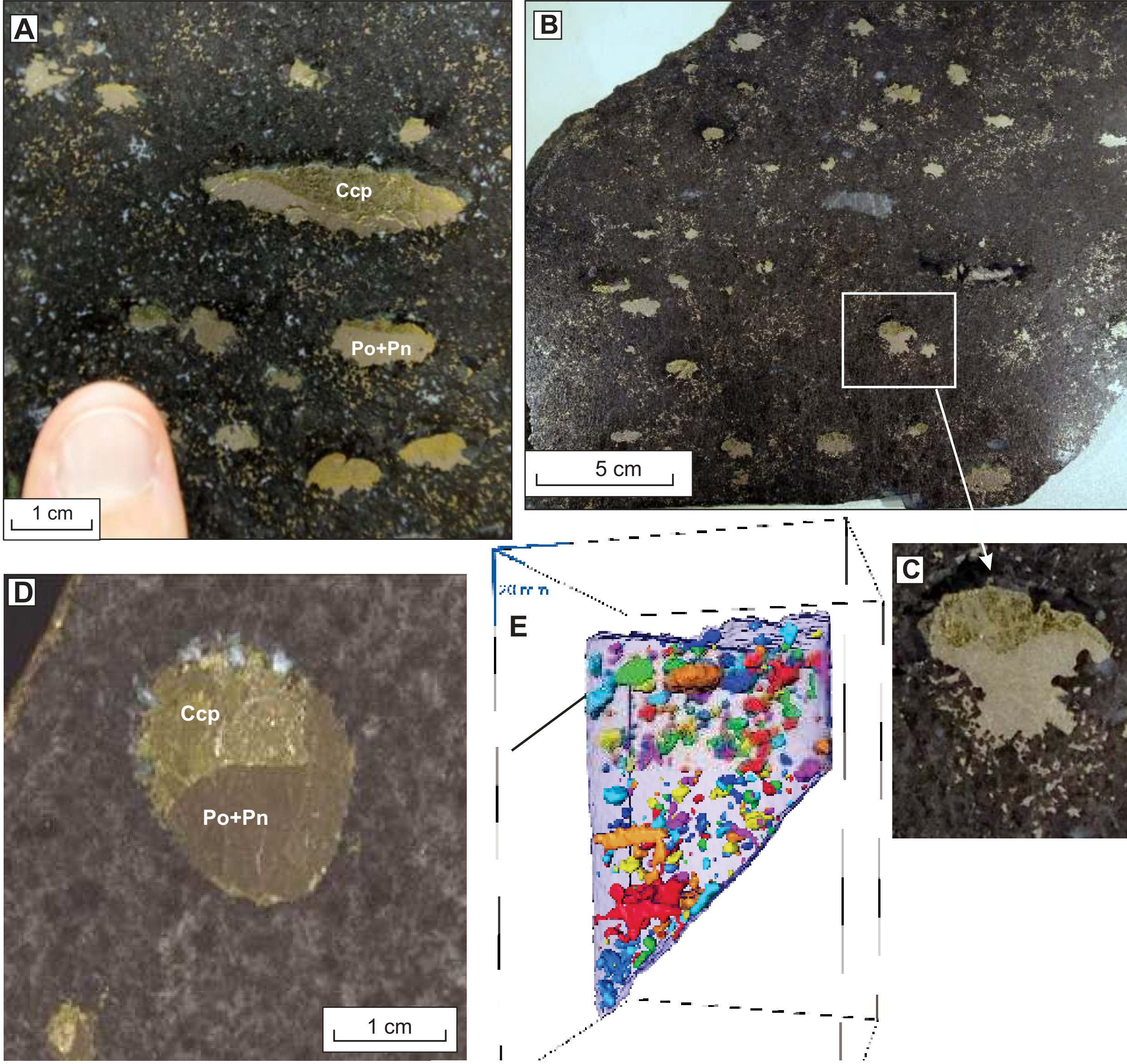
A
Ccp
Po+Pn
1 cm
B
5 cm
C
D
Ccp
Po+Pn
1 cm
E

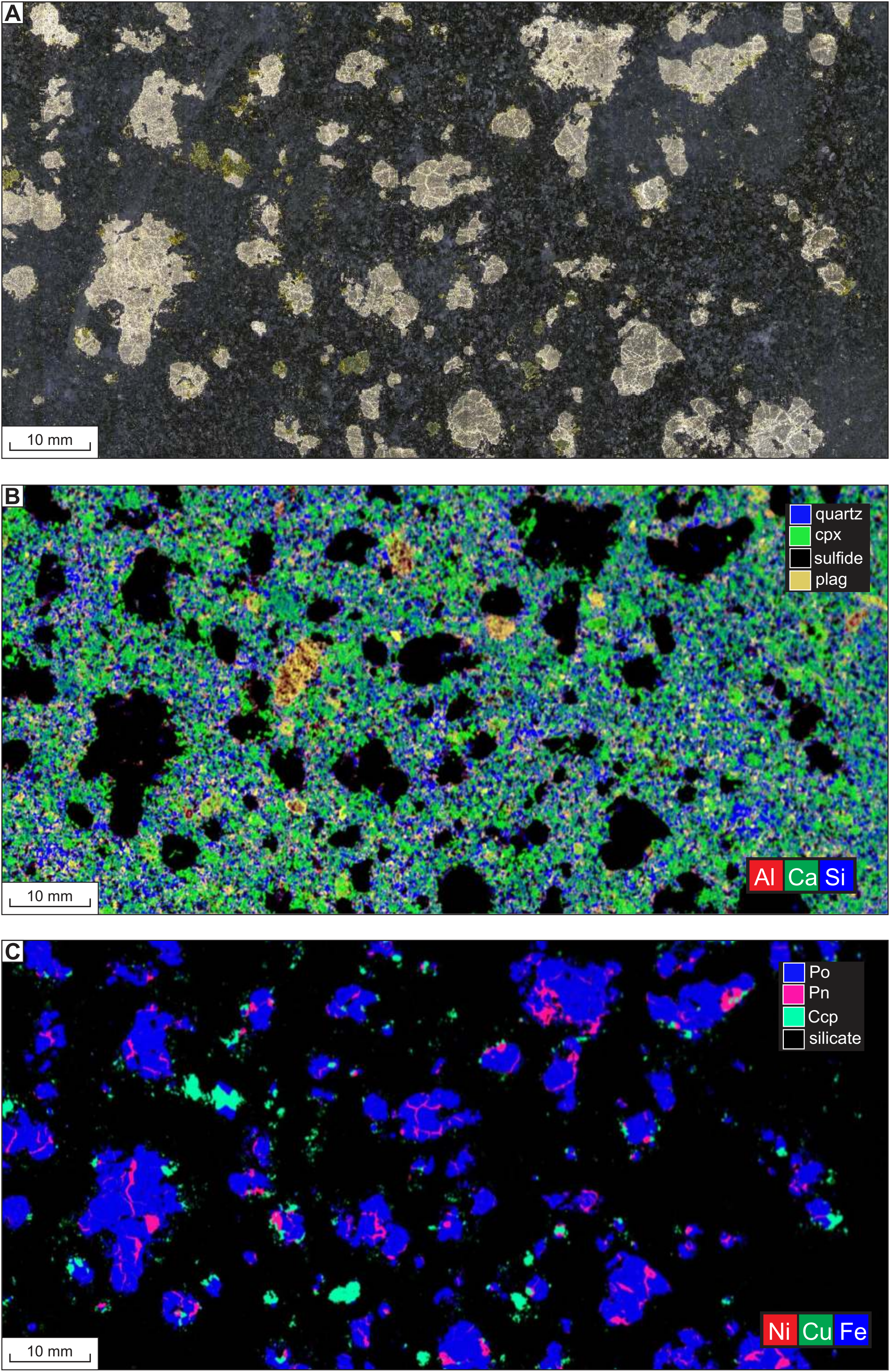
A
10 mm
B
quartz
cpx
sulfide
plag
Al
Ca
Si
10 mm
C
Po
Pn
Ccp
silicate
Ni
Cu
Fe
10 mm

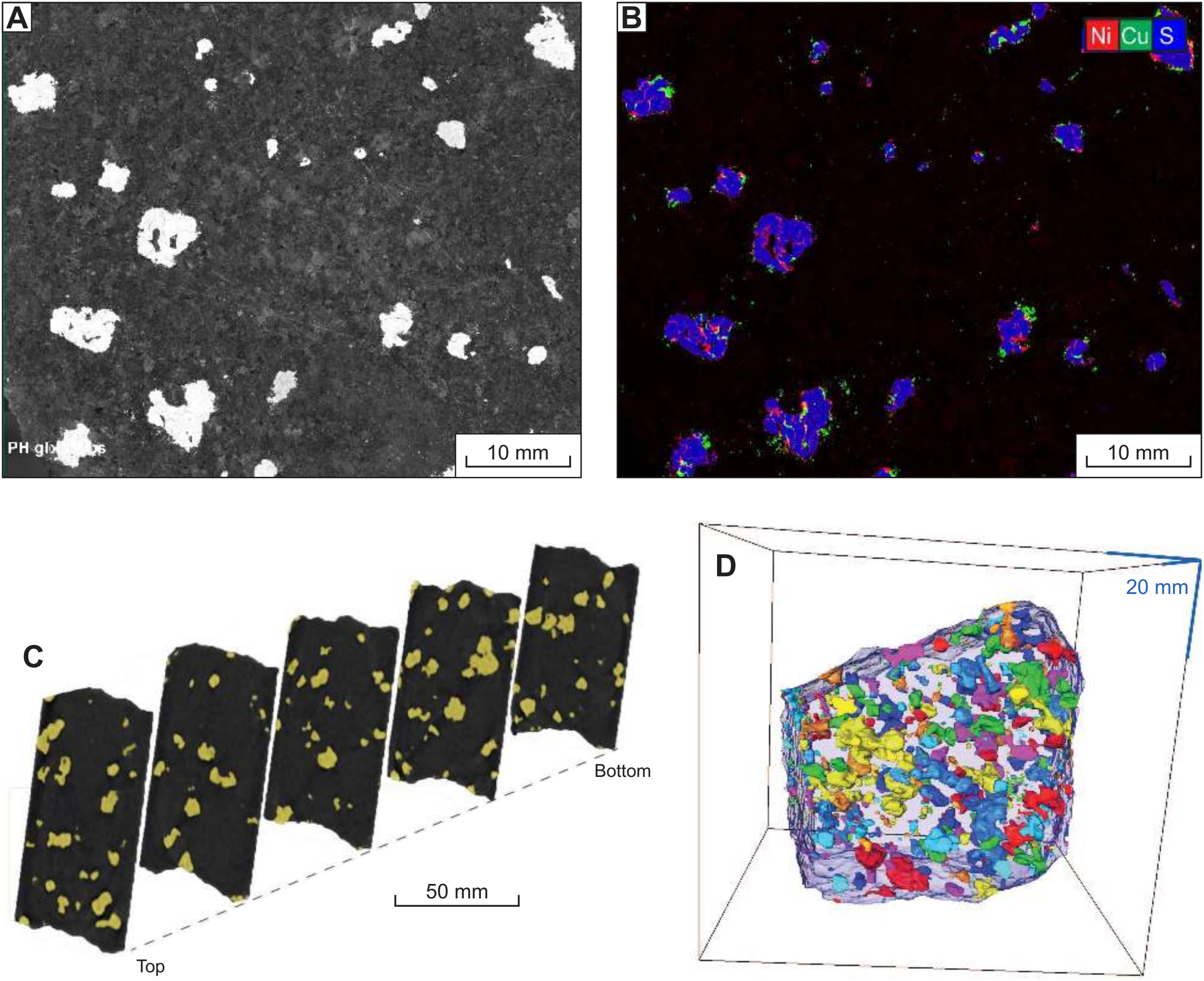

A
10 mm
B
Ni Cu S
10 mm
C
Top
Bottom
50 mm
D
20 mm

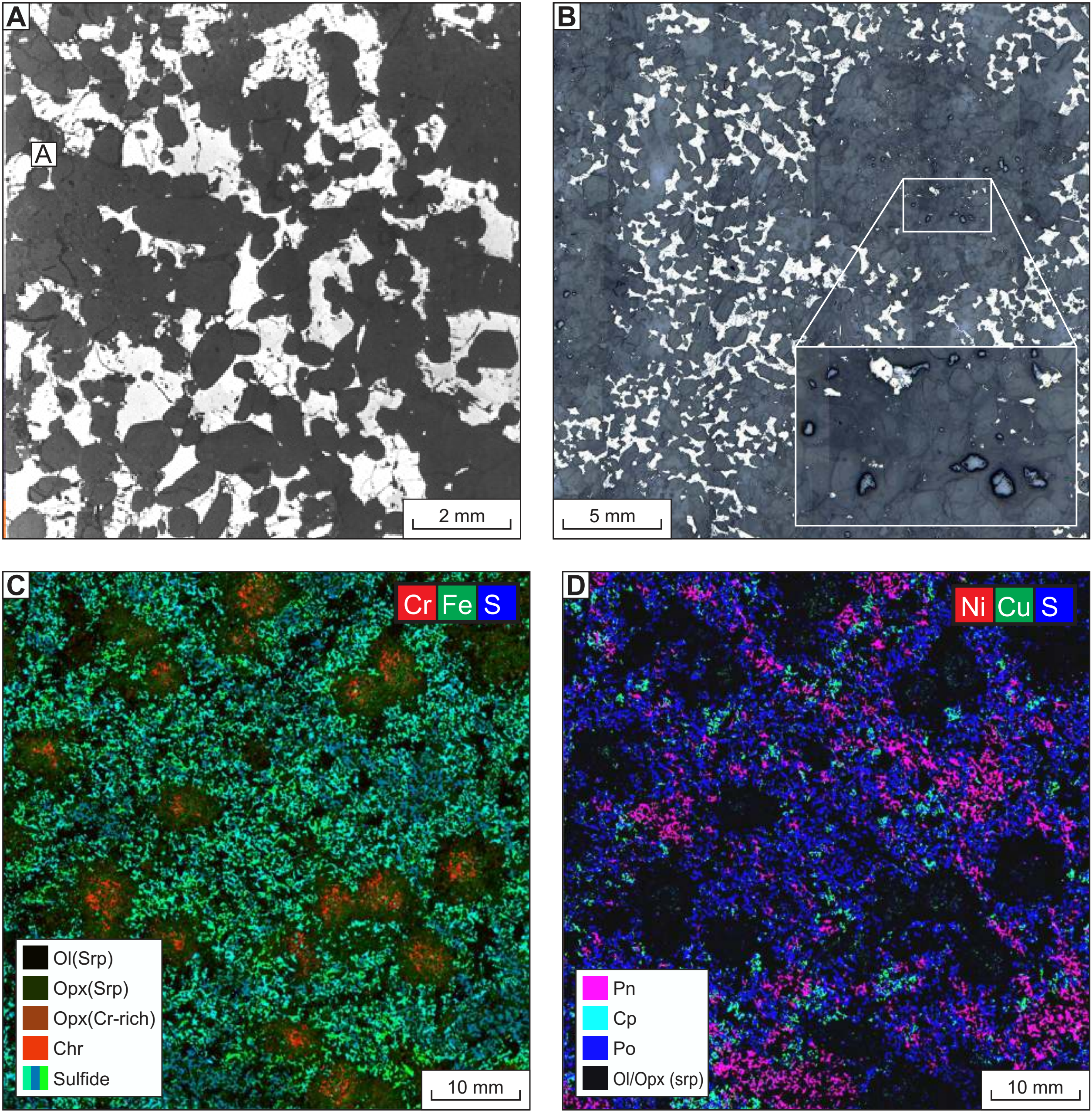
A
A
2 mm
B
5 mm
C
Cr Fe S
Ol(Srp)
Opx(Srp)
Opx(Cr-rich)
Chr
Sulfide
10 mm
D
Ni Cu S
Pn
Cp
Po
Ol/Opx (srp)
10 mm

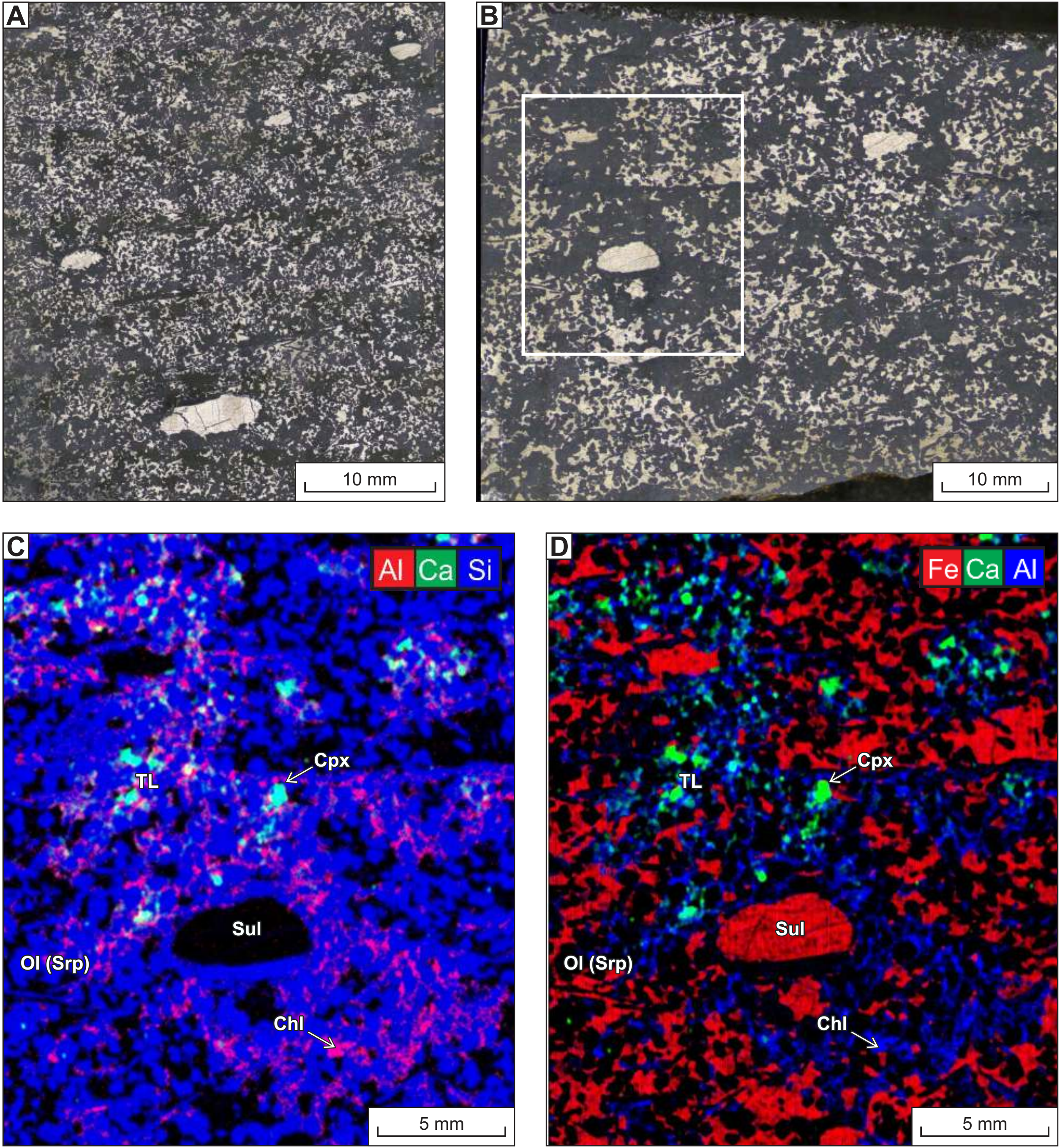
A
10 mm
B
10 mm
C
Al
Ca
Si
TL
Cpx
Sul
Ol (Srp)
Chl
5 mm
D
Fe
Ca
Al
TL
Cpx
Sul
Ol (Srp)
Chl
5 mm

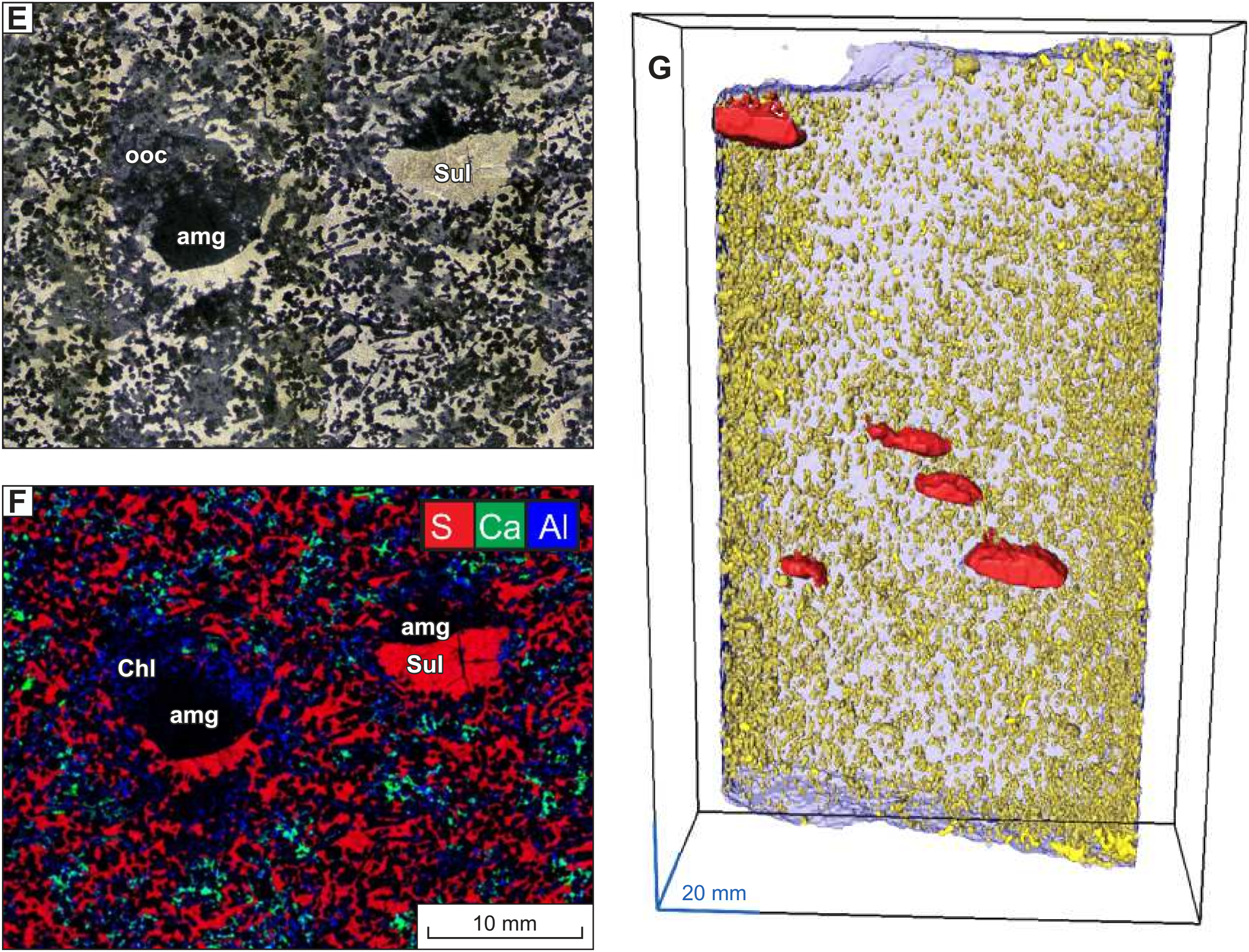
E
ooc
Sul
amg
F
S
Ca
Al
amg
Sul
Chl
amg
10 mm
G
20 mm

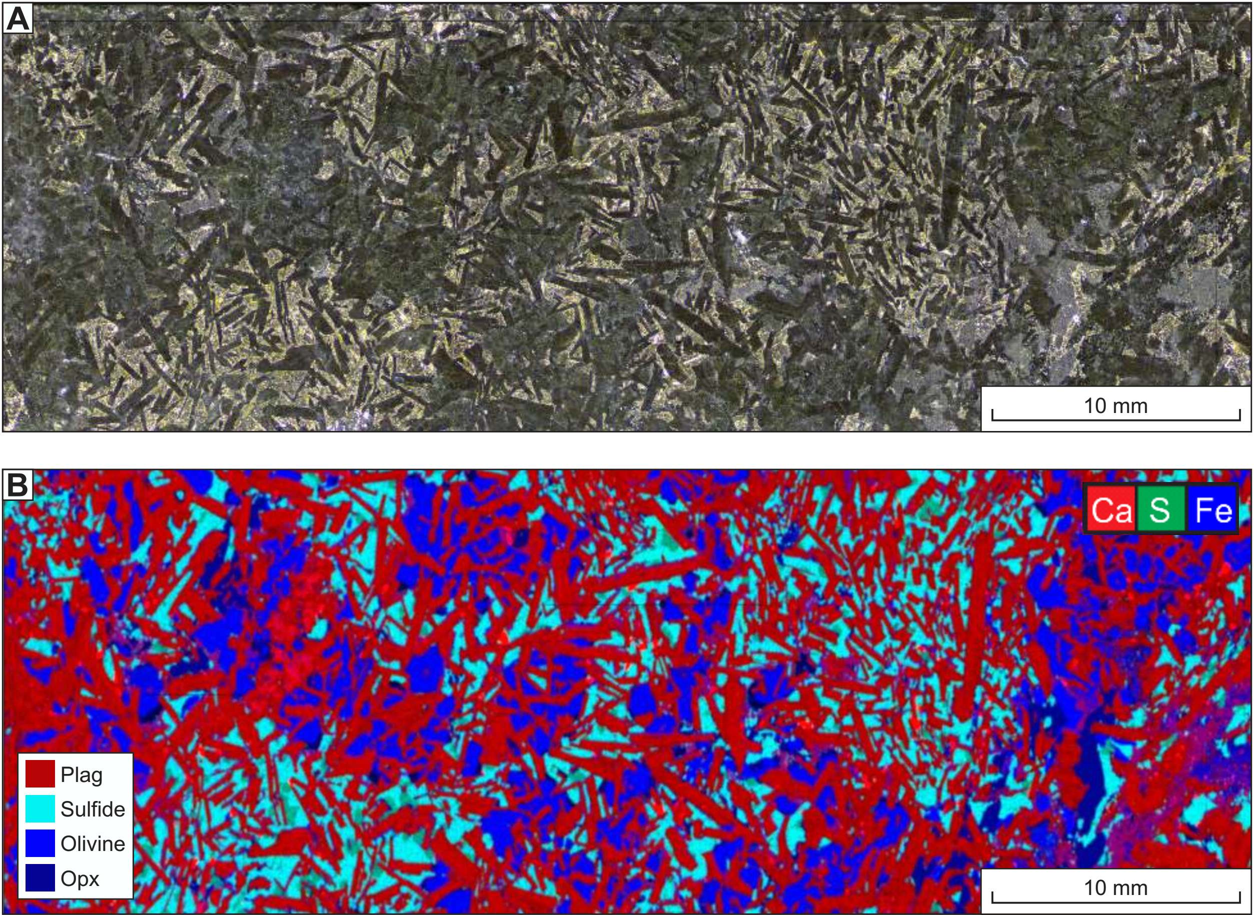
A
10 mm
B
Ca
S
Fe
Plag
Sulfide
Olivine
Opx
10 mm

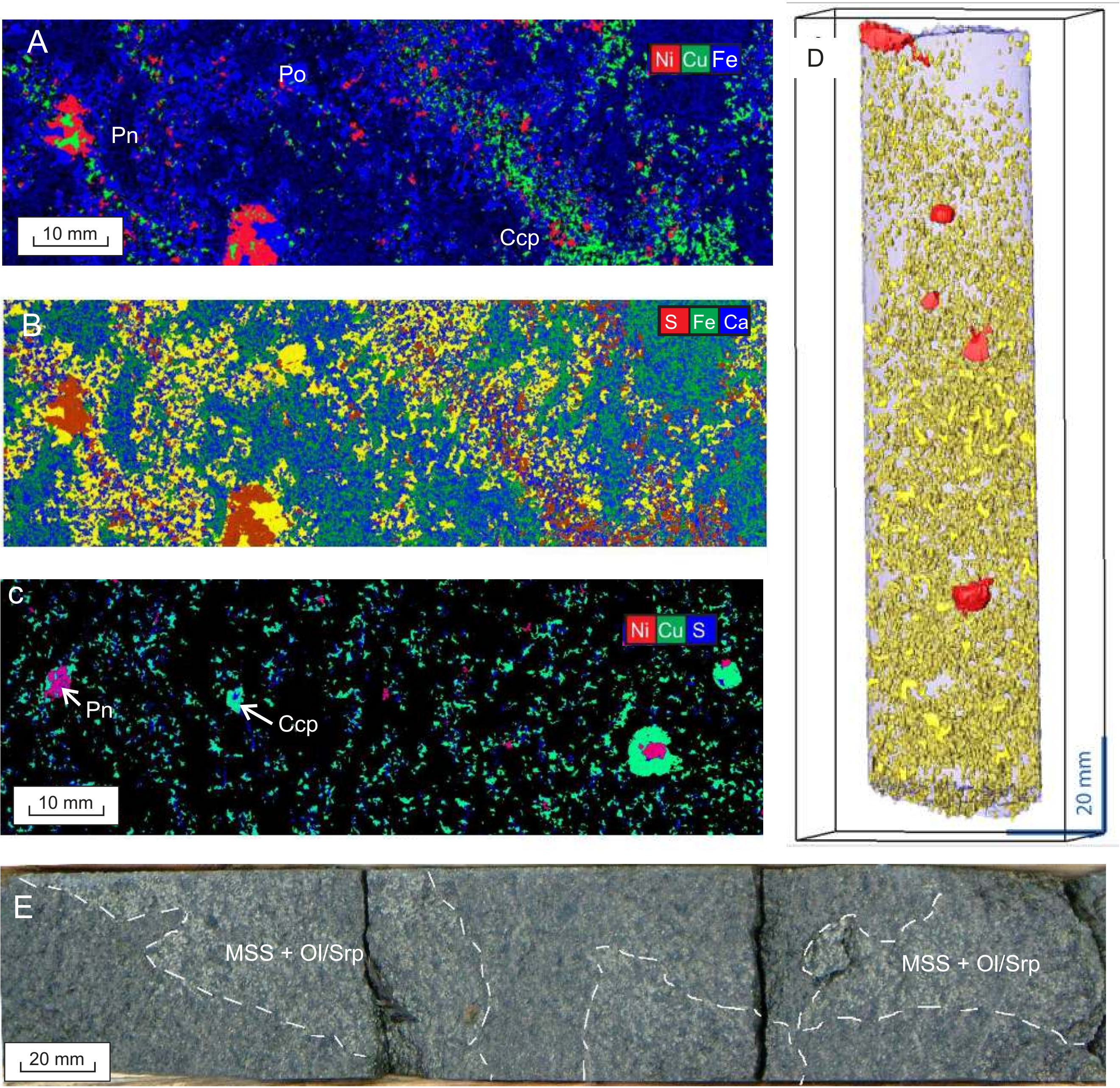
A
Ni Cu Fe
Po
Pn
Ccp
10 mm
B
S Fe Ca
C
Ni Cu S
Pn
Ccp
10 mm
D
20 mm
E
MSS + Ol/Srp
MSS + Ol/Srp
20 mm

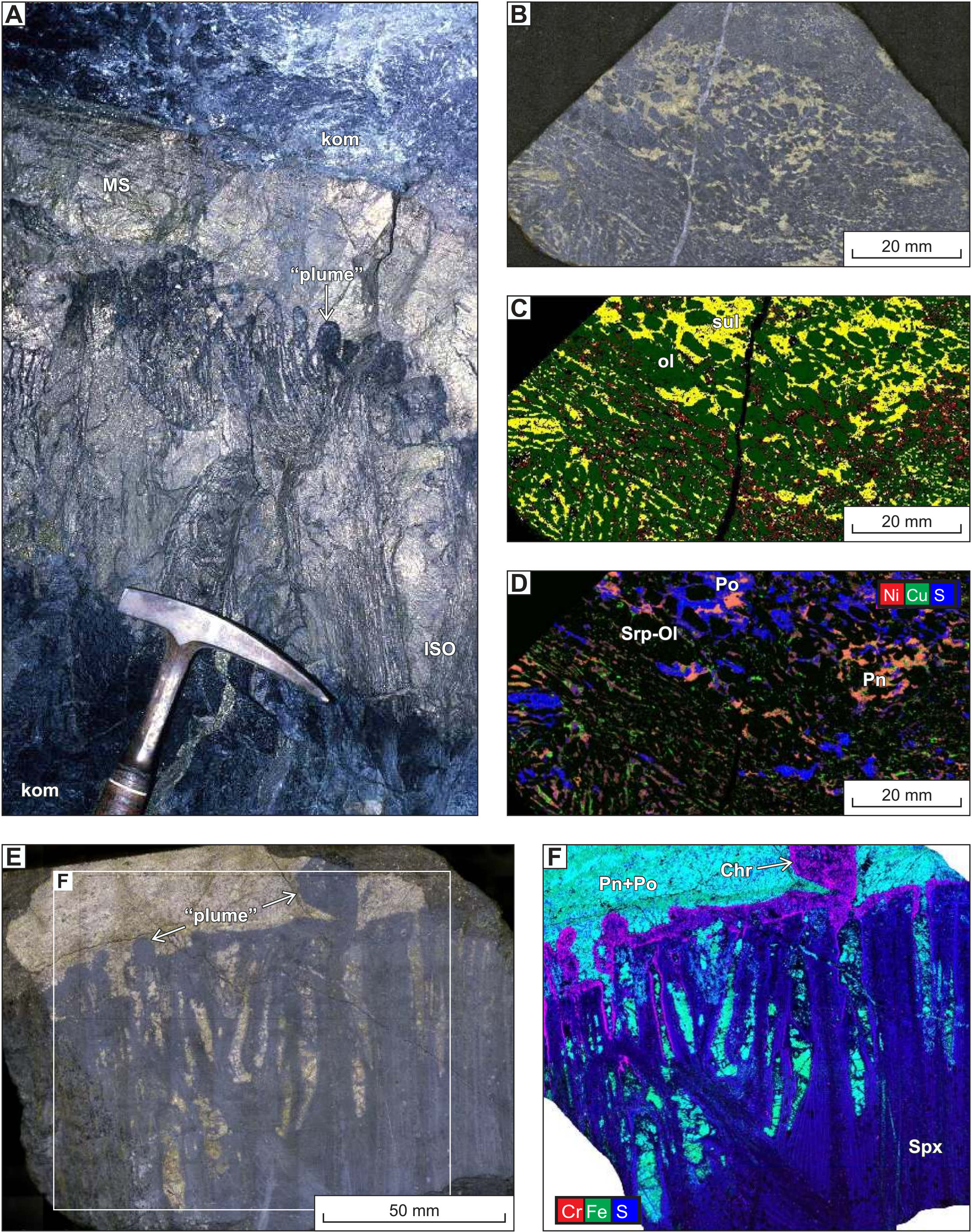
A
kom
MS
"plume"
ISO
kom
B
20 mm
C
sul
ol
20 mm
D
Po
Ni Cu S
Srp-Ol
Pn
20 mm
E
F
"plume"
50 mm
F
Chr
Pn+Po
Spx
Cr Fe S

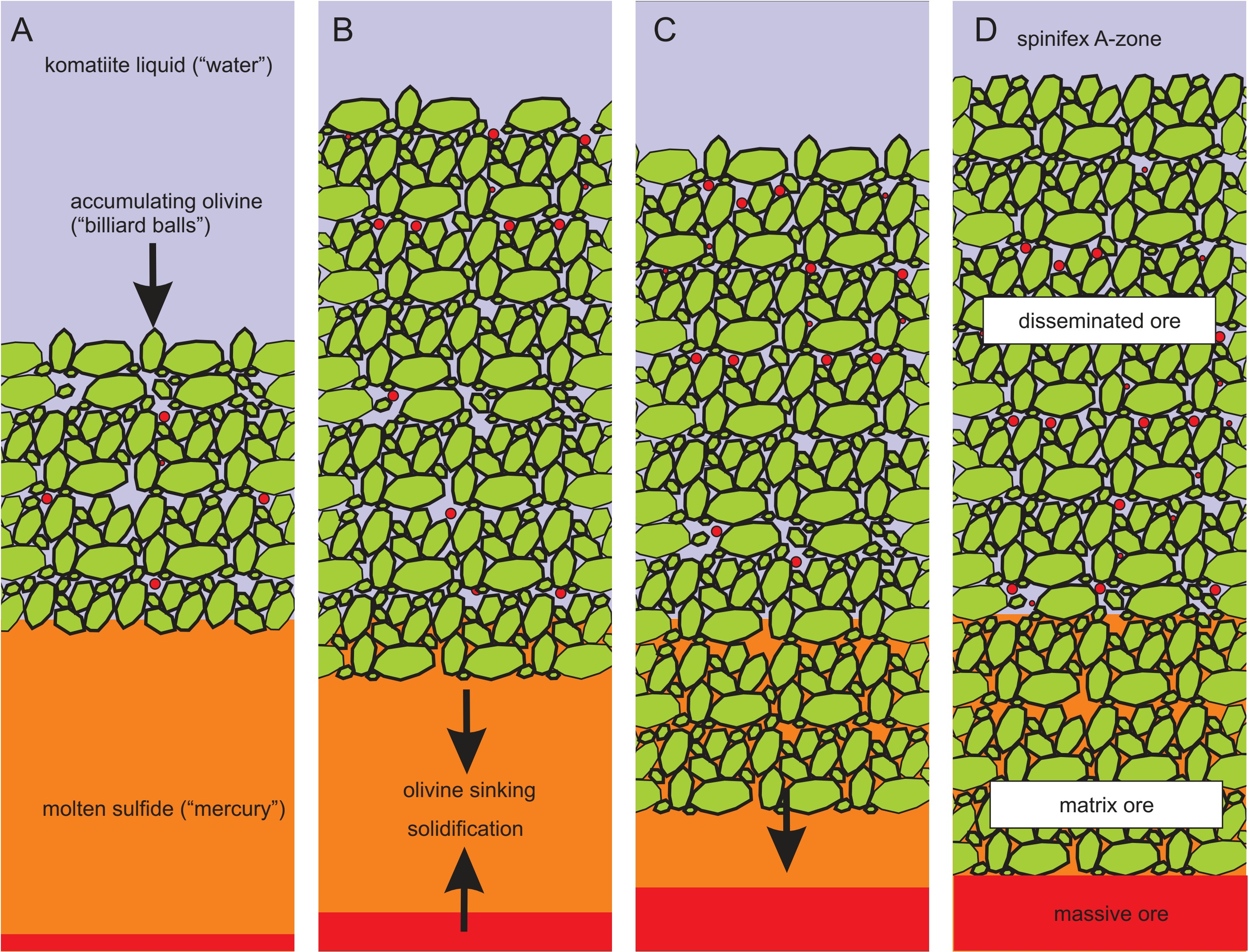
A
komatiite liquid ("water")
accumulating olivine
("billiard balls")
molten sulfide ("mercury")
B
olivine sinking
solidification
C
D
spinifex A-zone
disseminated ore
matrix ore
massive ore

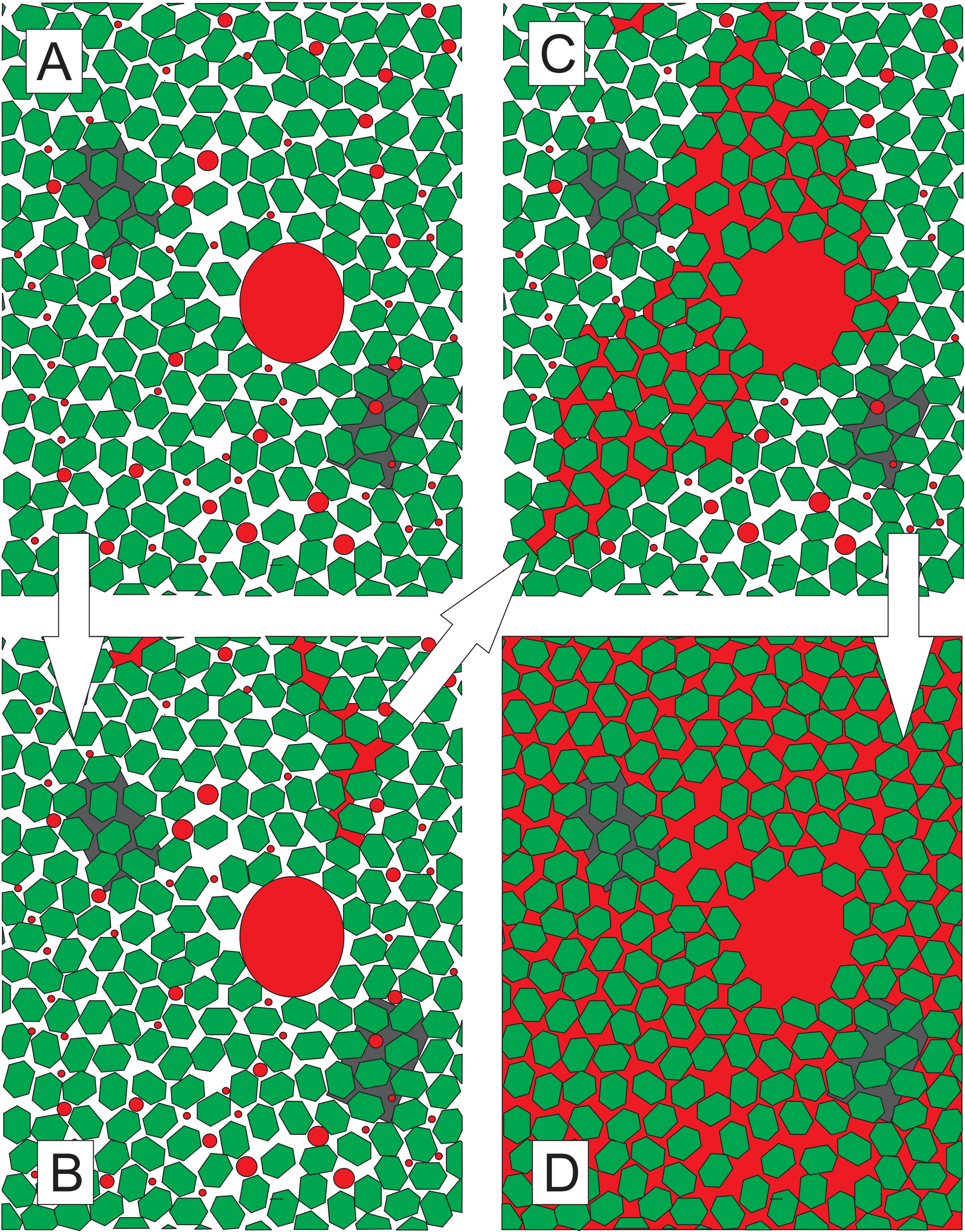
A
C
B
D


A
Sul Vein
2 cm
B
Sul Vein
2 cm
C
Globule
Matrix
Vein
Matrix
5 cm

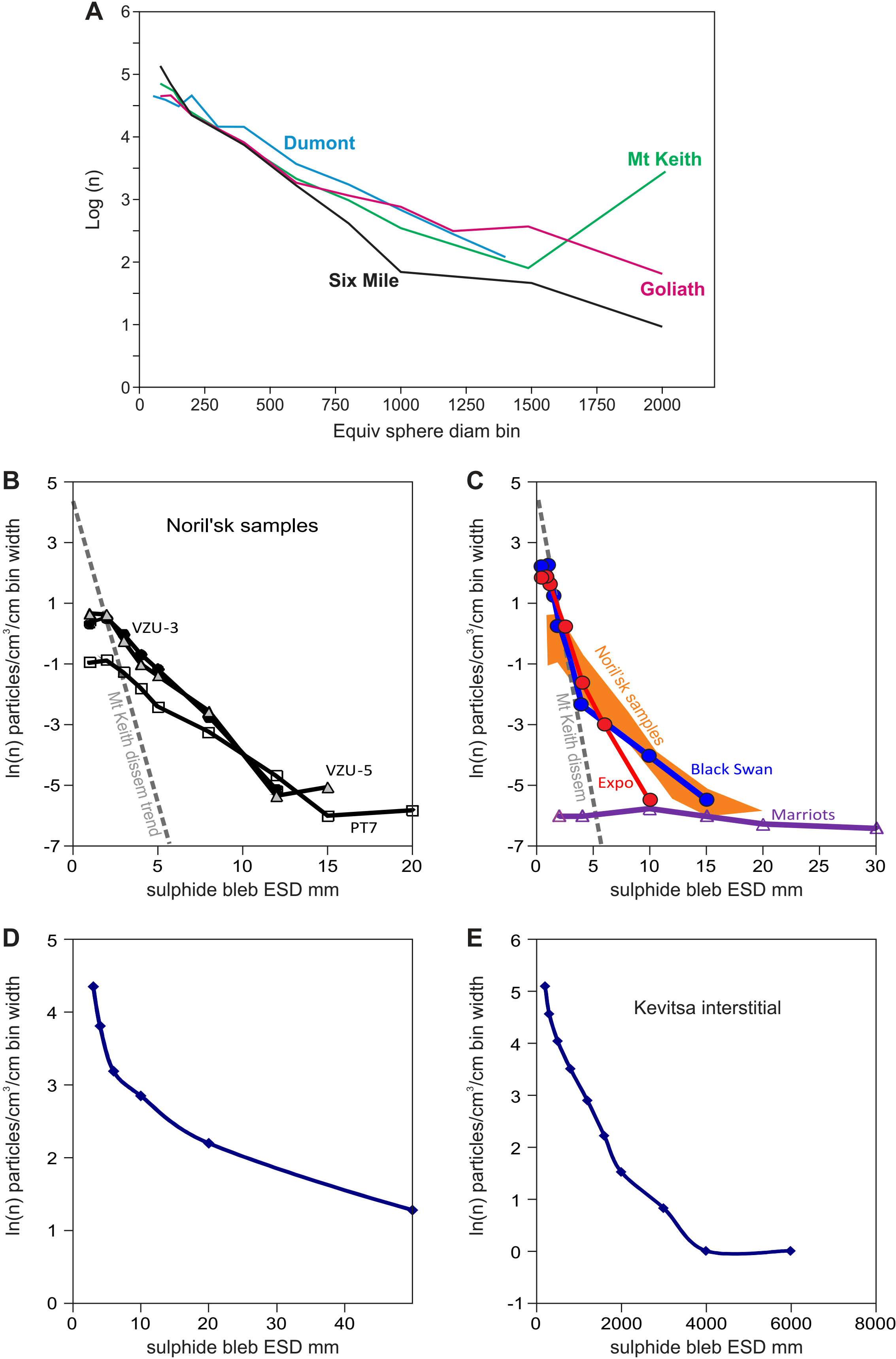
A
Log (n)
Equiv sphere diam bin
Dumont
Mt Keith
Six Mile
Goliath
B
Noril'sk samples
VZU-3
VZU-5
PT7
Mt Keith dissem trend
ln(n) particles/cm^3/cm bin width
sulphide bleb ESD mm
C
Noril'sk samples
Mt Keith dissem
Black Swan
Expo
Marriots
D
E
Kevitsa interstitial

Table 1. Summary of localities and sulfide textures discussed in the text.

Locality/deposit	Type of occurrence	Sulfide textural types dominant	Reference
Alexo, Ontario	Komatiite Ni	Net-textured, patchy and globular net-textured, massive	(Naldrett, 1973; Houle and Lesher, 2011; Houle et al., 2012)
Black Swan, WA	Komatiitic Ni	Disseminated interstitial and globular, some capped globules	(Barnes et al., 2009) (Dowling et al., 2004; Barnes, 2006)
Copper Cliff, Sudbury	Astrobleme-associated Ni-Cu-PGE	Disseminated interstitial and globular, massive	(Lightfoot et al., 1997a; Lightfoot et al., 1997b; Lightfoot and Farrow, 2002) (Naldrett, 1969; Mungall, 2002)
Dumont, Quebec	Komatiitic dunite Ni	Disseminated interstitial	(Sciortino et al., 2015)
Togeda macrodyke, Kangerlussuaq, East Greenland	Disseminated sulfides in dike margin	Disseminated globular (capped)	(Holwell et al., 2012)
Katinniq, Quebec	Komatiite Ni	Net-texture, “leopard” net-texture	(Barnes et al., 1982; Lesher, 2007)
Kevitsa, Finland	Mafic-ultramafic intrusion, disseminated Ni	Disseminated interstitial	(Yang et al., 2013; Santaguida et al., 2015)
Kharelakh and Noril’sk 1	Mafic intrusion, chonolith-style, Ni-	Wide variety from disseminated and	(Czamanske et al., 1992; Czamanske et

intrusions, Noril'sk-Talnakh, Siberia	Cu-PGE	disseminated interstitial to net-textured and massive ores,	al., 1995; Naldrett, 2004; Barnes et al., 2006; Lightfoot and Zotov, 2014; Sluzhenikin et al., 2014)
Langmuir, Ontario	Komatiite Ni	Interspinifex ore	(Green and Naldrett, 1981)
Lunnon, Kambalda, WA	Komatiite Ni	Interspinifex ore	(Groves et al., 1986)
Merensky Reef, Bushveld Complex	Reef-style disseminated PGE	Disseminated interstitial	(Godel et al., 2006; Godel et al., 2010)
Mesamax, Quebec	Komatiite Ni (intrusive)	Patchy and globular net-textured, massive	(Mungall, 2007a)
Mirabela (Santa Rita), Brazil	Mafic-ultramafic intrusion, disseminated Ni	Disseminated interstitial	(Barnes et al., 2011c)
Mount Keith, Western Australia	Komatiitic dunite Ni	Disseminated interstitial	(Barnes et al., 2011a; Godel et al., 2013)
Piaohechuan, China	Mafic-ultramafic intrusion, disseminated Ni	Disseminated globular	(Wei et al., 2015)
Voisey's Bay	Mafic intrusion, Ni-Cu	Net-texture, "leopard" net-texture, massive	(Evans-Lamswood et al., 2000)
Yakabindie (including Goliath), Western Australia	Komatiitic dunite Ni	Disseminated interstitial	(Barnes et al., 2011a; Barnes et al., 2011b; Godel et al.,

			2013)

Table 1. Summary of characteristics of disseminated and net-textured ore types

	Sulfide abundance		
Host rock characteristic	**0-5 % - Disseminated ores**	**5-40% Patchy Net Textured**	**40-70% Net-Textured ores**
Sulfide-olivine adcumulate - no silicate melt	**Disseminated interstitial** - low wetting angles, sulfides form weakly connected triple-point channels - e.g. Mt Keith-type komatiitic dunite setting.		**Net-textured ores** - standard variety, e.g. Kambalda, Katinniq **Error! Reference source not found.**
Sulfide-olivine orthocumulate - 30-50% silicate melt	**Disseminated globular** - high wetting angles, sulfides form unconnected or weakly coalesced convex globules - e.g. Black Swan-type komatiitic peridotite setting.	**Patchy net-textured ores** - standard variety, e.g. Jinchuan	
Sulfide-olivine orthocumulate - 20-50% silicate melt plus amygdales/vesicles	**Interstitial capped globular** - high wetting angles, sulfides form unconnected spherical globules inside segregation vesicles - e.g. Black Swan-type komatiitic peridotite setting.	**Patchy net-texture with capped globules** - sulfides form unconnected spherical globules inside segregation vesicles within low-sulfide domains in otherwise net-textured ores - e.g. Alexo	
Poikilitic sulfide-olivine or sulfide-pyroxene orthocumulate with pyroxene oikocrysts	**Interstitial disseminated "leopard" variety** - e.g. Kevitsa	**Patchy net-textured ores** - "Leopard" variety, e.g. Jinchuan	"Leopard" net-texture - e.g. Katinniq
Poikilitic sulfide-plagioclase or sulfide-olivine-plagioclase orthocumulate with pyroxene and/or olivine oikocrysts		**"Leopard Troctolite" ores** - e.g. Voisey's Bay	**"Leopard Troctolite" ores** - e.g. Voisey's Bay
Non-cumulate, porhyritic or aphyric chilled silicate melt, non-vesicular	**Disseminated globular** - subspherical sulfide globules in marginal phase rocks, narrow dikes or sulfide-poor flows e.g. Raglan South	**Patchy net-texture** in pyroxene-rich marginal facies rocks, with or without minor globules - e.g. Raglan South	

Non-cumulate, porhyritic or aphyric chilled silicate melt, vesicular	**Disseminated capped globular** -spherical sulfide globules with silicate caps in marginal phase rocks - e.g. East Greenland macrodikes, Uruguay mafic dikes		
Non-cumulate, porhyritic or aphyric chilled silicate melt, overlapping melting range between silicate and sulfide		**Disseminated globular** - non-spherical blebs with MSS facets e.g. Sudbury Copper Cliff	